

3784

NACA TN 4501

NATIONAL ADVISORY COMMITTEE FOR AERONAUTICS

TECHNICAL NOTE 3501

THE TRANSONIC CHARACTERISTICS OF 22 RECTANGULAR,
SYMMETRICAL WING MODELS OF VARYING
ASPECT RATIO AND THICKNESS

By Warren H. Nelson and John B. McDevitt

Ames Aeronautical Laboratory
Moffett Field, Calif.



Washington

June 1955

AMERICAN
AERONAUTICAL

AIR LIBRARY

ML 281



0066619

NATIONAL ADVISORY COMMITTEE FOR AERONAUTICS

TECHNICAL NOTE 3501

THE TRANSONIC CHARACTERISTICS OF 22 RECTANGULAR,

SYMMETRICAL WING MODELS OF VARYING

ASPECT RATIO AND THICKNESS¹

By Warren H. Nelson and John B. McDevitt

SUMMARY

An investigation to determine the aerodynamic characteristics of a series of thin, rectangular wings was conducted in the Ames 16-foot high-speed wind tunnel, utilizing the transonic-bump technique over a Mach number range from 0.40 to 1.10, corresponding to a Reynolds number range from 1.25 to 2.05 million. The lift, drag, and pitching-moment data are presented for wings having aspect ratios of 6, 4, 3, 2, 1.5, 1, and 0.5, and NACA 63AOXX sections with thickness-to-chord ratios of 10, 8, 6, 4, and 2 percent.

INTRODUCTION

The purpose of this investigation was to provide comprehensive data on the effects of aspect ratio and thickness on the aerodynamic characteristics of a family of symmetrical, straight wings through the transonic speed range.

Twenty-two wings in all were investigated, with aspect ratios of 6, 4, 3, 2, 1.5, 1, and 0.5. Rectangular plan forms were used, and the profiles were NACA 63AOXX sections having thickness-to-chord ratios of 10, 8, 6, 4, and 2 percent.

In order to obtain an indication of the reliability of the bump data, a semispan scale model of the larger, full-span, aspect-ratio-2 wing reported in reference 1 was also constructed and tested on the bump.

¹Supersedes recently declassified NACA RM A51A12 by Warren H. Nelson and John B. McDevitt, 1951.

NOTATION

C_D	drag coefficient, $\frac{\text{twice semispan drag}}{qS}$
ΔC_D	total drag coefficient minus drag coefficient at zero lift
C_L	lift coefficient, $\frac{\text{twice semispan lift}}{qS}$
C_m	pitching-moment coefficient, referred to 0.25 \bar{c} , $\frac{\text{twice semispan pitching moment}}{qS\bar{c}}$
A	aspect ratio, $\frac{b^2}{S}$
$\frac{L}{D}$	lift-drag ratio
$(\frac{L}{D})_{\max}$	maximum lift-drag ratio
M	Mach number
R	Reynolds number based on mean aerodynamic chord
S	total wing area (twice wing area of semispan model), sq ft
V	velocity, ft/sec
b	twice span of semispan model, ft
c	local wing chord, ft
\bar{c}	mean aerodynamic chord, $\frac{\int_0^{b/2} c^2 dy}{\int_0^{b/2} c dy}$, ft
q	dynamic pressure, $\frac{1}{2} \rho V^2$, lb/sq ft
$\frac{t}{c}$	thickness-to-chord ratio
y	spanwise distance from plane of symmetry, ft
α	angle of attack, deg
ρ	air density, slugs/cu ft
$\frac{dC_L}{da}$	slope of lift curve measured at zero lift, per deg

$\frac{dC_m}{dC_L}$ slope of pitching-moment curve measured at zero lift

APPARATUS

Wind Tunnel and Equipment

These tests were conducted on a transonic bump in the Ames 16-foot high-speed wind tunnel. The bump is described in detail in reference 2. The aerodynamic forces and moments were measured by means of a strain-gage balance mounted inside the bump.

Models

The sting-supported full-span model mounted centrally in the wind tunnel and the similar reduced-scale, semispan model mounted on the bump are shown in figure 1. These wings, used to provide a comparison of the results obtained with the two testing techniques, had NACA 65₁-210 sections, aspect ratios of 2, and taper ratios of 0.4.

A typical mounting of the rectangular wings on the bump is shown in figure 2. The principal dimensions and plan forms of the rectangular wings are shown in figure 3. Five aspect-ratio-6 wings of the various thicknesses used were constructed and the aspect ratios of 4, 3, 2, 1.5, 1 and 0.5 were obtained by successively cutting off the tips. The profiles were NACA 63AOXX sections having thickness-to-chord ratios of 10, 8, 6, 4, and 2 percent (fig. 4).

A fence located 3/16 inch from the bump surface was used to keep leakage, originating inside the bump, from affecting the flow over the model. This leakage is the result of clearance between the wing and bump surface required for this type of mounting.

TESTS AND PROCEDURE

Range of Test Variables

The characteristics of the rectangular wings were investigated for a Mach number range from 0.4 to 1.10. The variation of Reynolds number with Mach number for the rectangular wings is shown in figure 5. The angle-of-attack range was limited from -2° to 20° by the balance mechanism, and for some of the thinner wings it was limited to a smaller angle-of-attack range by the bending stress at the root.

The aspect ratios and thickness ratios tested are shown in the following table:

Aspect ratio	Thickness-to-chord ratio				
	0.10	0.08	0.06	0.04	0.02
6	x	x	x	---	---
4	x	x	x	x	---
3	---	---	---	x	---
2	x	x	x	x	x
1.5	---	---	---	x	x
1	x	x	x	x	x
0.5	---	---	---	x	x

Reduction of Data

The test data have been reduced to standard NACA coefficient form. A drag correction was applied to account for an interaction between the lift and drag components of the balance. A tare correction to the drag of the rectangular wings to account for the drag of the fence was evaluated by cutting the wing off flush with the fence and testing the fence alone.

The magnitude of the tare-drag coefficient, which depended on the areas of the wings, was 0.0175 for the aspect-ratio-0.5 wings and 0.0014 for the aspect-ratio-6 wings. The measured fence tare-drag coefficient did not change appreciably with Mach number or with changes in angle of attack. The interference effects of the fence and the effects of leakage around the fence are unknown; corrections for these effects have not been made. These effects would be greatest on the lower aspect-ratio wings since they have the smaller area.

The models investigated on the transonic bump are mounted in a local, high-velocity region. Typical contours of local Mach number in the bump flow field are shown in figure 6. Outlines of the rectangular wings have been superimposed on these diagrams to indicate the Mach number gradients which existed across the wings during the tests. No attempt has been made to evaluate the effects of these gradients. The test Mach numbers presented in this report are the average Mach numbers over the wings.

RESULTS

The drag data presented herein should be used with caution, particularly that for the lower Mach numbers or aspect ratios where the measured loads were small compared to the capacity of the balance. For this reason,

only data above 0.70 Mach number have been used in the cross plots involving drag measurements. Other factors which contribute to the uncertainty of the drag data are the large drag tares (for the lower aspect ratios), the fact that the lift-drag interaction mentioned previously may have varied slightly with time, and the Mach number gradients existing throughout the flow field of the bump. However, it is believed that the trends shown throughout the transonic speed range are qualitatively correct.

Figure 7 presents a comparison of the lift, drag, and pitching-moment data for the tapered, aspect-ratio-2, NACA 65₁-210 wings for the full-span model mounted on a sting in the center of the wind tunnel, and for the semispan model mounted on the bump. The Reynolds number range was about 2 to 3 million for the bump test, and it was about 6 to 9 million for the sting test.

The basic lift, drag, and pitching-moment data from the bump tests of the rectangular wings are presented in figures 8 through 10.

The variation of lift-drag ratio with lift coefficient is shown in figure 11. The maximum lift-drag ratios and the lift coefficients at which they occurred are shown as functions of Mach number in figures 12 and 13, respectively. The maximum lift-drag ratios appear erratic for some of the wings (especially the aspect-ratio-1 wings), particularly at the lower transonic Mach numbers. However, it is believed that the trends shown at the higher Mach numbers are correct. Phenomena of flow separation and reattachment as well as changes in the boundary layer may occur as the Mach number changes, so that it seems probable that some of the irregularities indicated do actually exist.

The variations with Mach number of the lift-curve slopes, the drag coefficients, and the pitching-moment-curve slopes are shown in figures 14 through 16 for rectangular wings. All the slopes shown in these summary curves were measured at zero lift. It should be noted that slopes are shown even for those cases in which the curves were nonlinear.

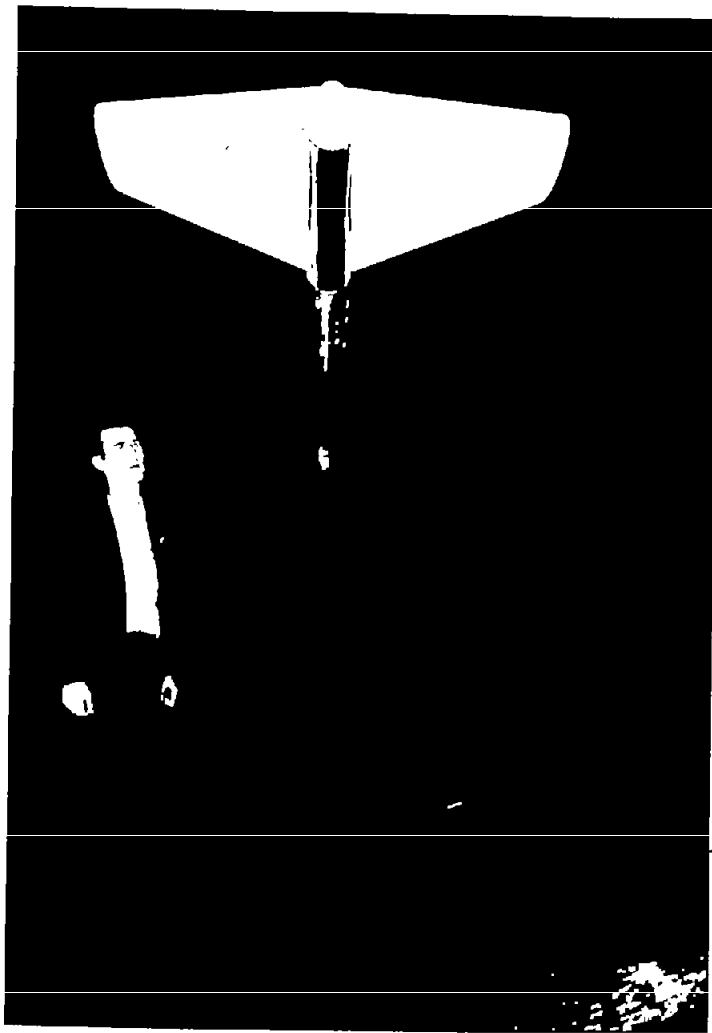
The data presented in this report have been analyzed in reference 3, utilizing the transonic similarity rules.

Ames Aeronautical Laboratory
National Advisory Committee for Aeronautics
Moffett Field, Calif., Jan. 12, 1951.

REFERENCES

1. Nelson, Warren H., and Erickson, Albert L.: The Effect of Aspect Ratio on the Subsonic Aerodynamic Characteristics of Wings With NACA 65₁-210 Sections. NACA RM A9K18, 1949.

2. Axelson, John A., and Taylor, Robert A.: Preliminary Investigation of the Transonic Characteristics of an NACA Submerged Inlet. NACA RM A50C13, 1950.
3. McDevitt, John B.: A Correlation by Means of the Transonic Similarity Rules of the Experimentally Determined Characteristics of 22 Rectangular Wings of Symmetrical Profile. NACA RM A51L17b, 1952.



(a) Full-span model.

A-13852



(b) Semispan model.

A-15649

Figure 1.- The two methods of mounting the tapered, aspect-ratio-2, NACA 65₁-210 wing models.



A-15628

Figure 2.- An aspect-ratio-2, rectangular wing model with an NACA 63A004 section mounted on the transonic bump in the 16-foot high-speed wind tunnel.

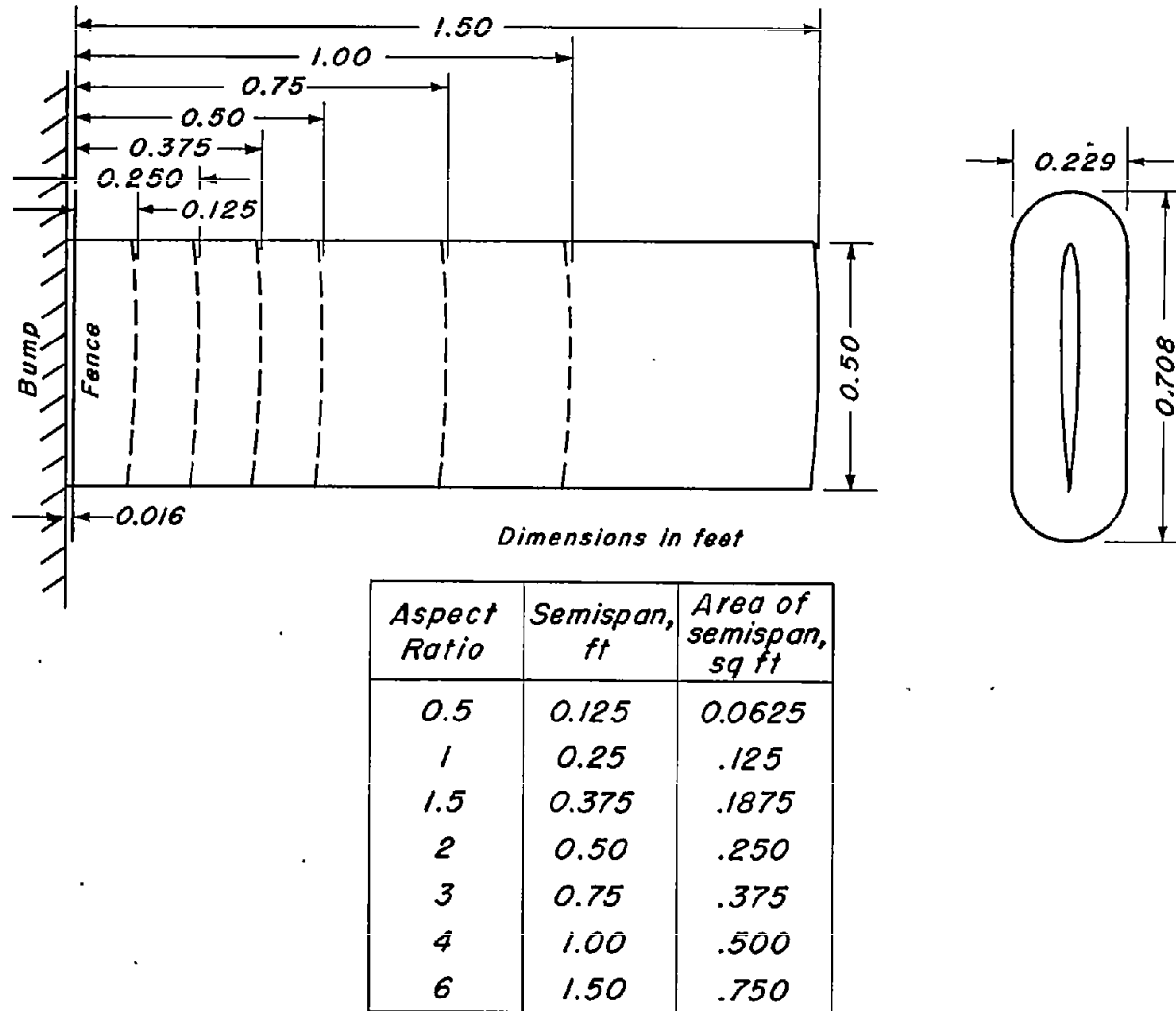
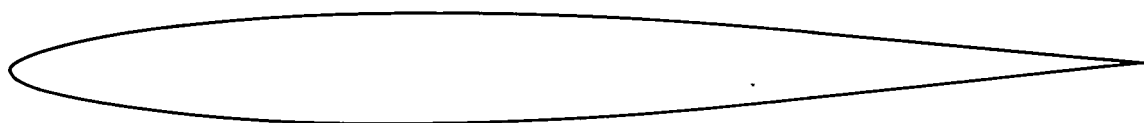
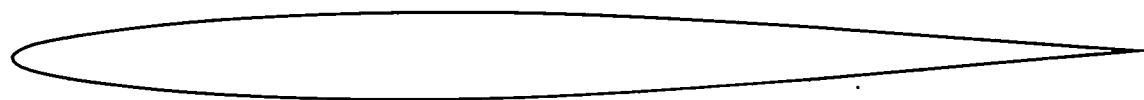


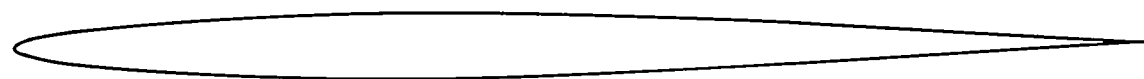
Figure 3.- Dimensions and plan forms of the rectangular wings.



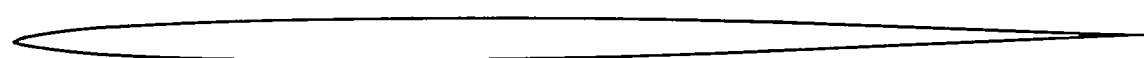
NACA 63A010



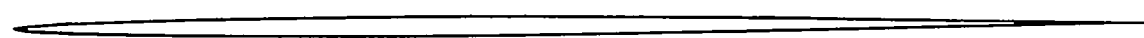
NACA 63A008



NACA 63A006



NACA 63A004



NACA 63A002

Figure 4.- Airfoil profiles used for the rectangular wings.

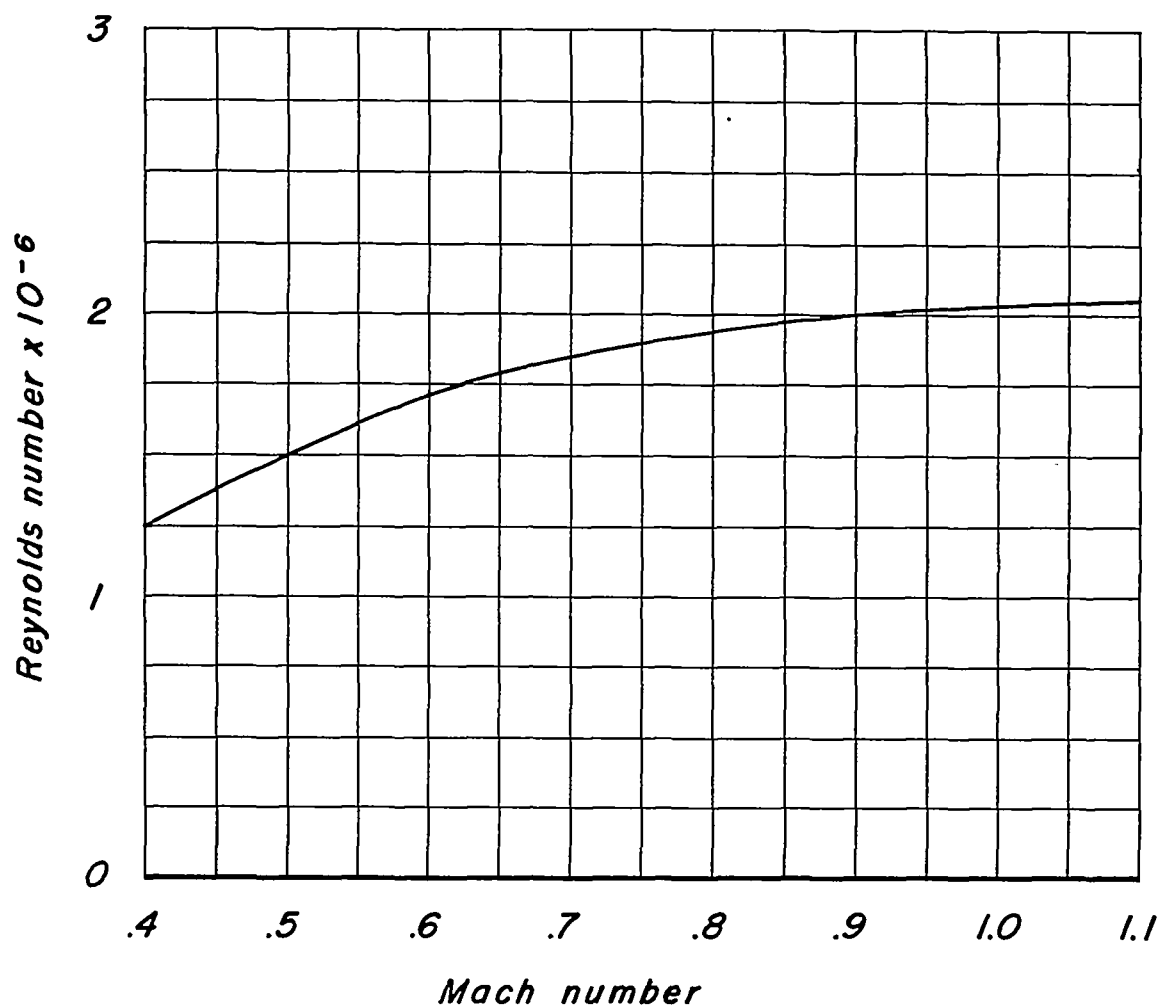


Figure 5.—The variation of Reynolds number with Mach number for the rectangular wings.

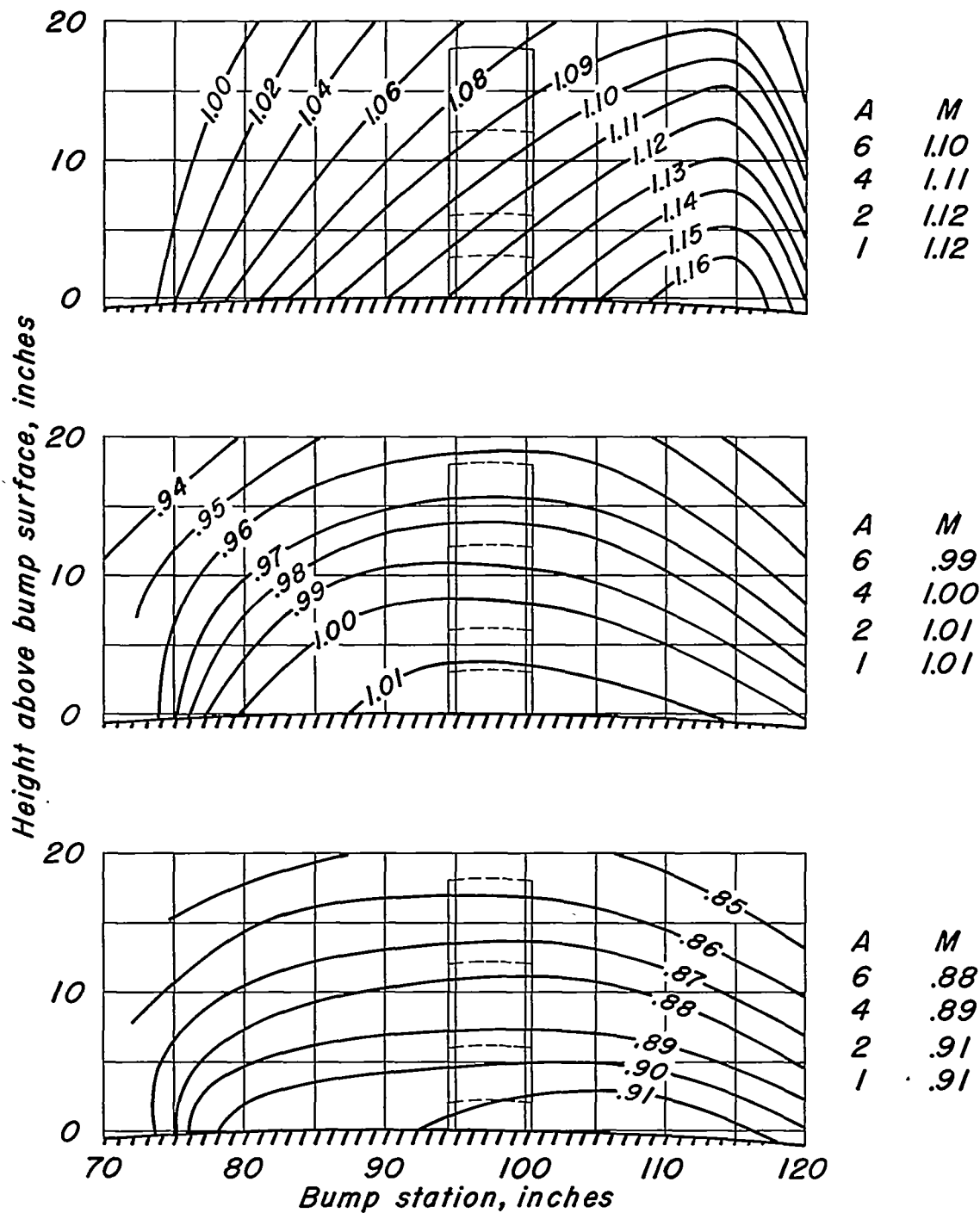


Figure 6.- Typical Mach number contours over the transonic bump in the Ames 16-foot high-speed wind tunnel.

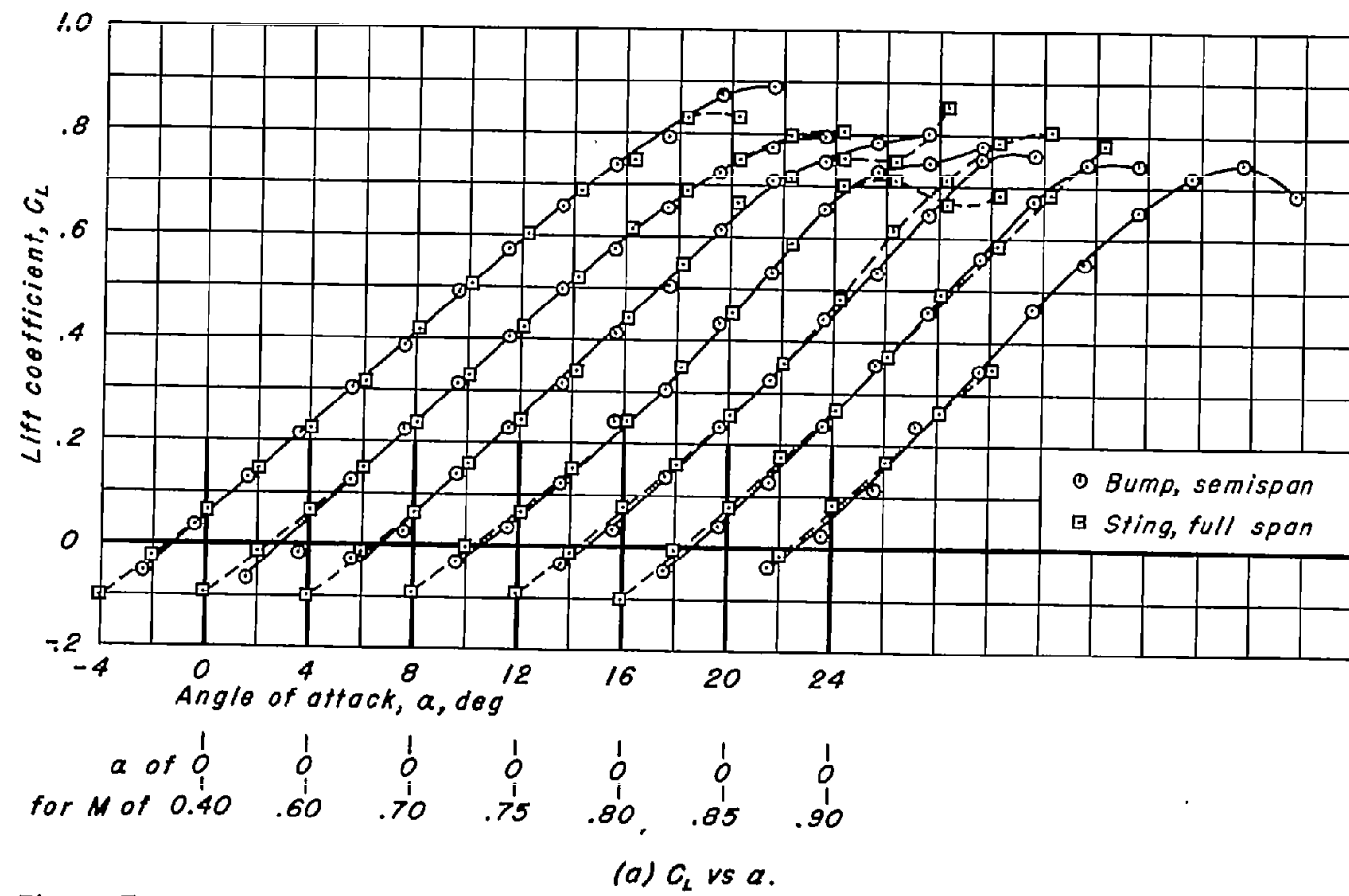


Figure 7.—Comparison of the aerodynamic characteristics of the tapered, aspect-ratio-2, NACA 65-210 wings, as obtained with a sting-mounted model and a bump-mounted model.

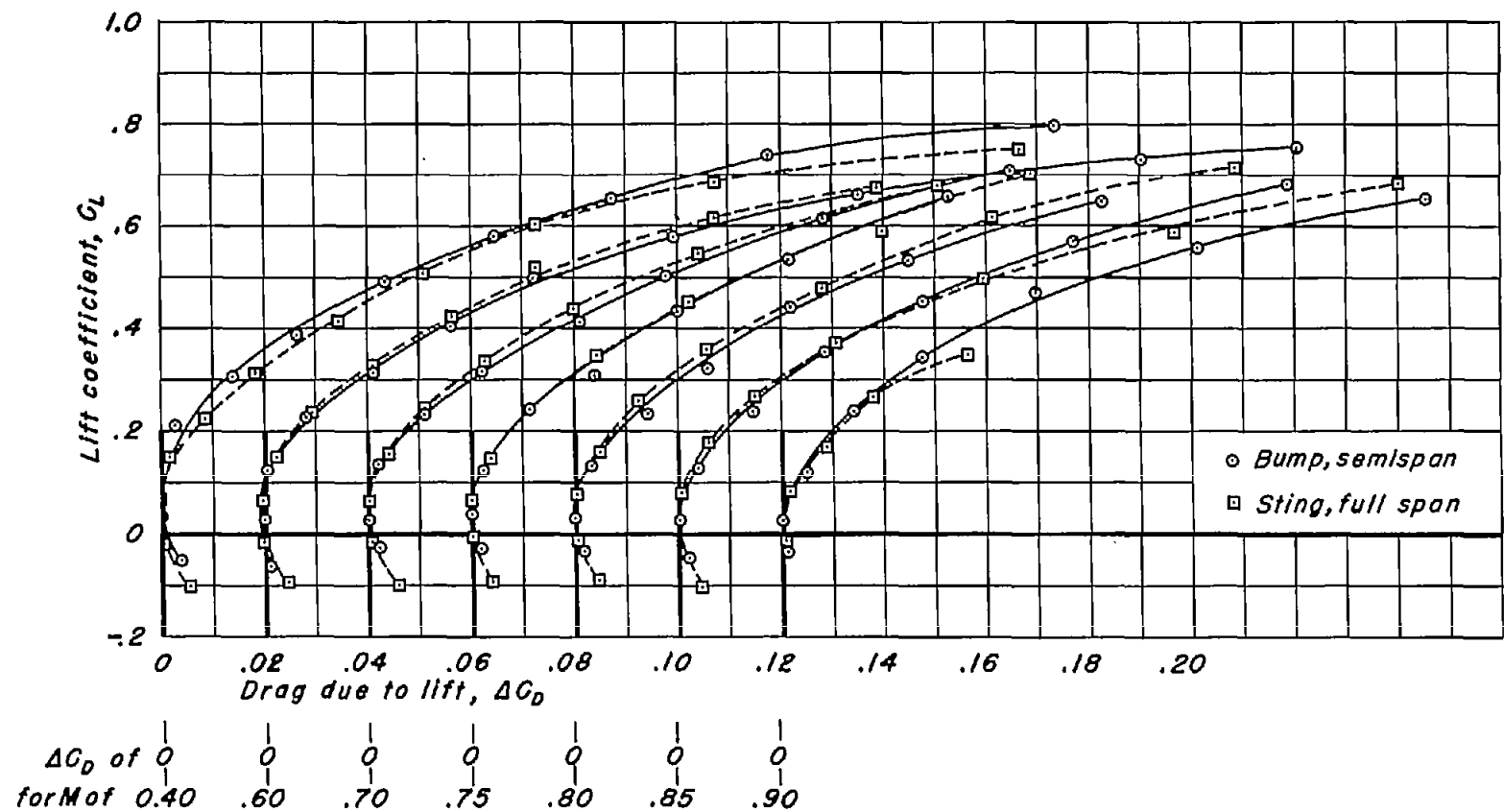
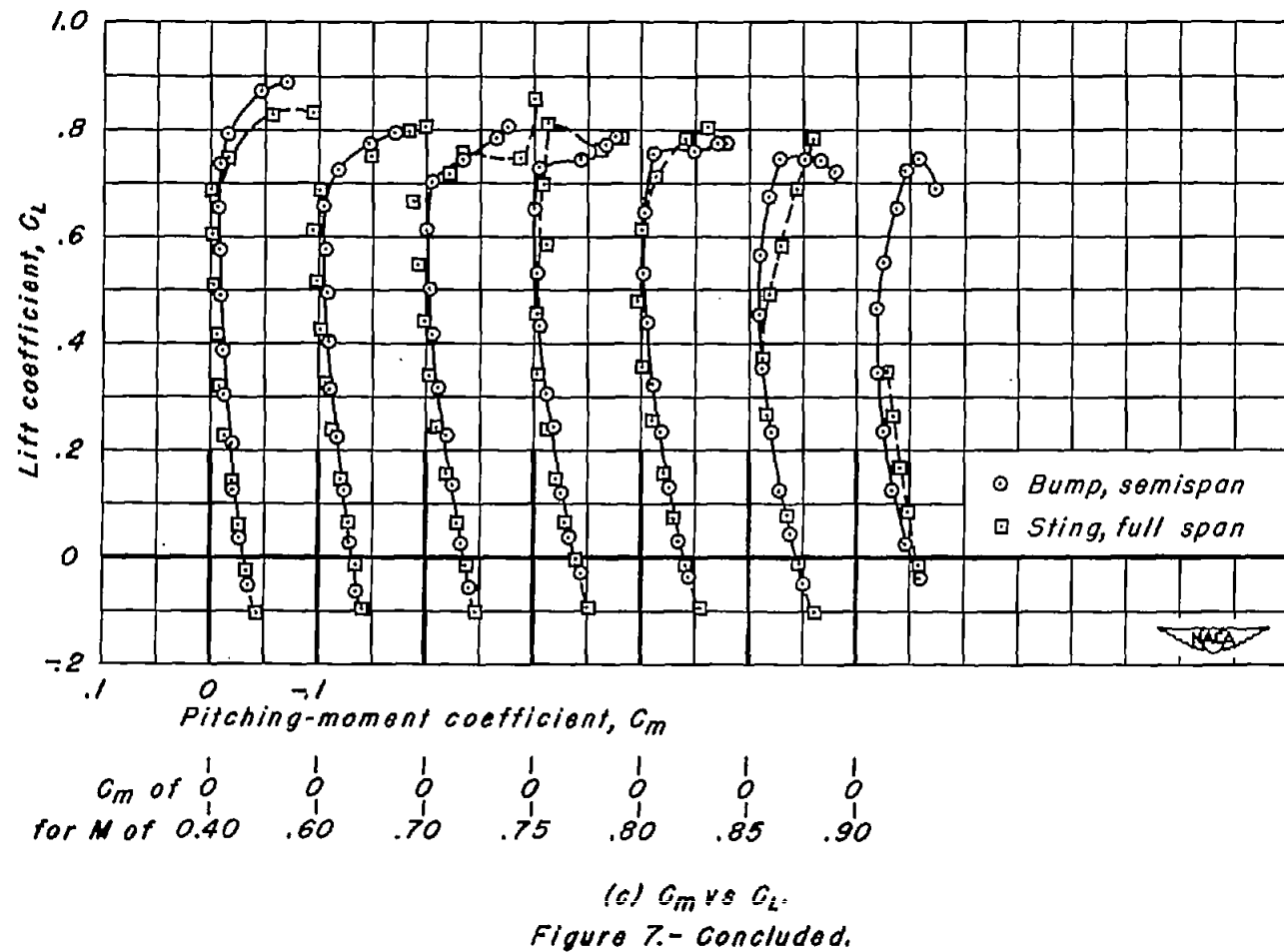
(b) Drag due to lift, ΔC_D vs C_L .

Figure 7.- Continued.



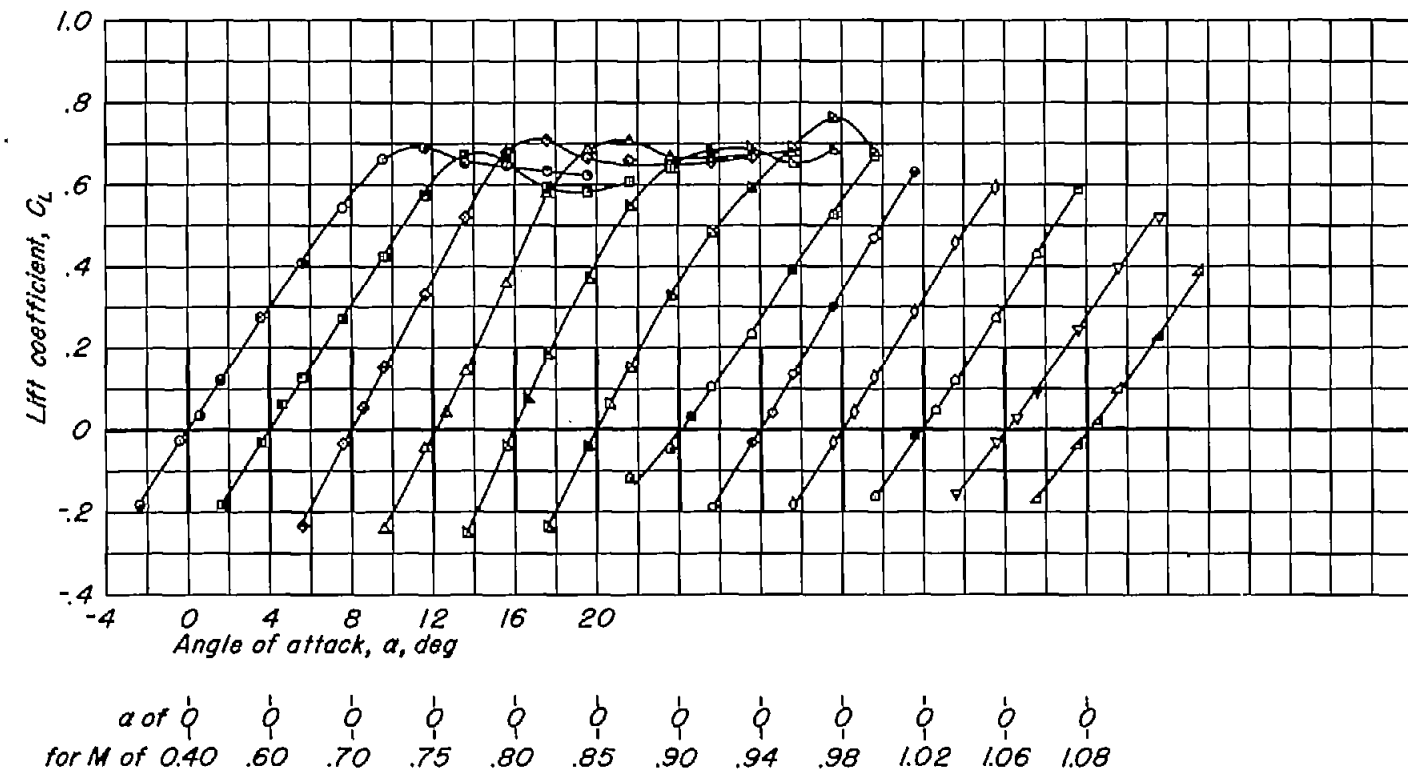
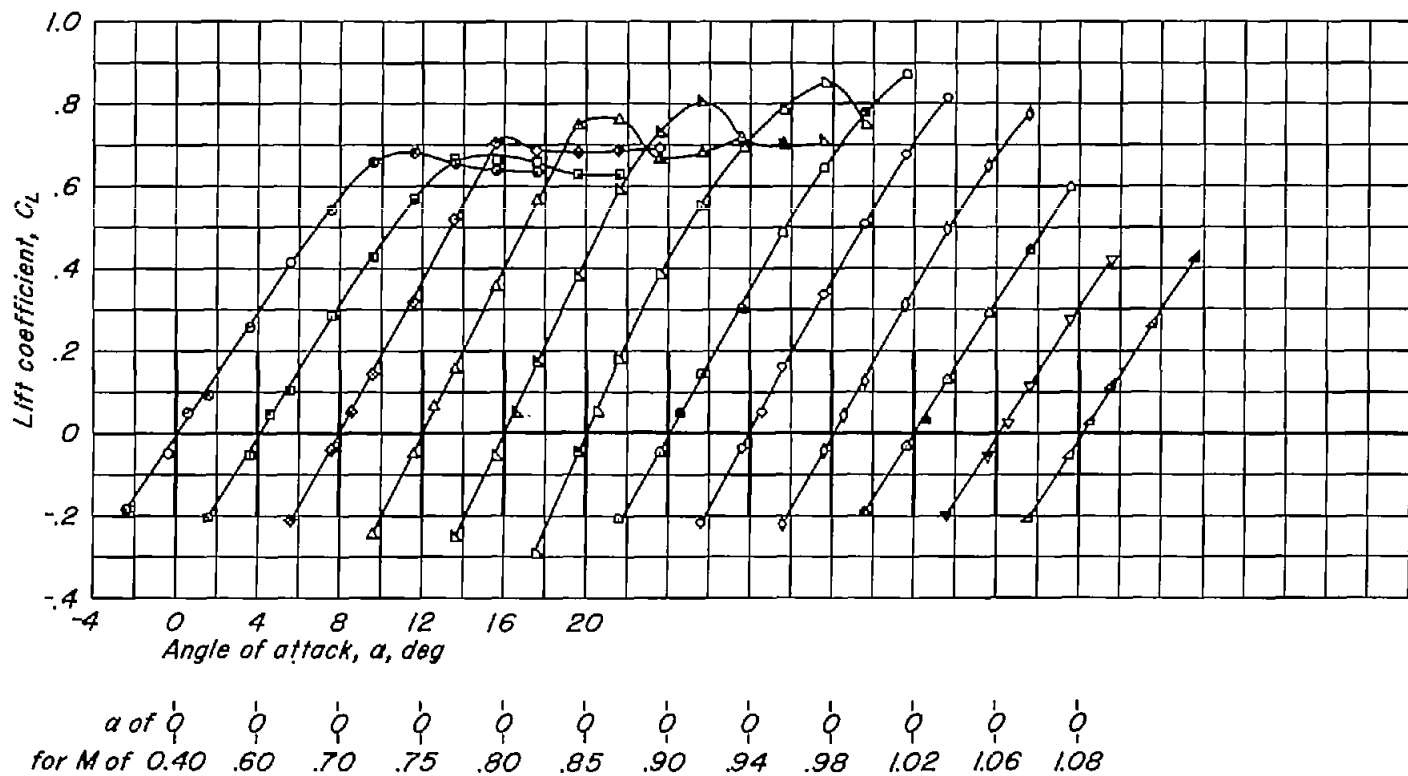
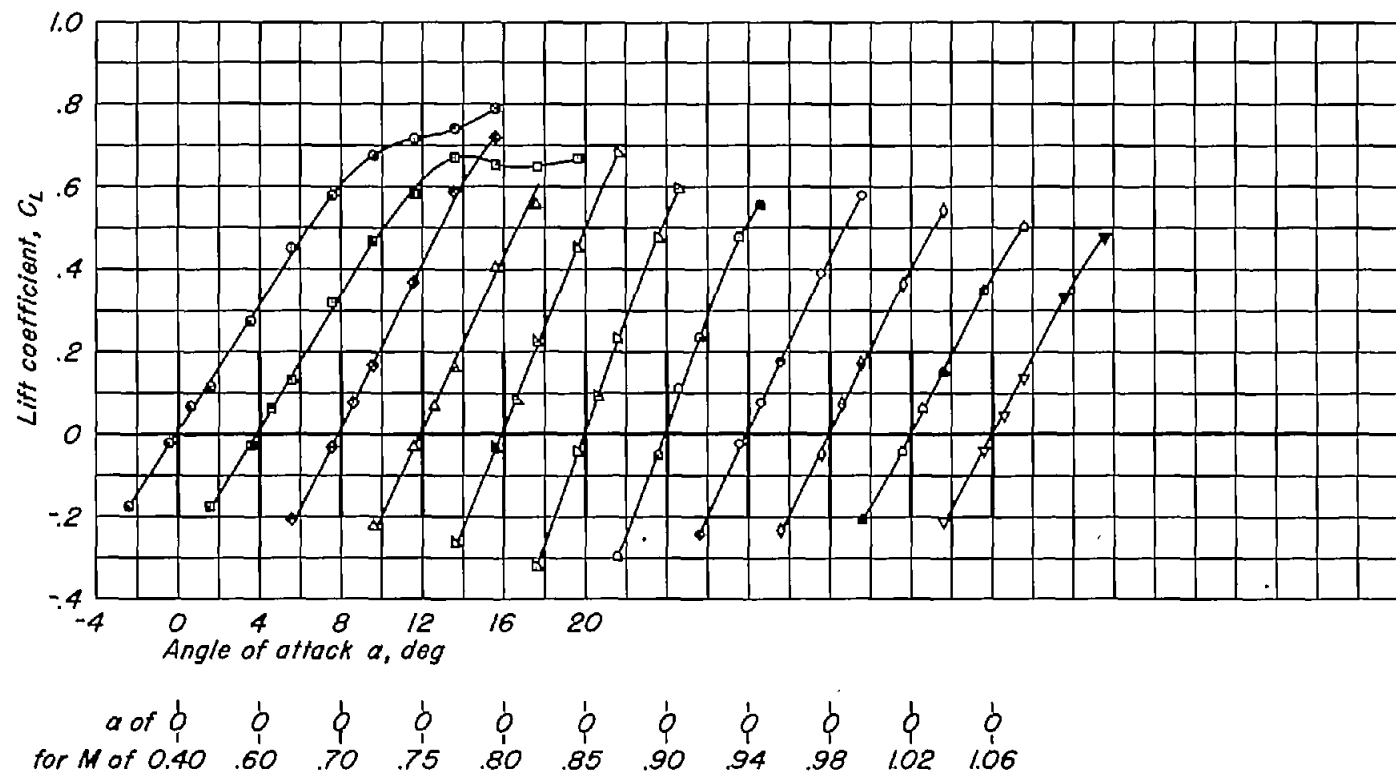
(a) $A, 6; t/c, 0.10.$

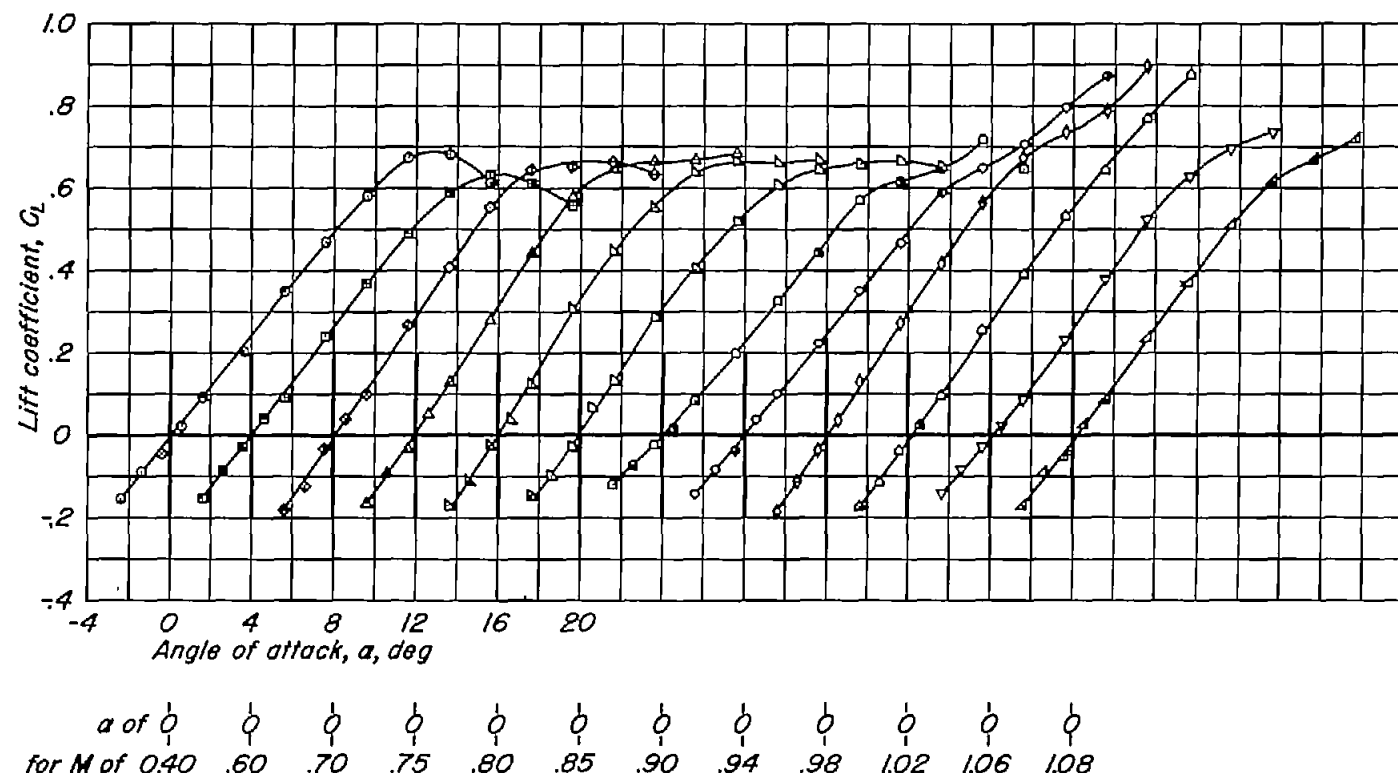
Figure 8.-The variation of lift coefficient with angle of attack for the rectangular wings with NACA 63AOXX sections.



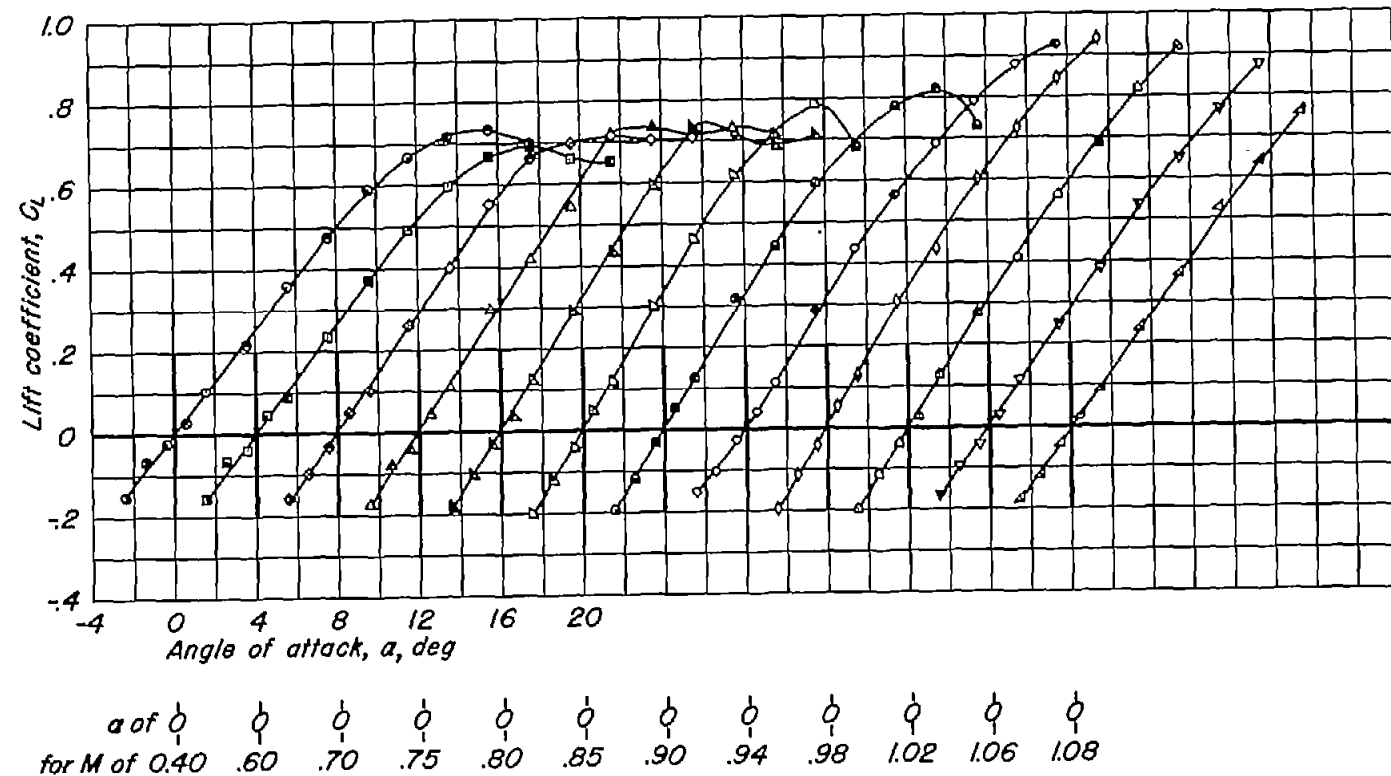
(b) A, 6; t/c , 0.08.
Figure 8.-Continued.



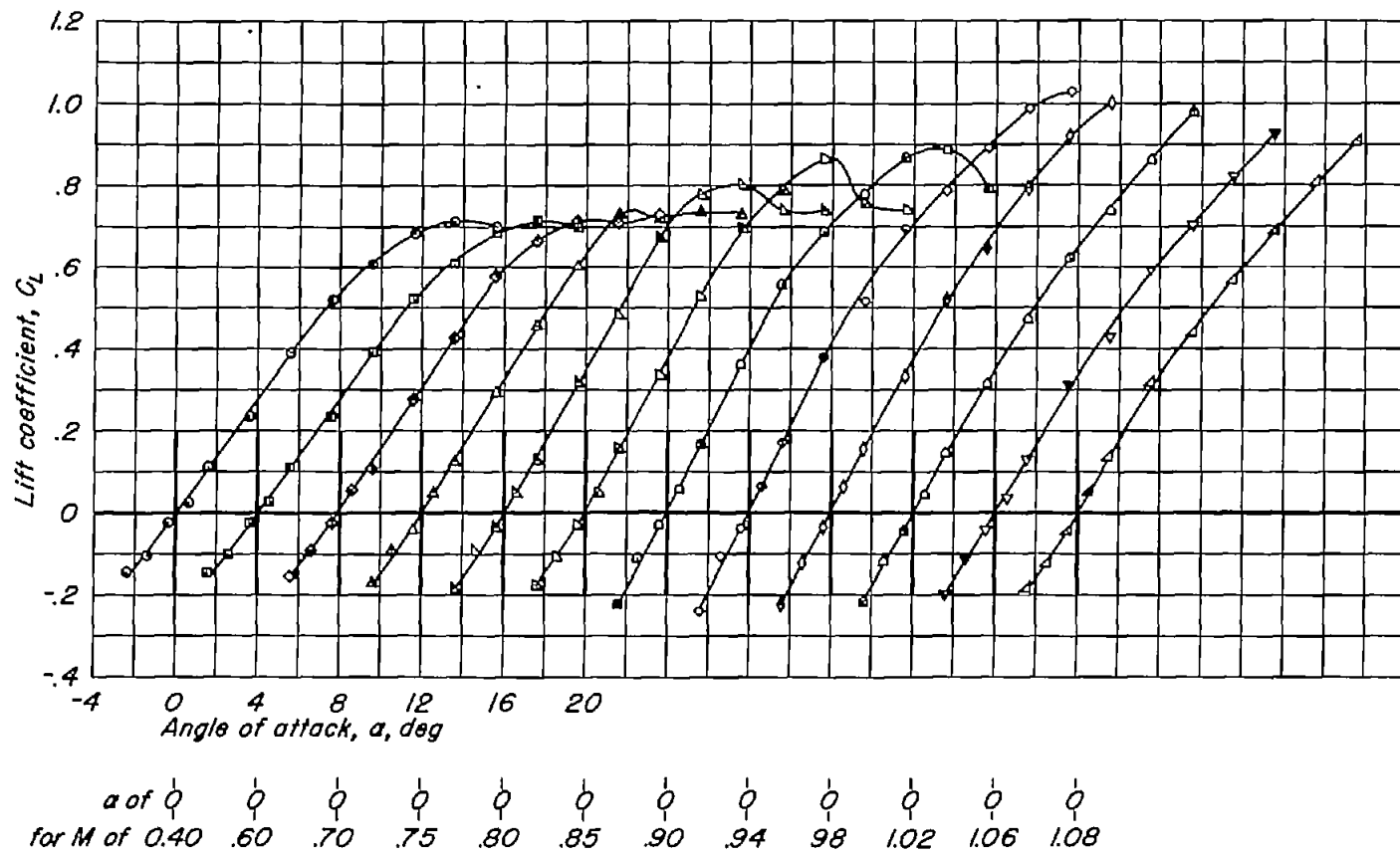
(c) $A, 6; t/c, 0.06$.
Figure 8.-Continued.



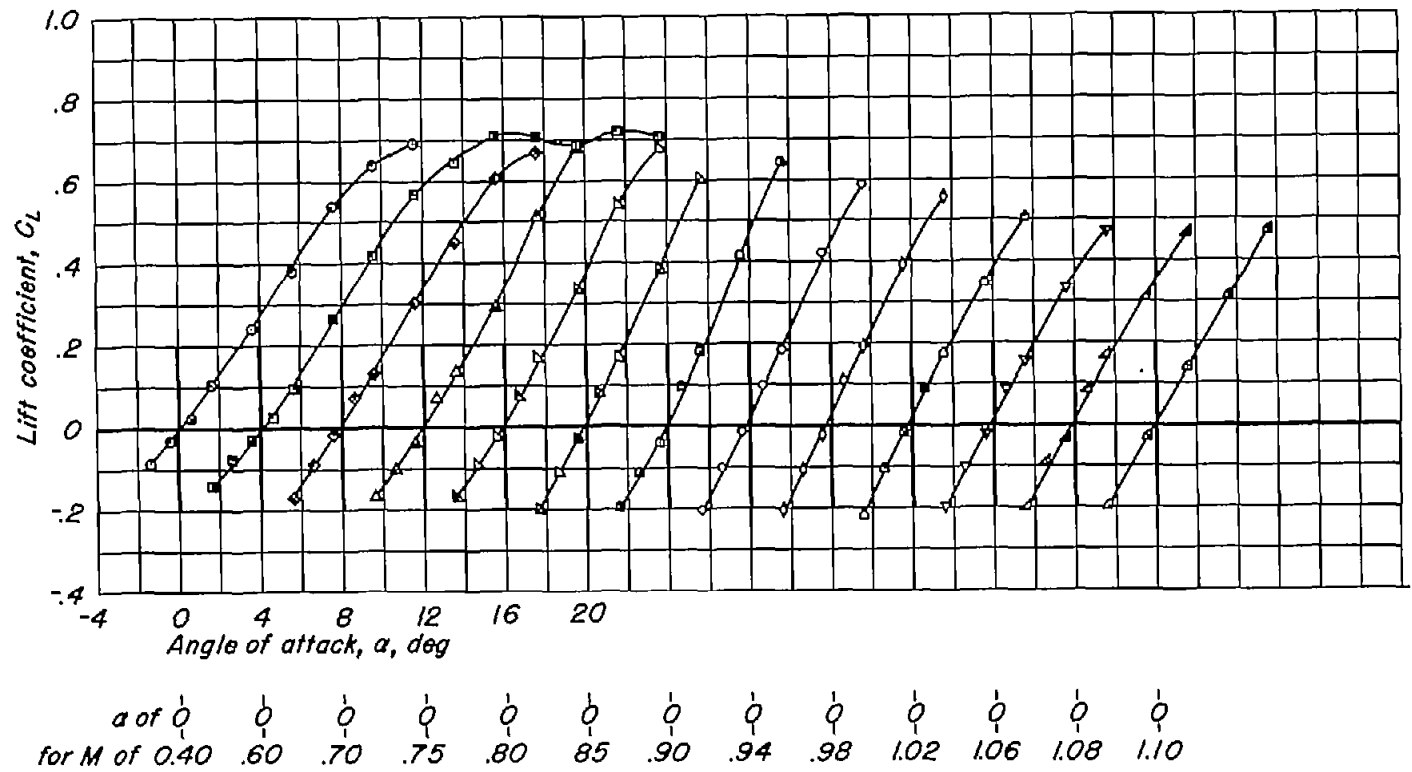
(d) $A, 4; t/c, 0.10$.
Figure 8.-Continued.



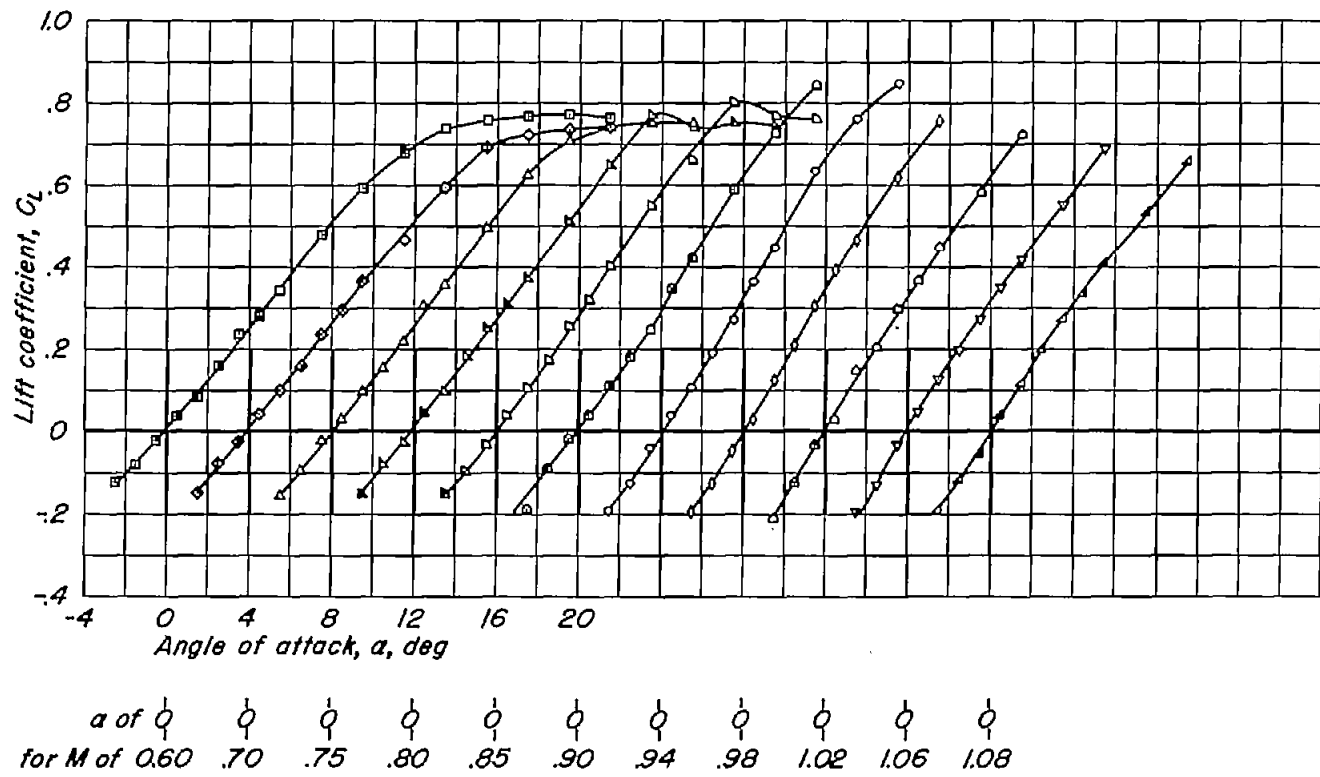
(e) $A, 4; t/c, 0.08$.
Figure 8.-Continued.



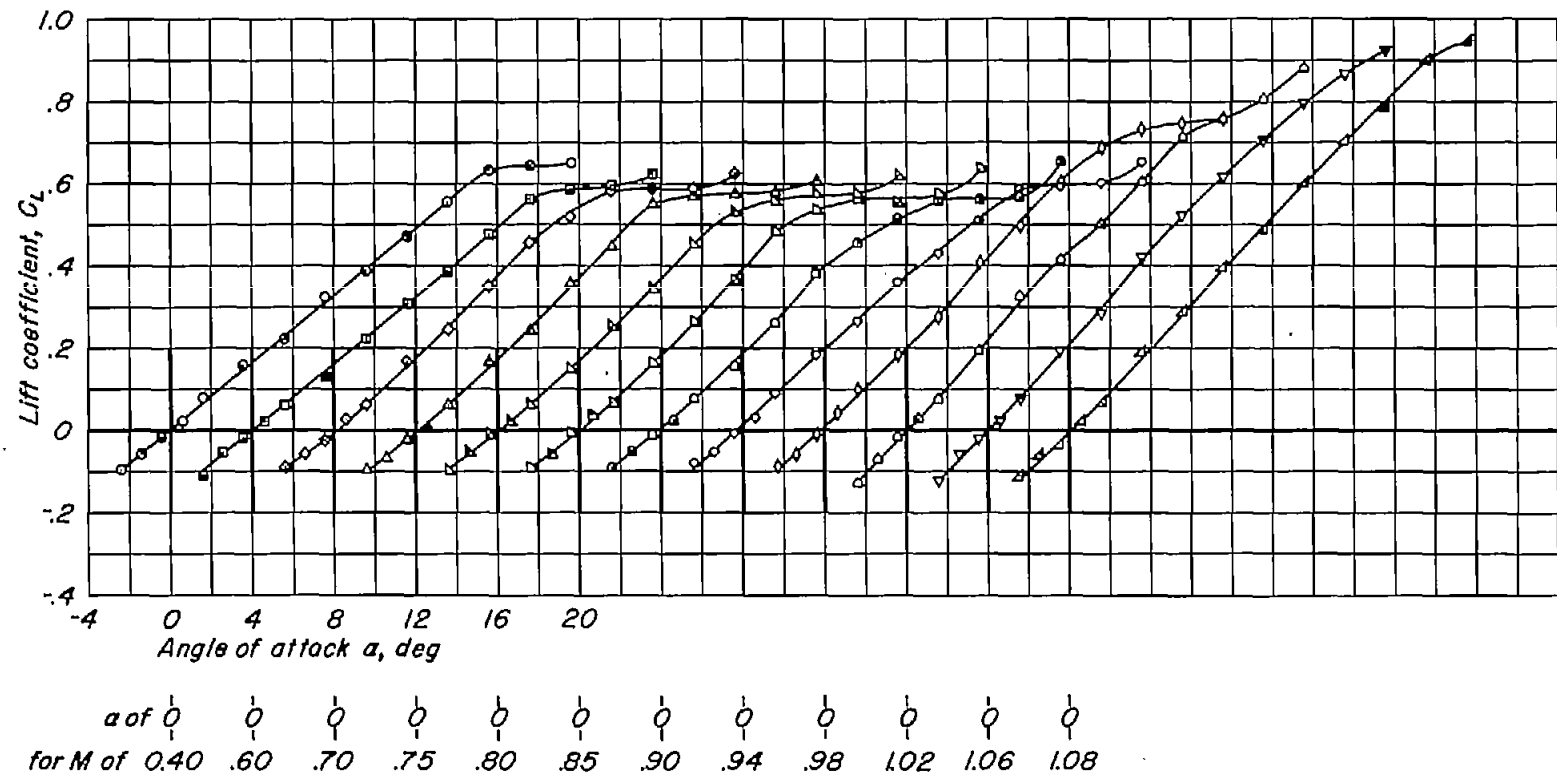
(f) $A, 4; t/c, 0.06.$
Figure 8.-Continued.



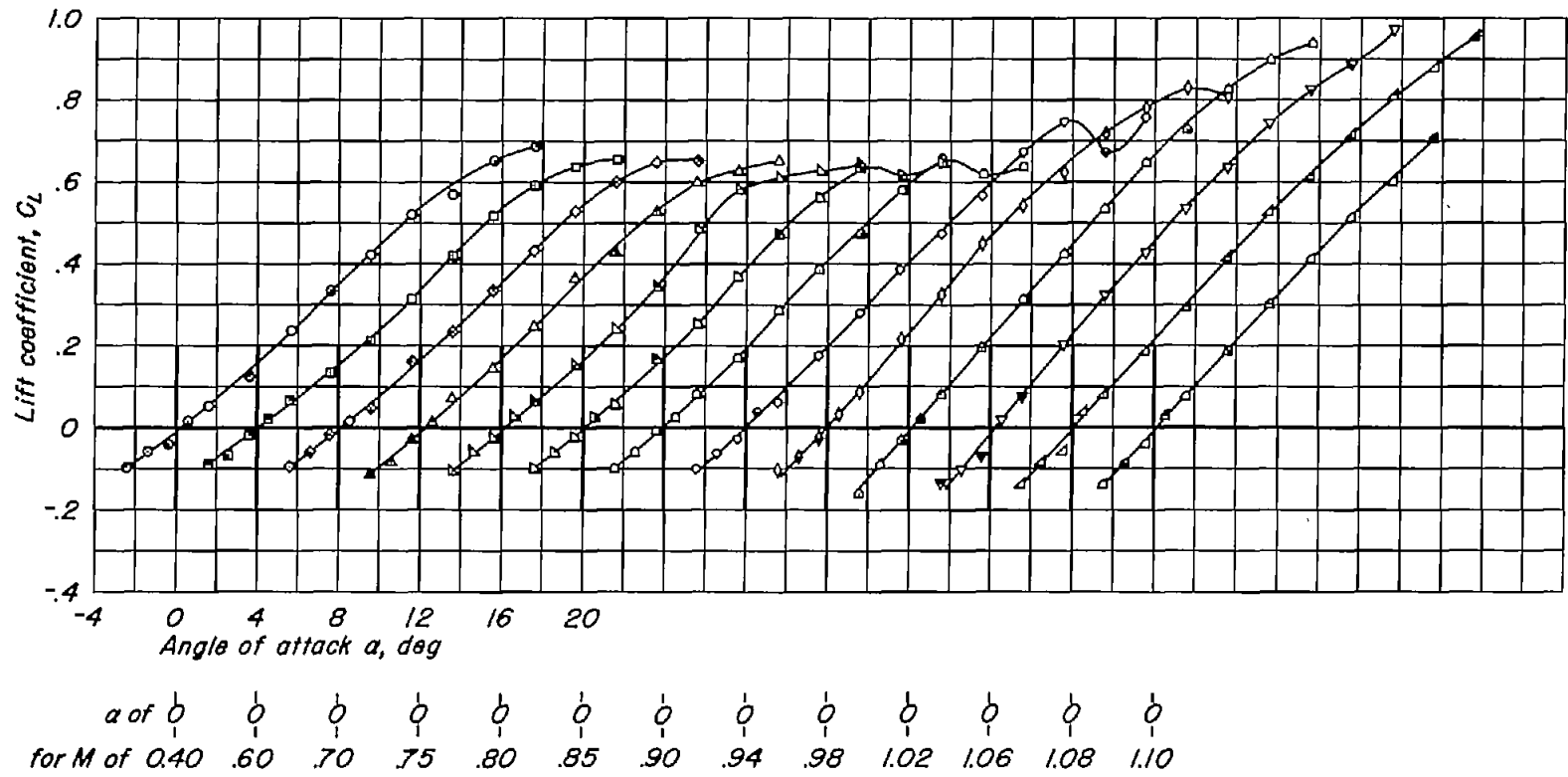
(g) $A, 4; t/c, 0.04$.
Figure 8.-Continued.



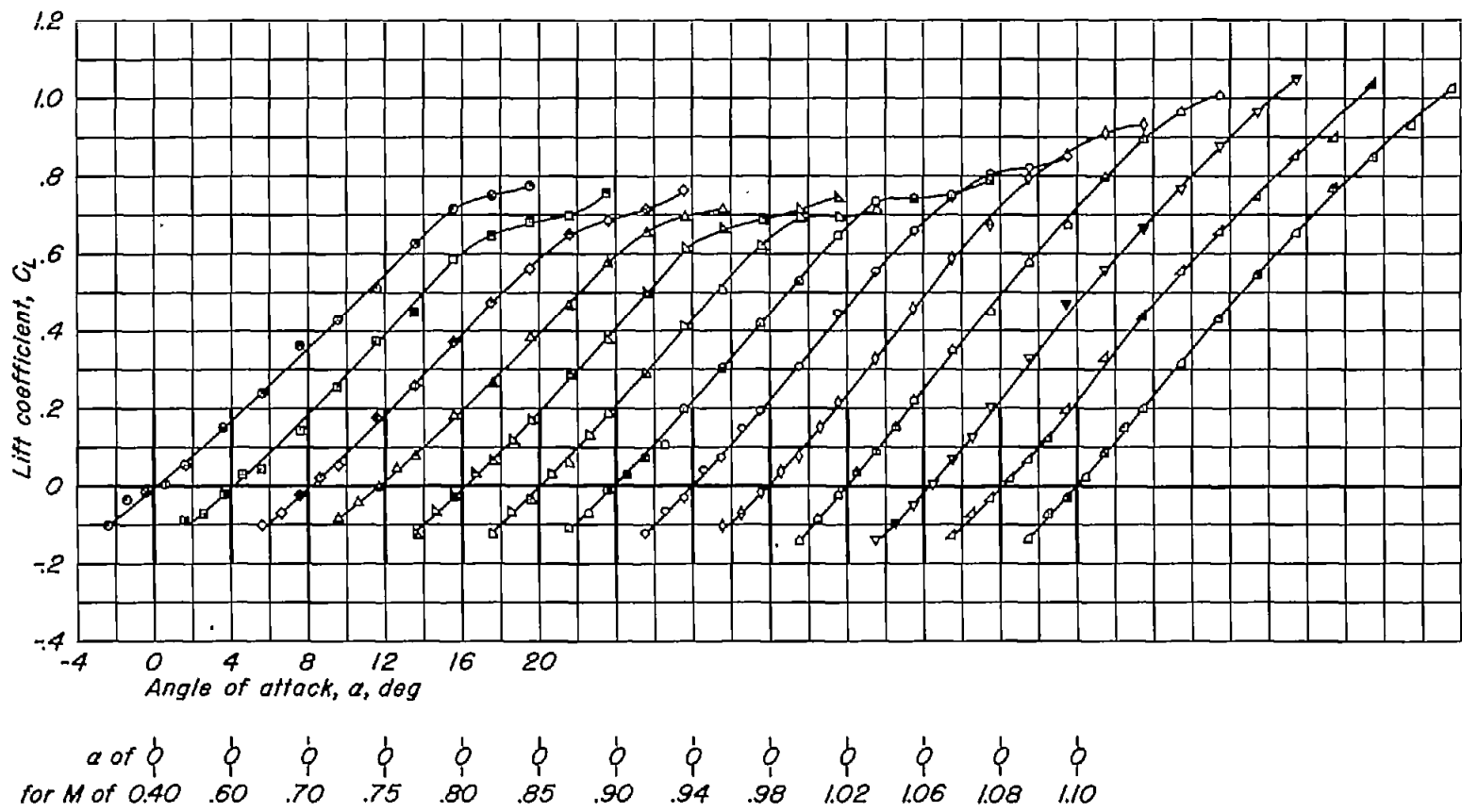
(h) $A, 3; t/c, 0.04$.
Figure 8.- Continued.



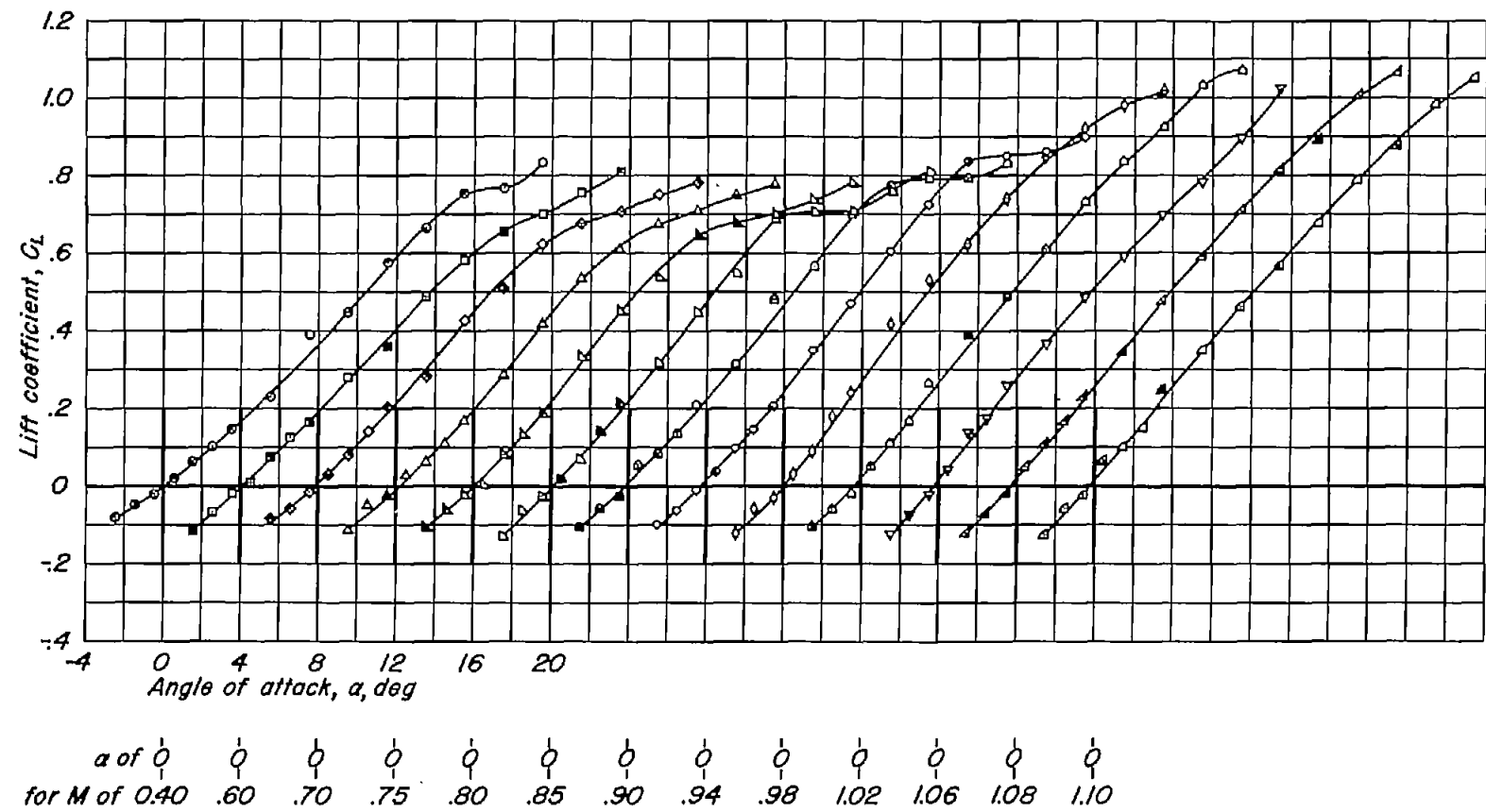
(i) A, 2; t/c , 0.10.
Figure 8.-Continued.



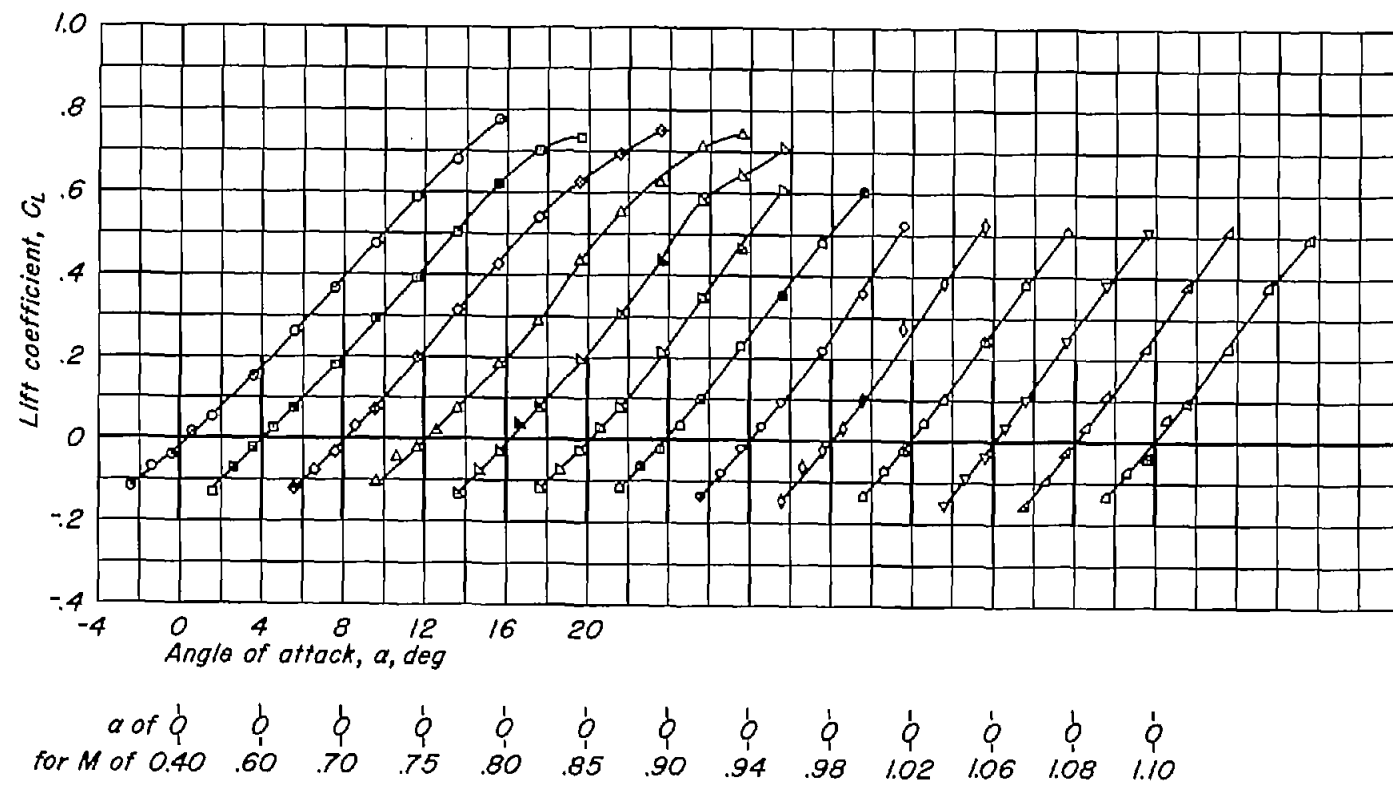
(1) A, 2; t/c , 0.08.
Figure 8.-Continued.



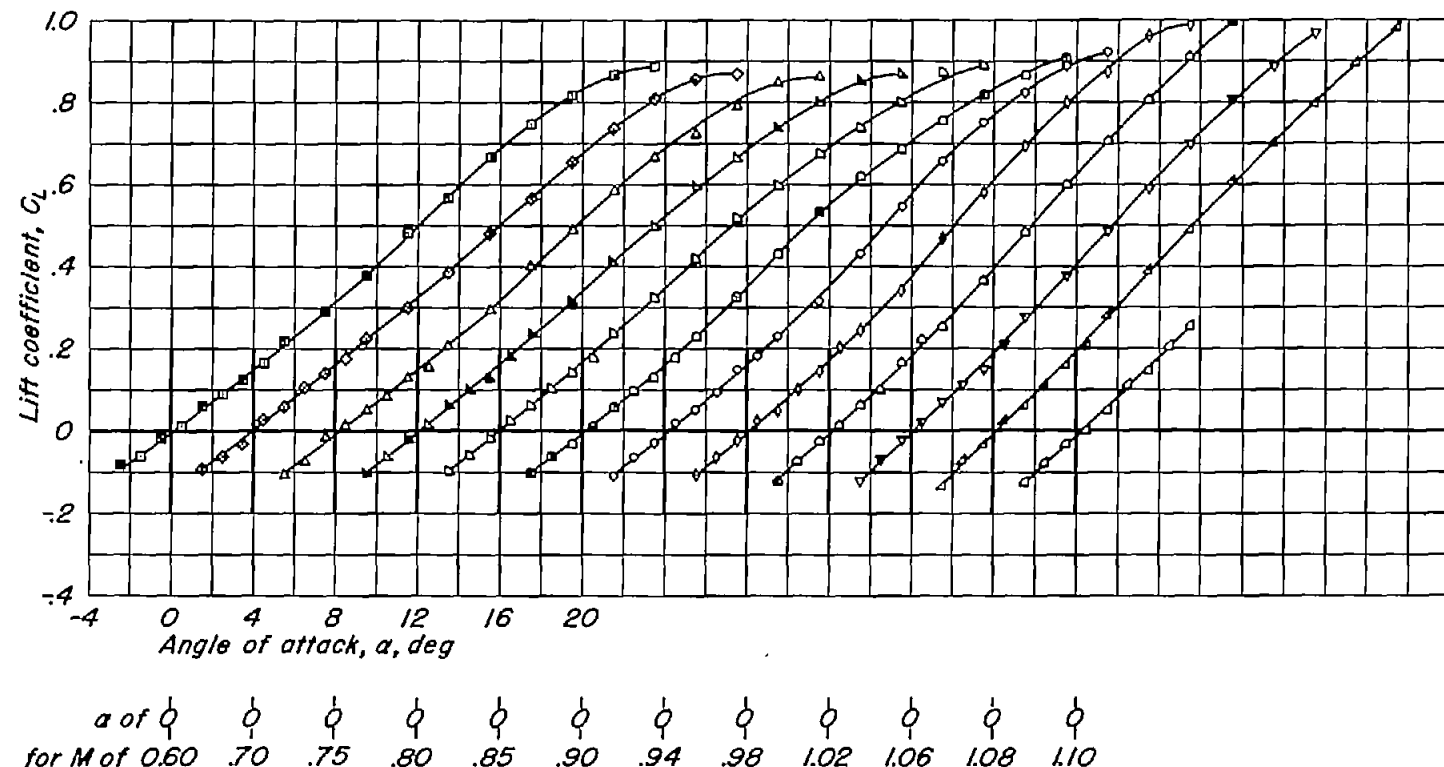
(k) $A, 2; t/c, 0.06.$
Figure 8.-Continued.



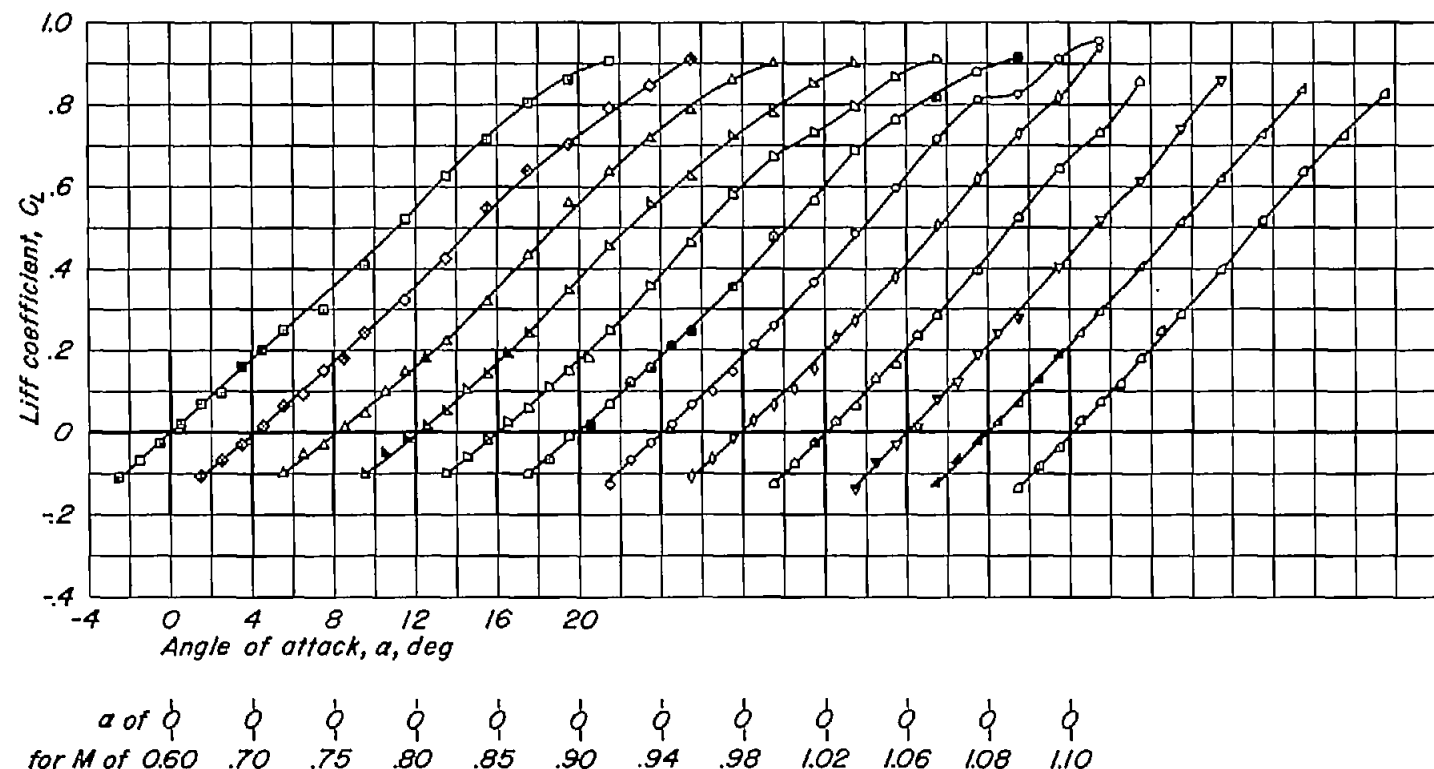
(1) A, 2; t/c, 0.04.
Figure 8.-Continued.



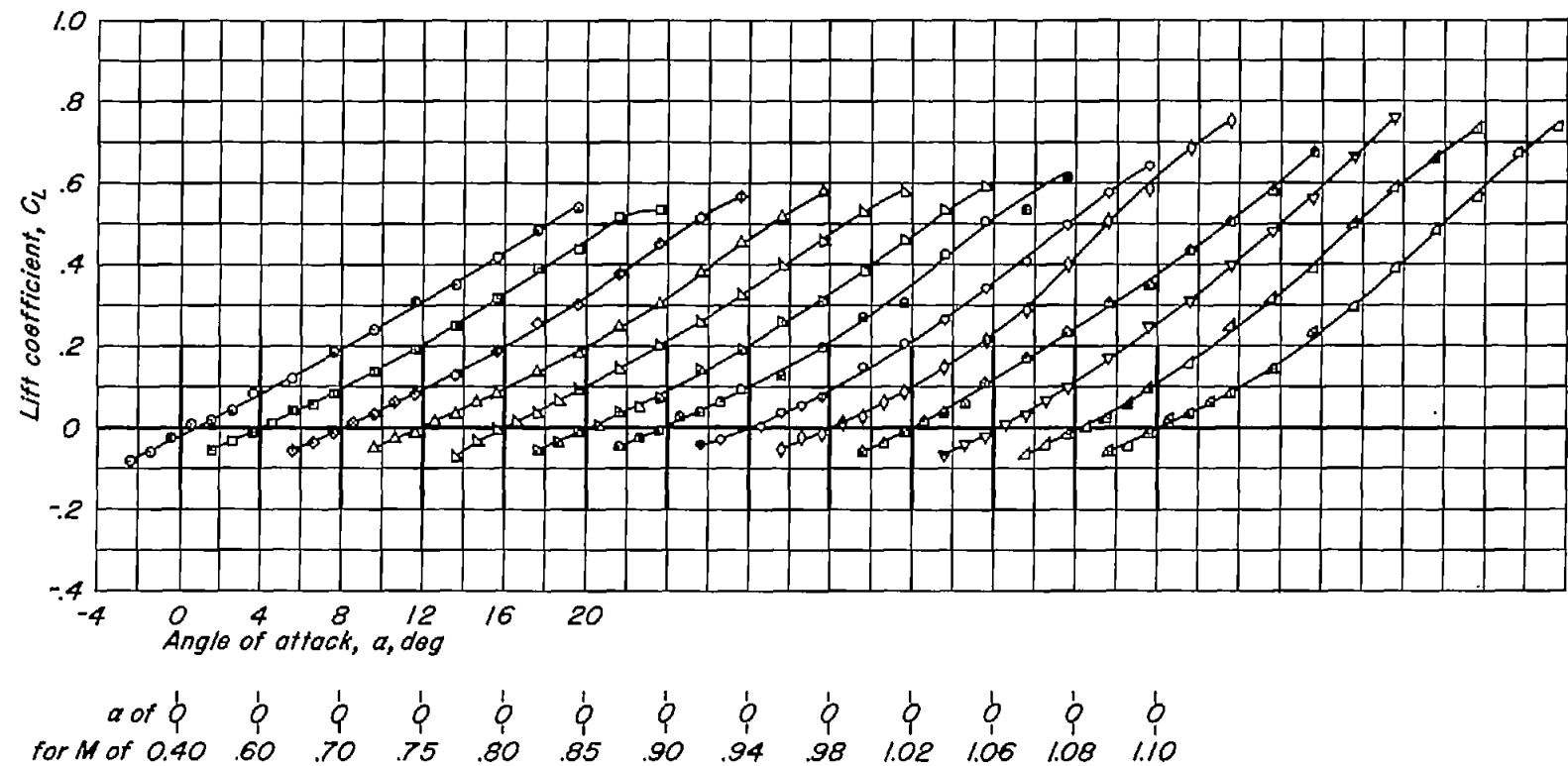
(m) A, 2; t/c , 0.02.
Figure 8.-Continued.



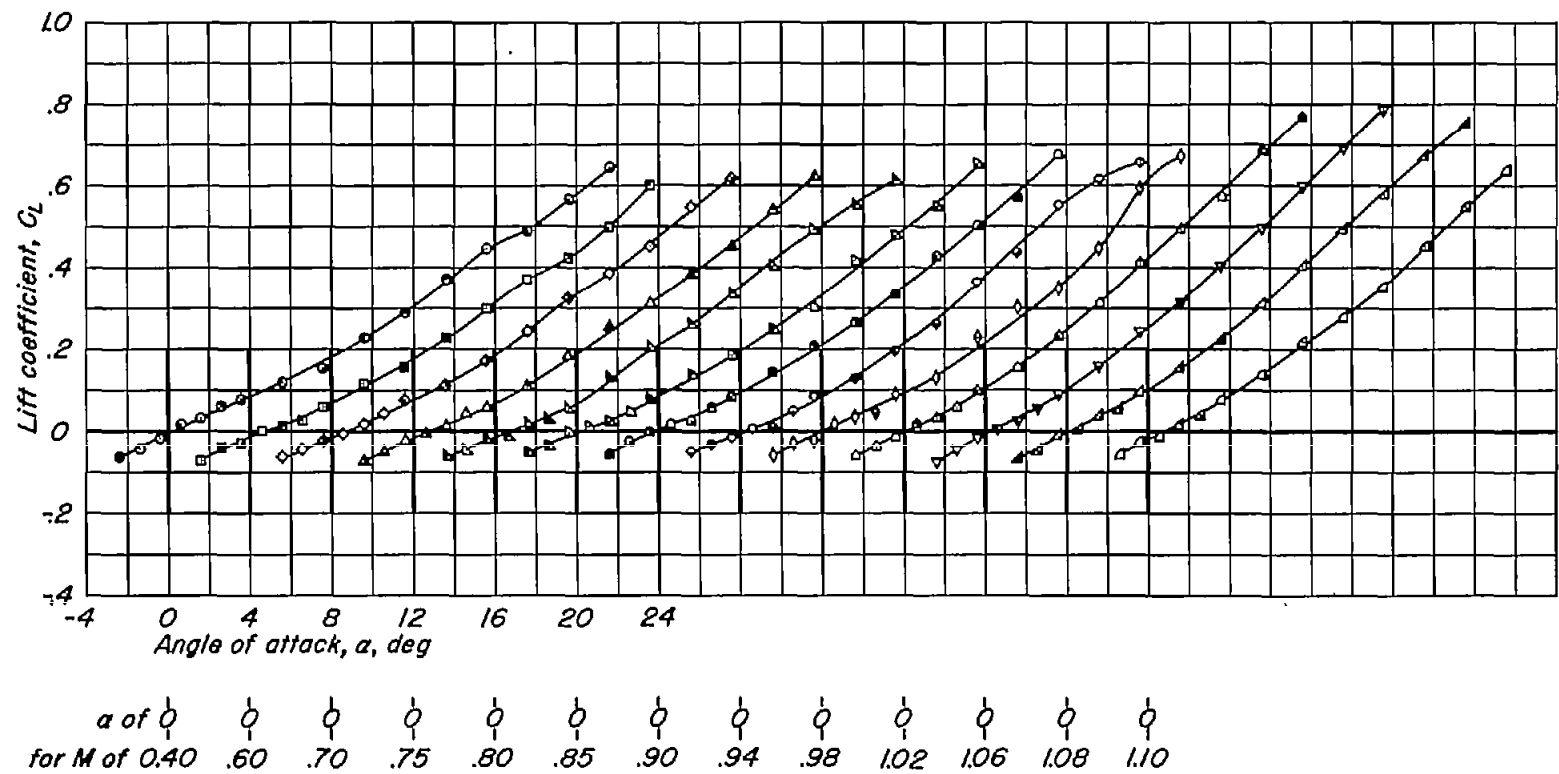
(n) $A, 1.5; t/c, 0.04$.
Figure 8.- Continued.



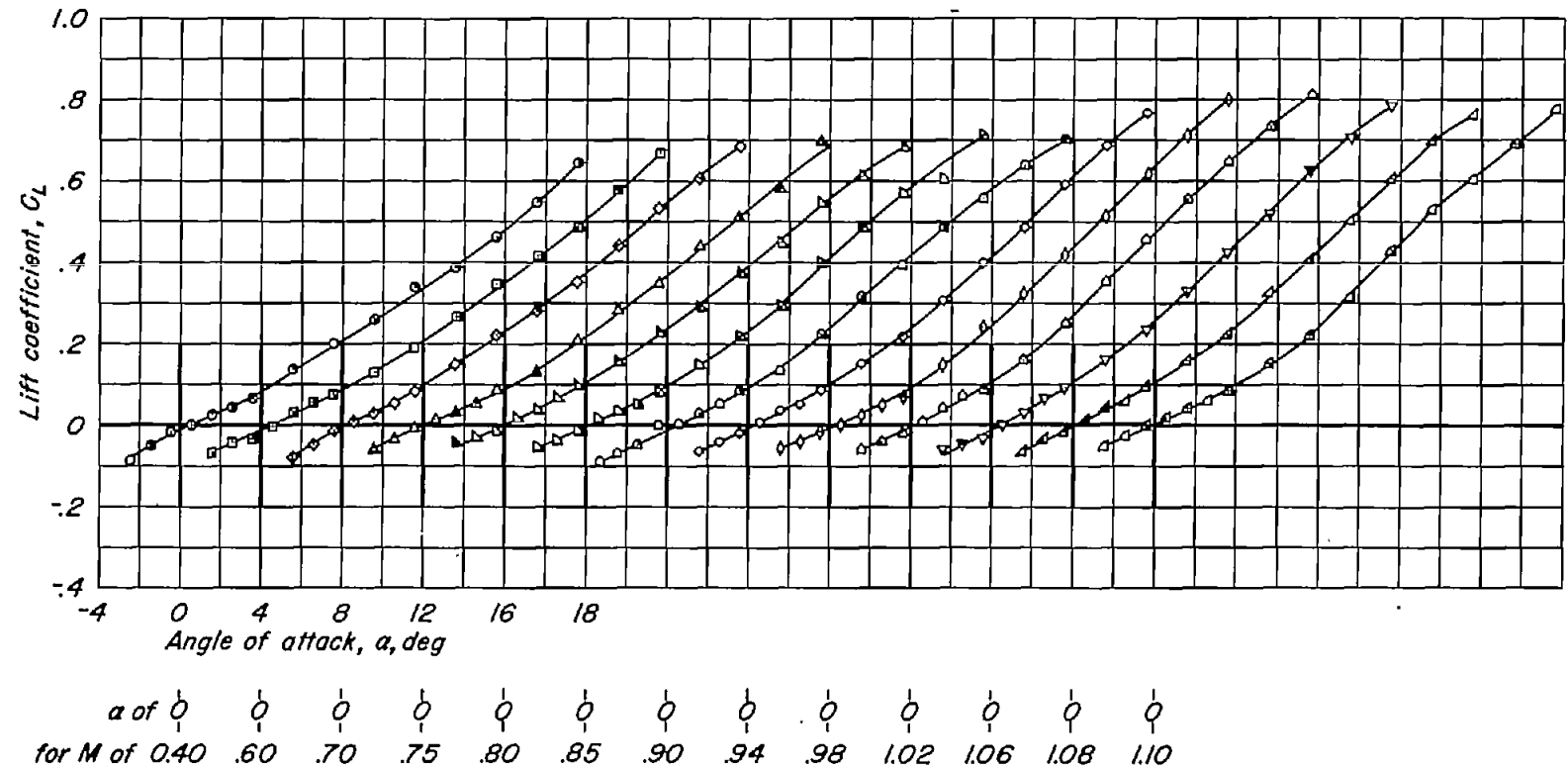
(a) $A, 1.5; t/c, 0.02.$
Figure 8- Continued.



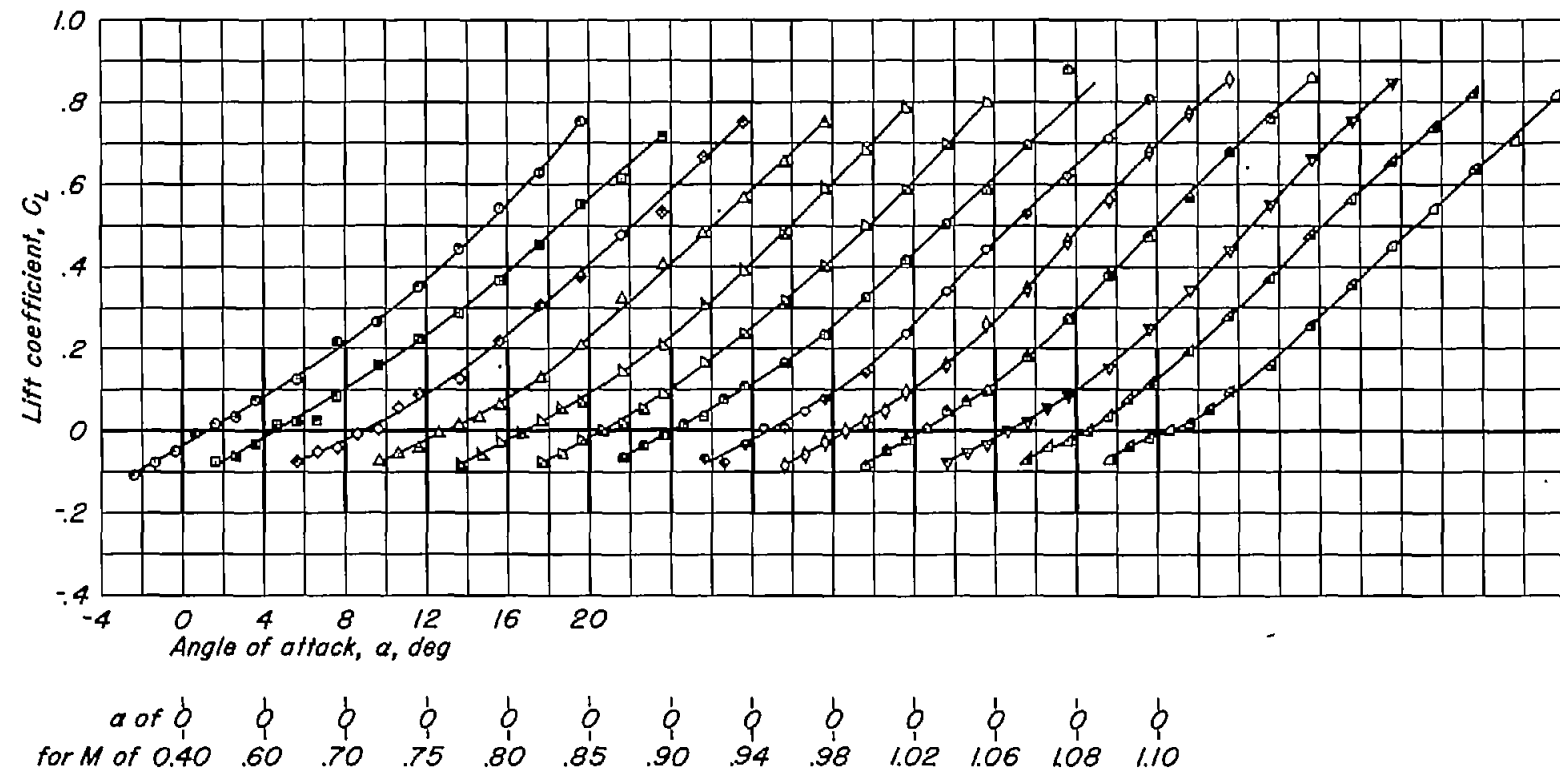
(p) $A, 1; t/c, 0.10$.
Figure 8.-Continued.



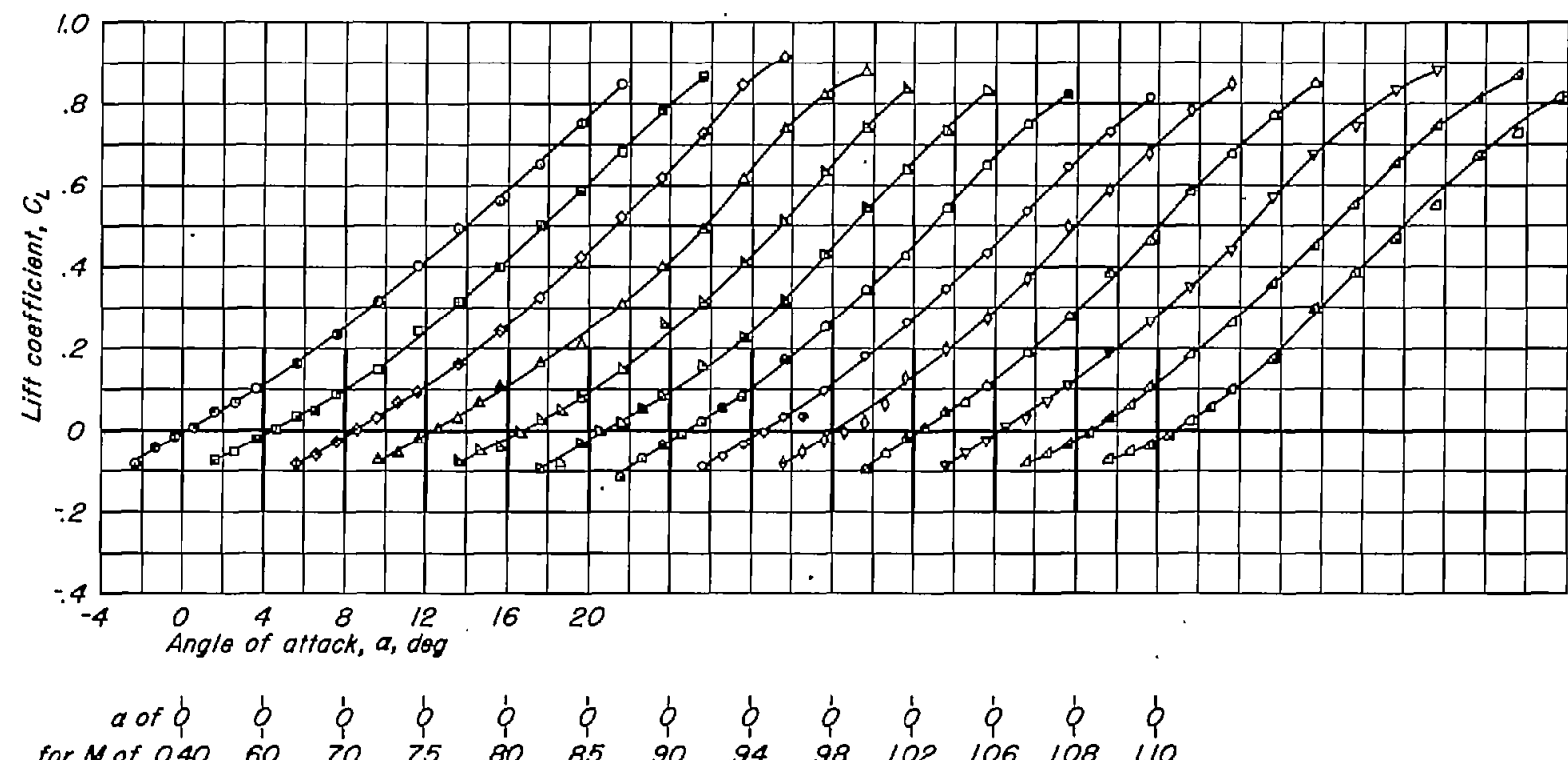
(q) $A_1; t/c, 0.08.$
Figure 8-Continued.



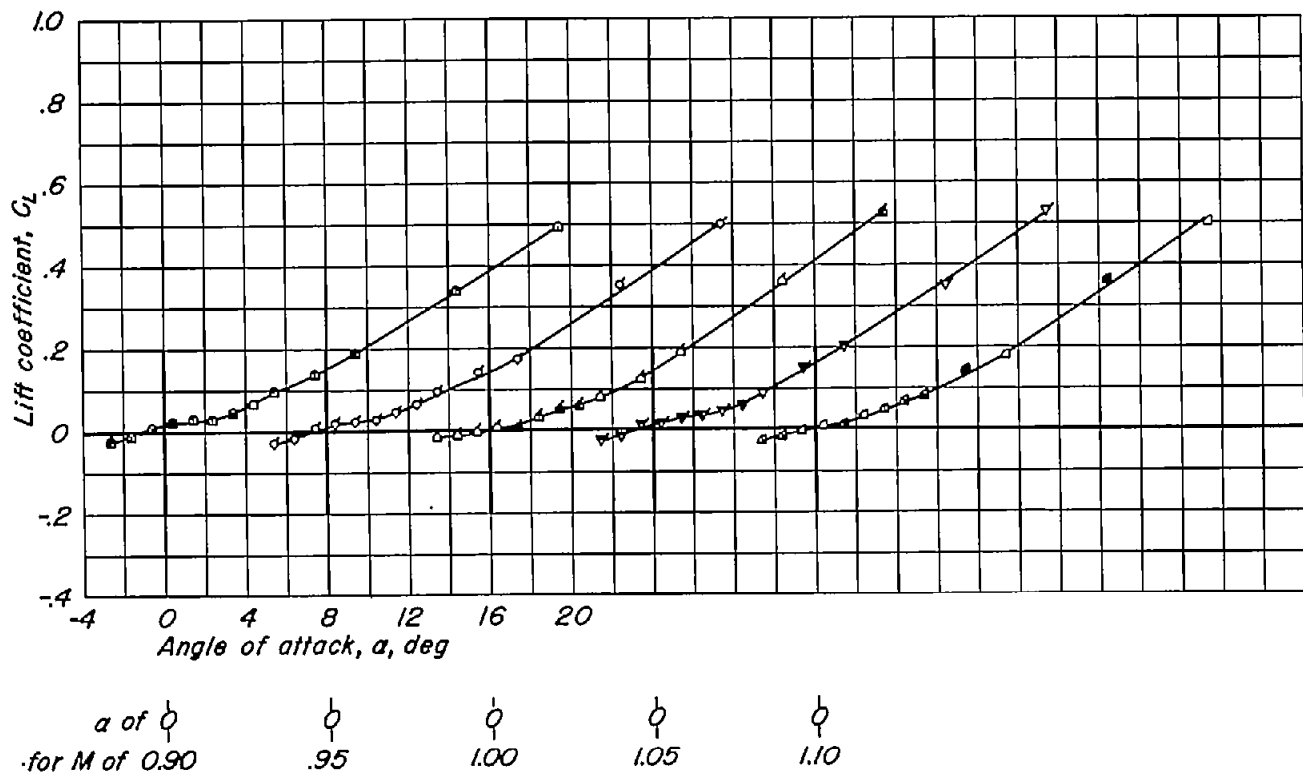
(r) $A, 1; t/c, 0.06$.
Figure 8.-Continued.



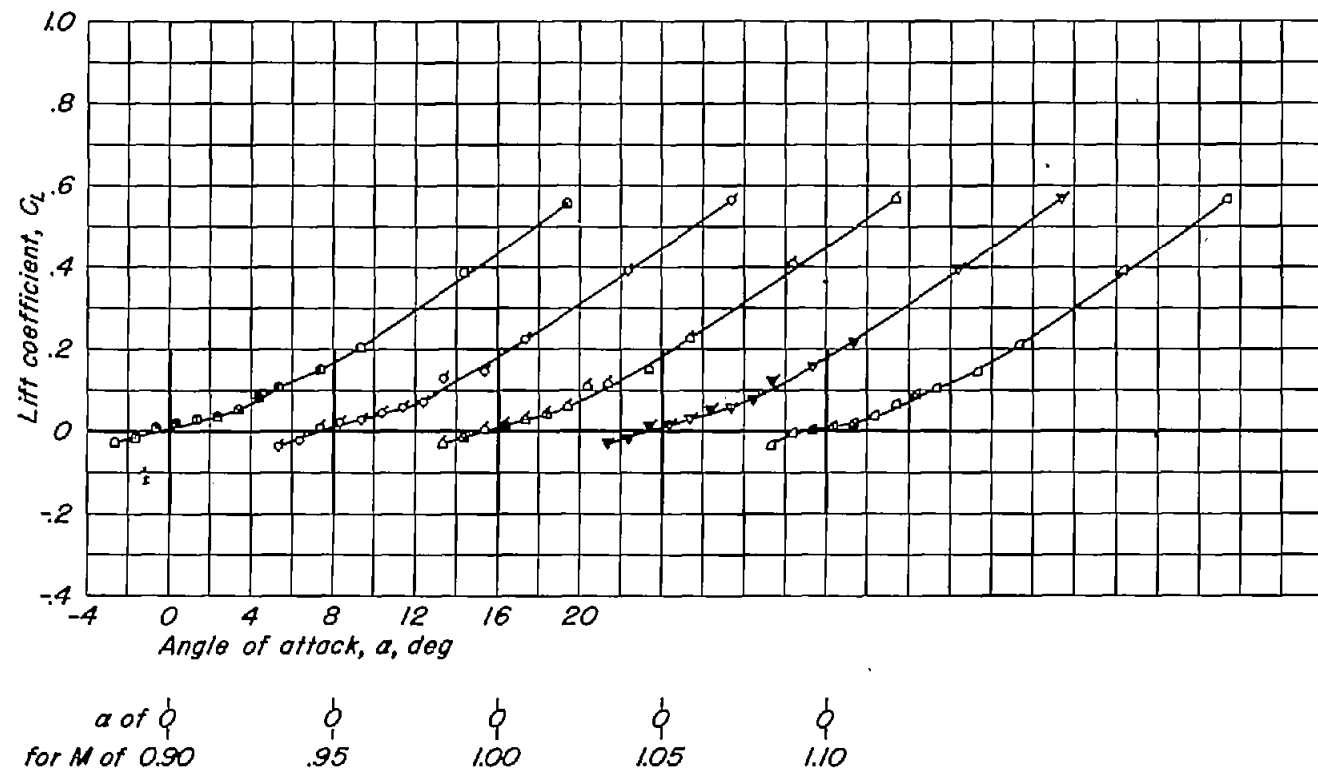
(s) A, 1; t/c , 0.04.
Figure 8.-Continued.



(t) $A, 1; t/c, 0.02$.
Figure 8.-Continued.



(u) $A, 0.5, t/c, 0.04$.
Figure 8- Continued.



(v) $A, 0.5; t/c, 0.02$.
Figure 8.- Concluded.

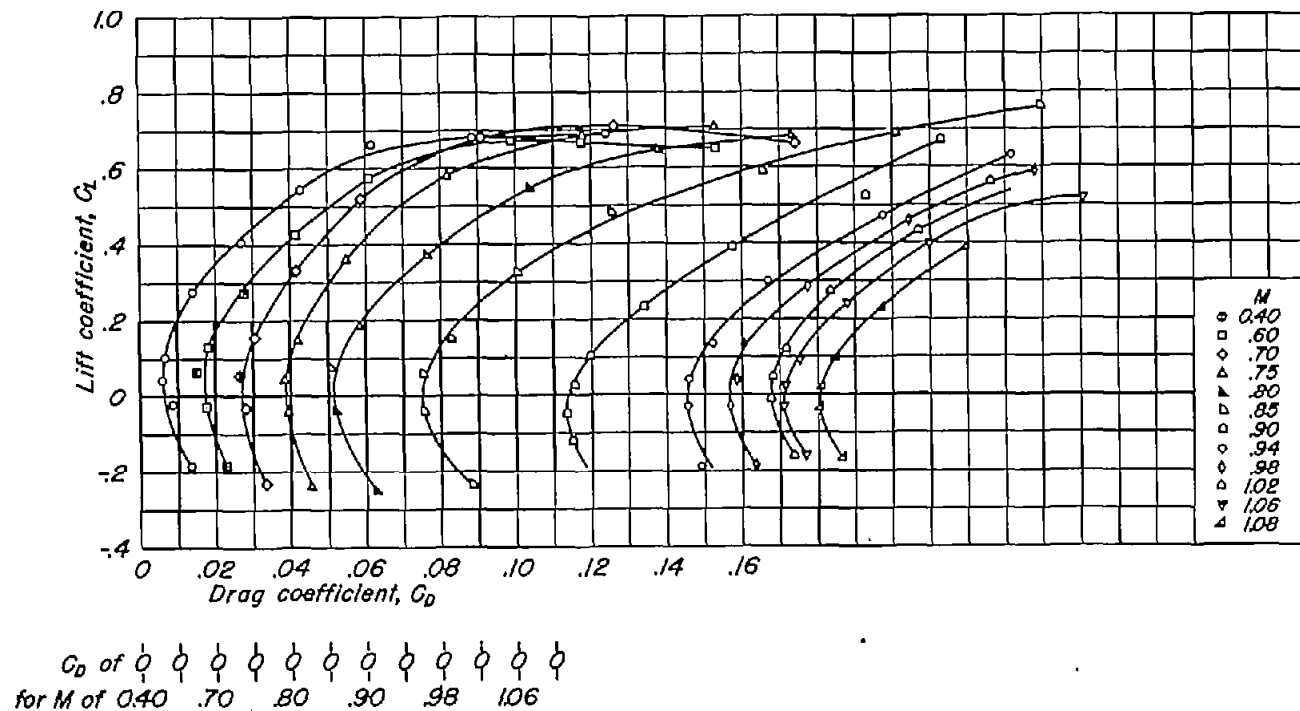
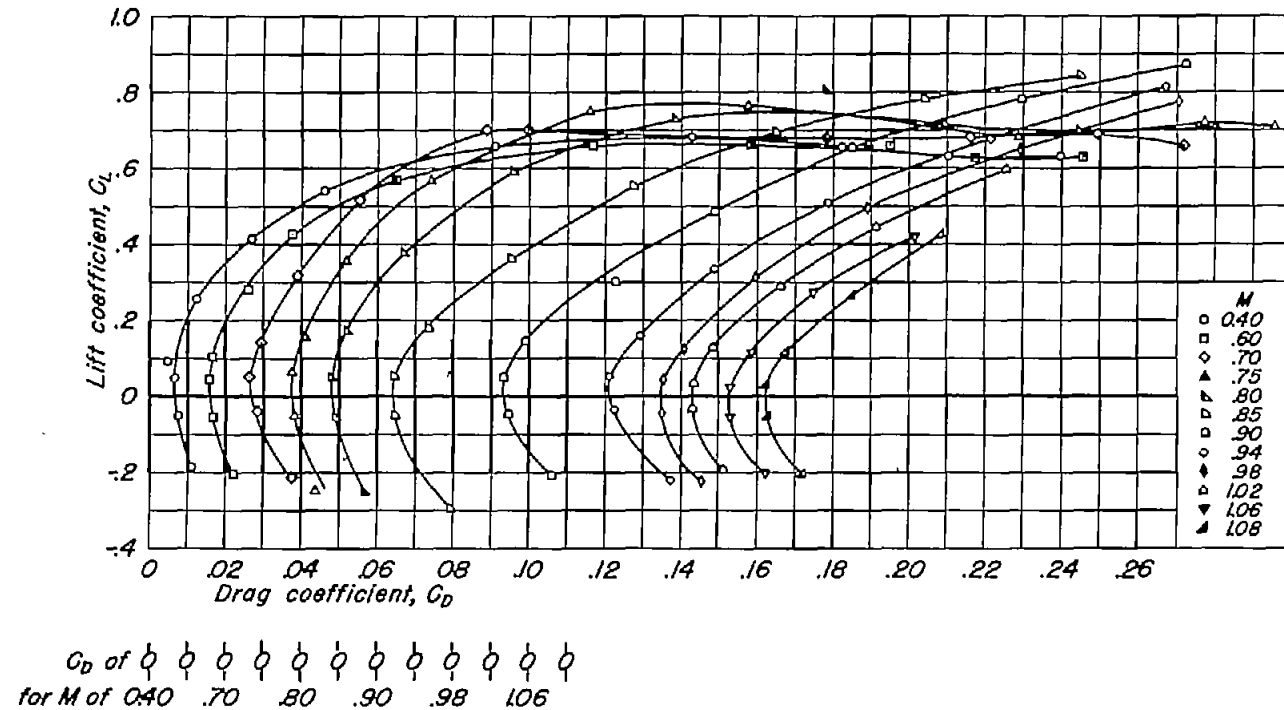
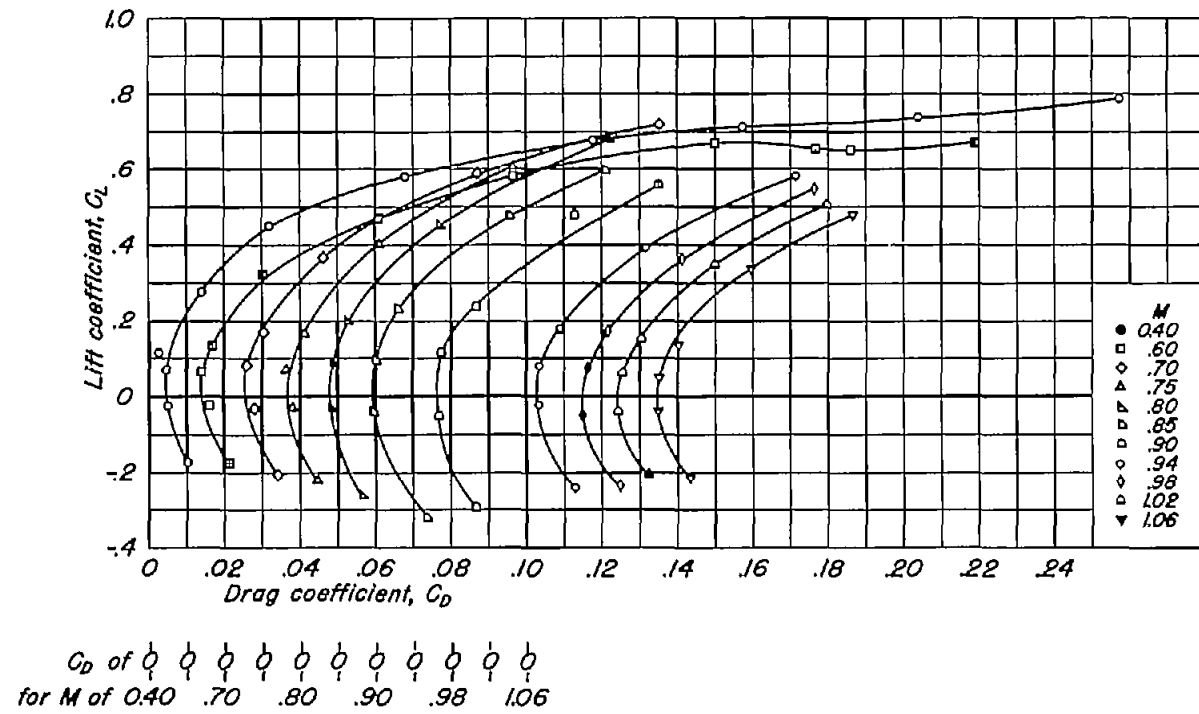
(a) $A, 6; t/c, 0.10.$

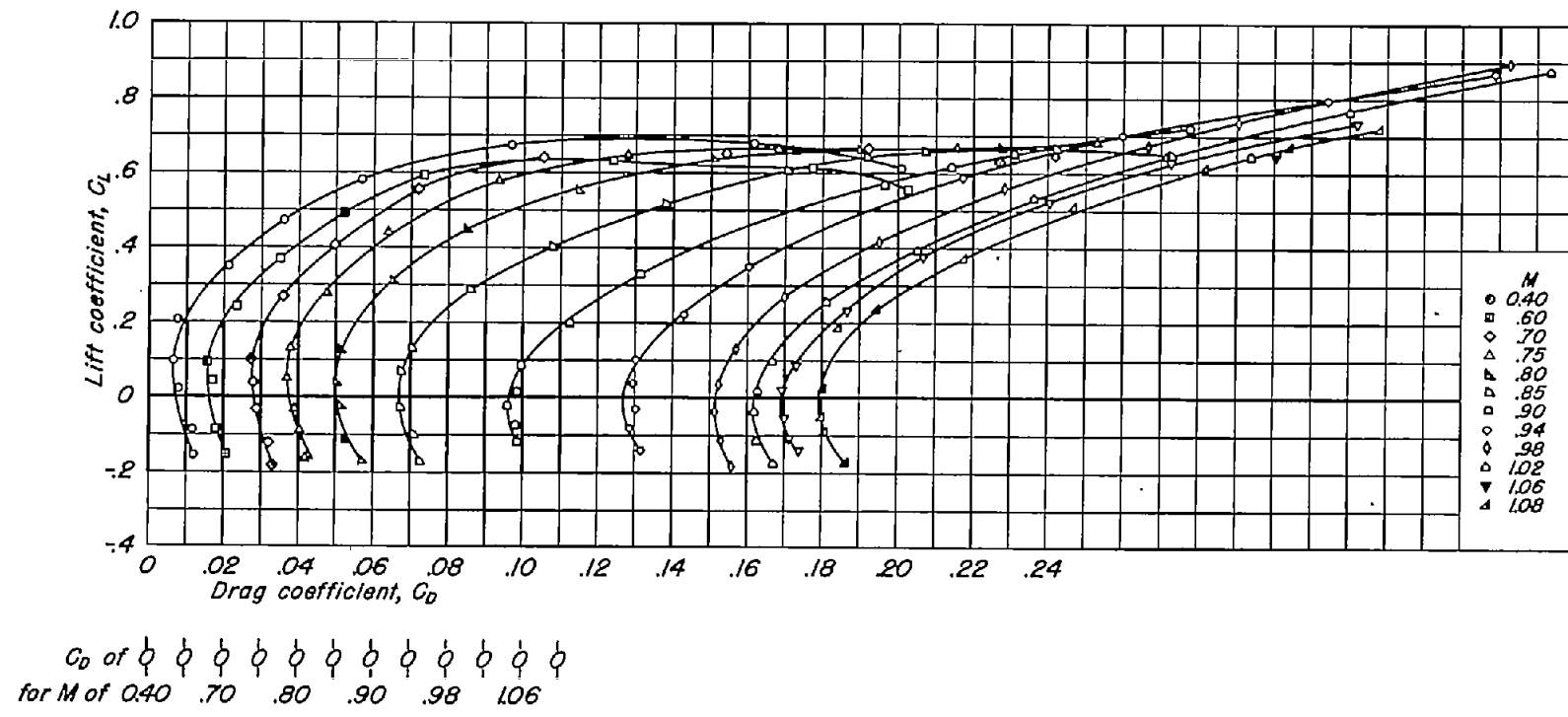
Figure 9.-The variation of drag coefficient with lift coefficient for the rectangular wings with NACA 63AOXX sections.



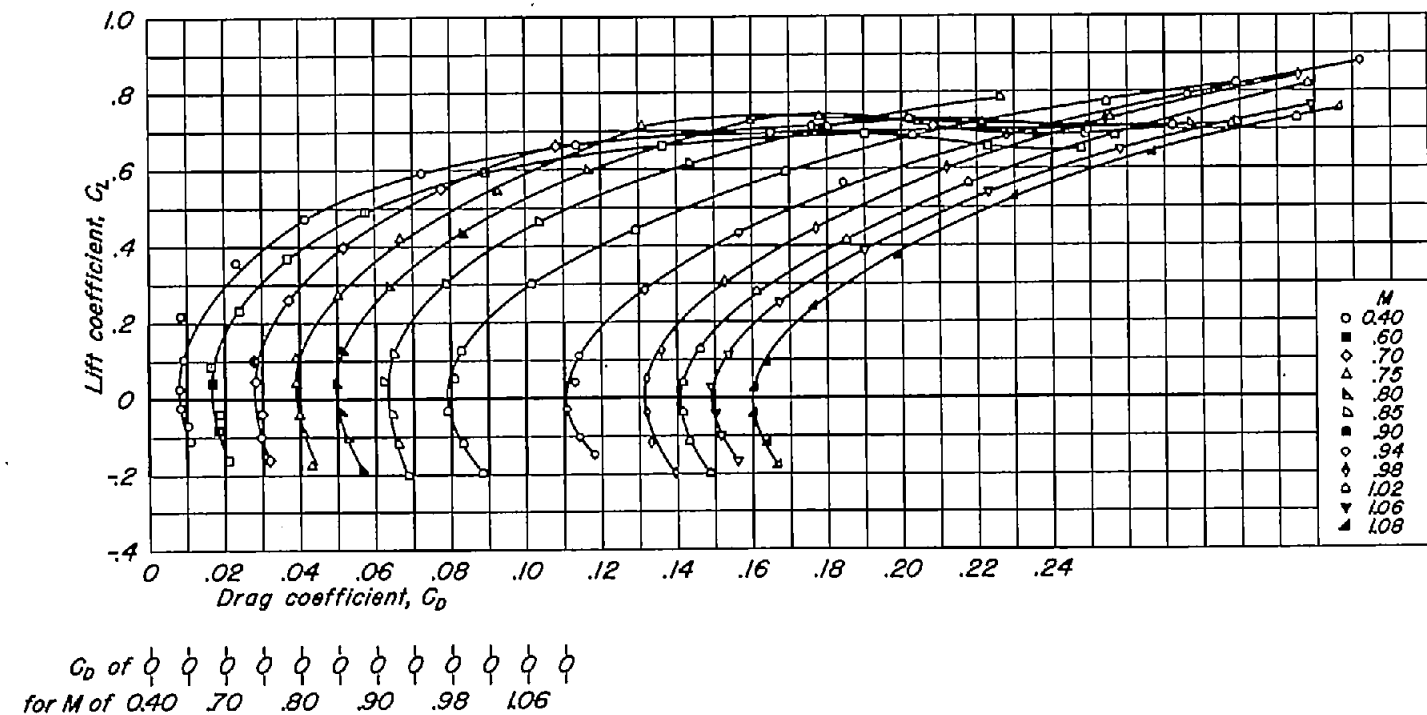
(b) A, 6; t/c, 0.08.
Figure 9.- Continued.



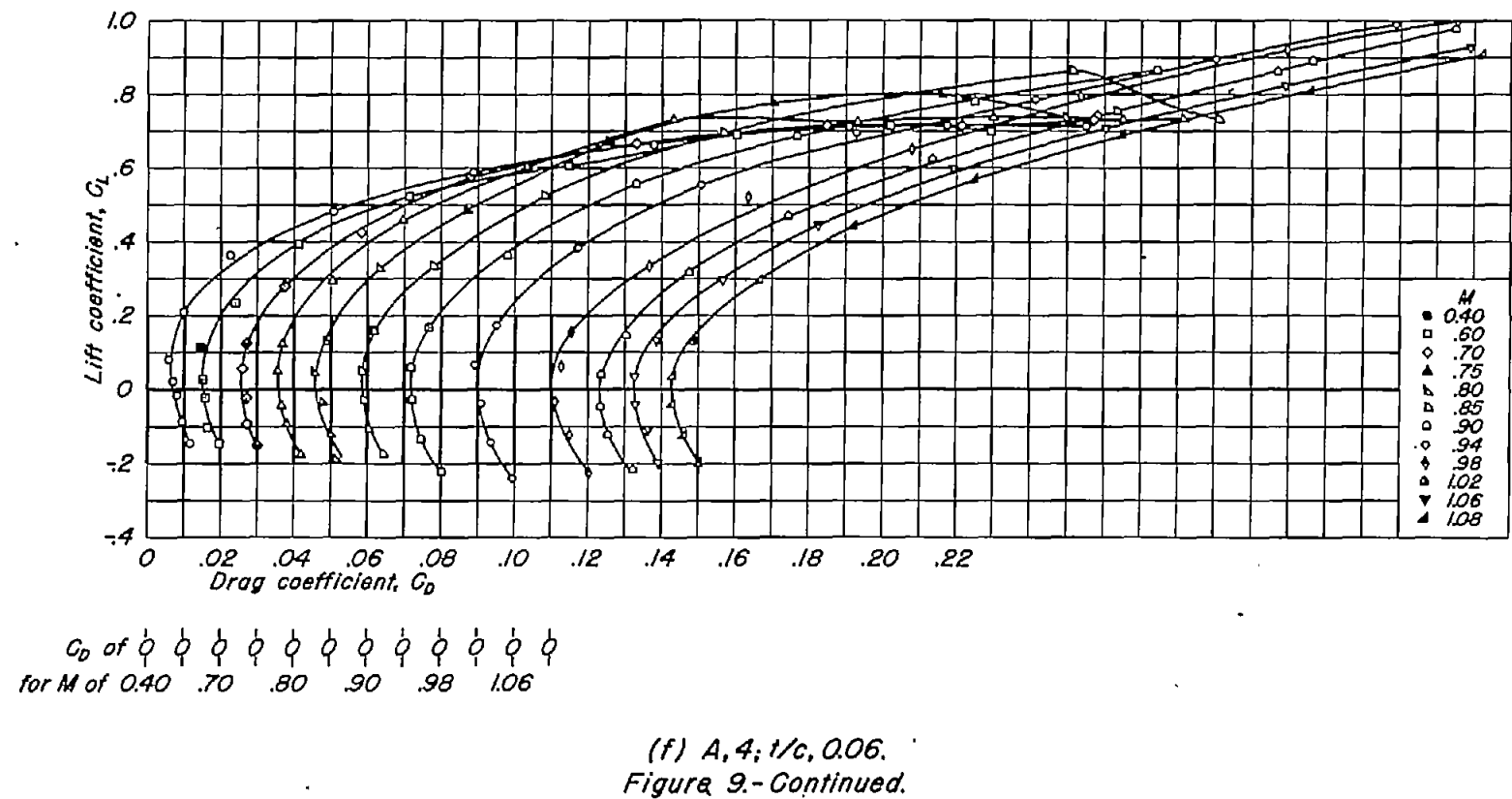
(c) A, 6; 1/c, 0.06.
Figure 9-Continued.

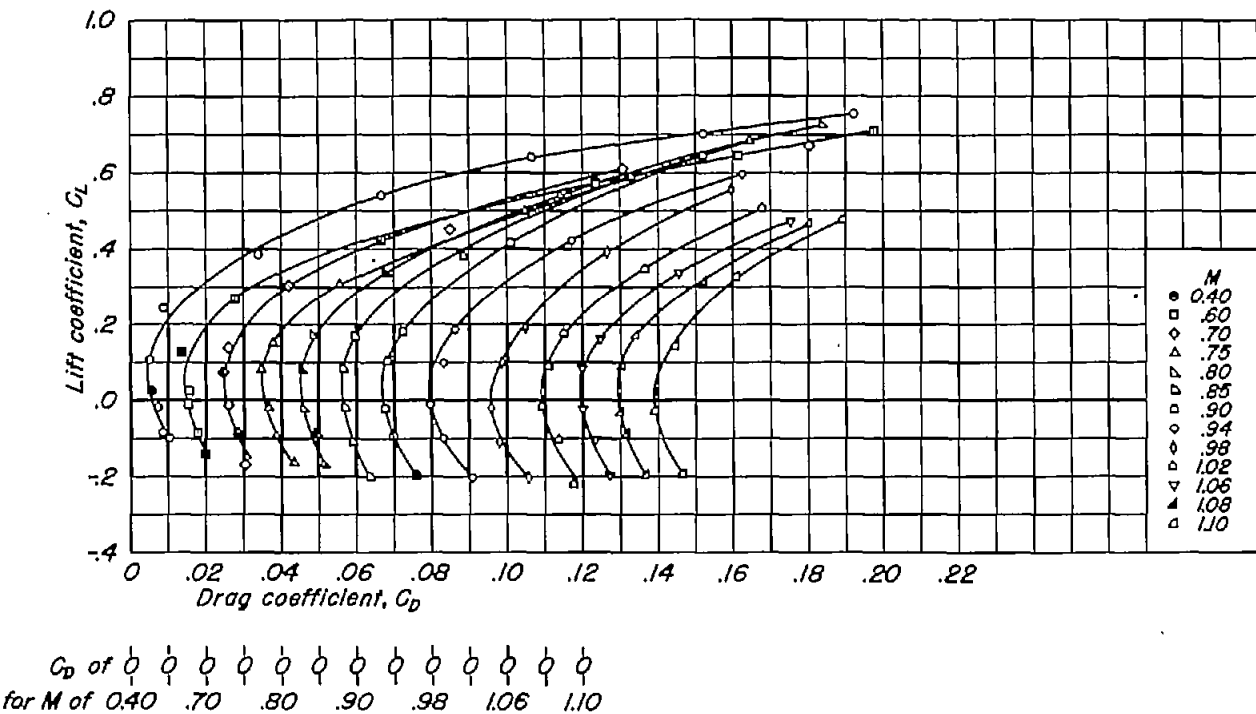


(d) A, 4; t/c, 0.10.
Figure 9.-Continued.

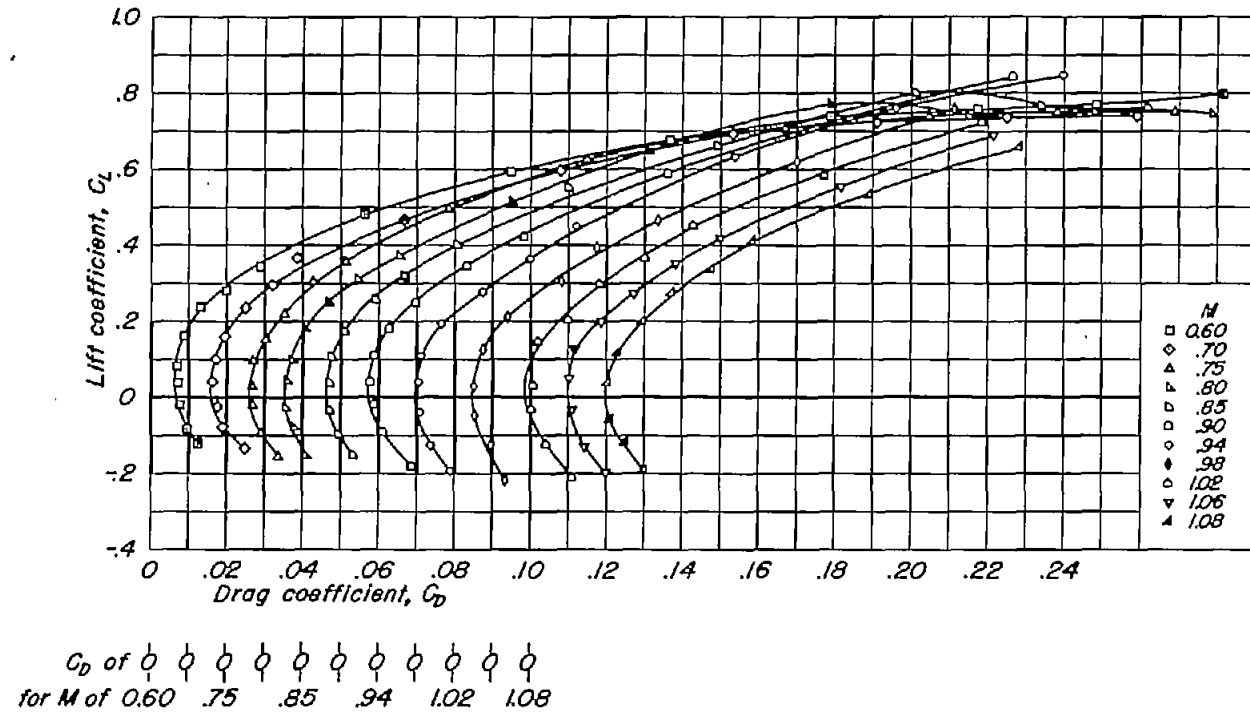


(e) A, 4; t/c, 0.08.
Figure 9.-Continued.

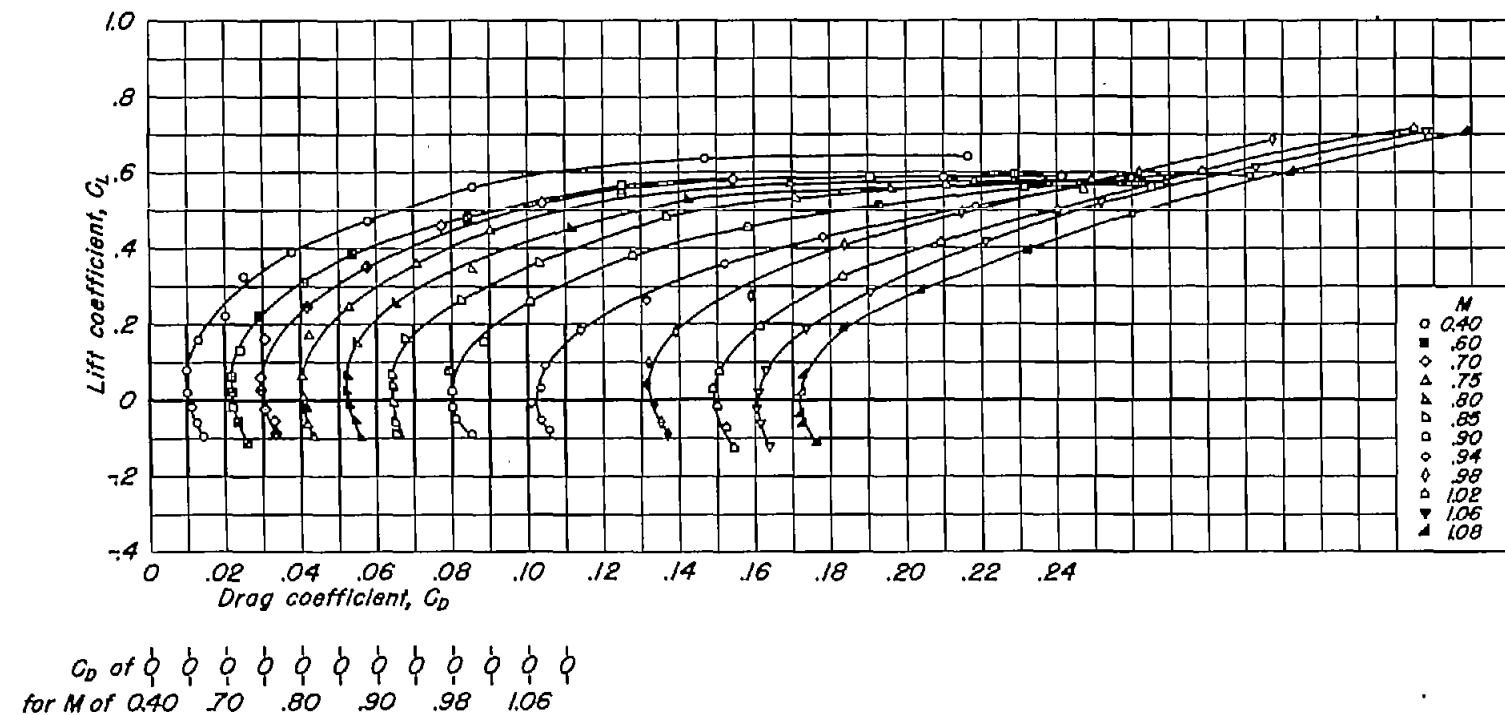




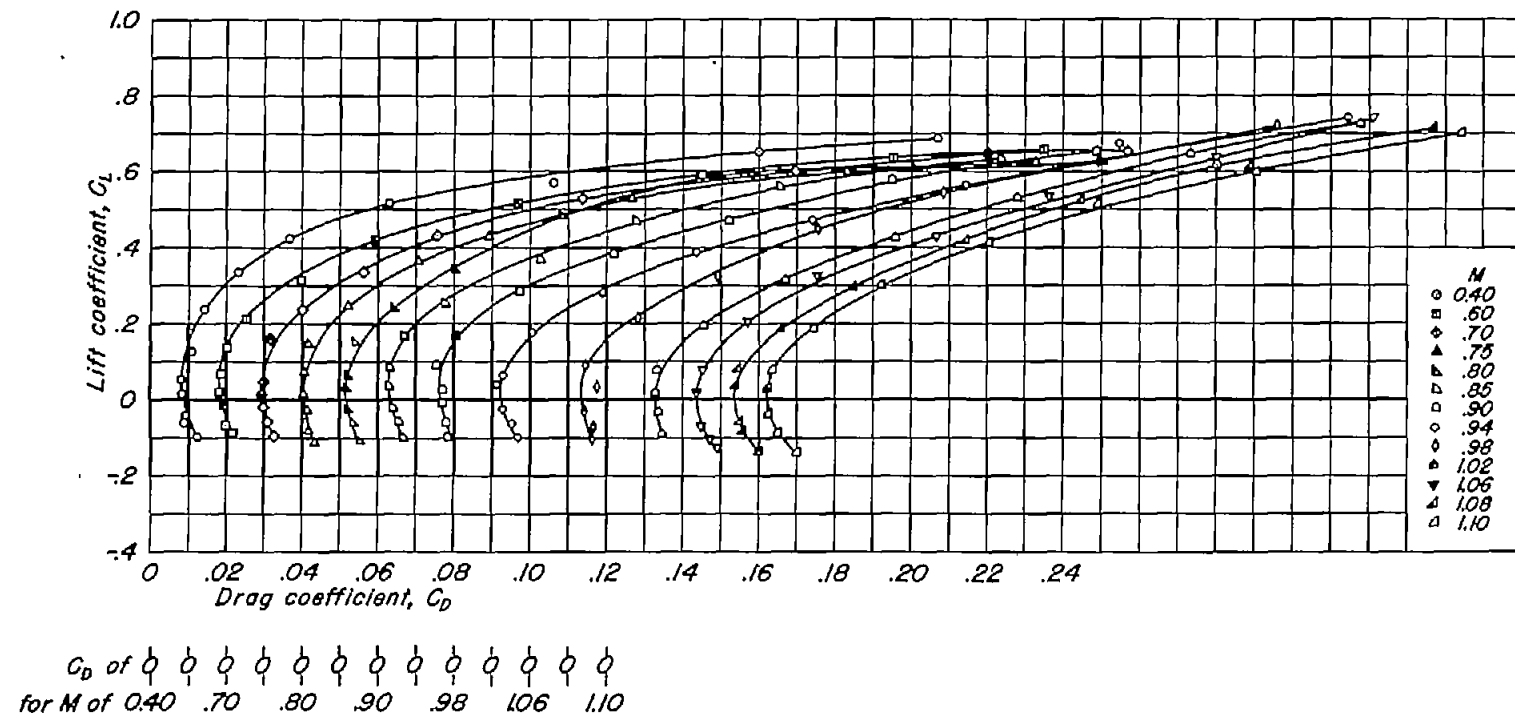
(g) $A, 4; t/c, 0.04$.
Figure 9.-Continued.



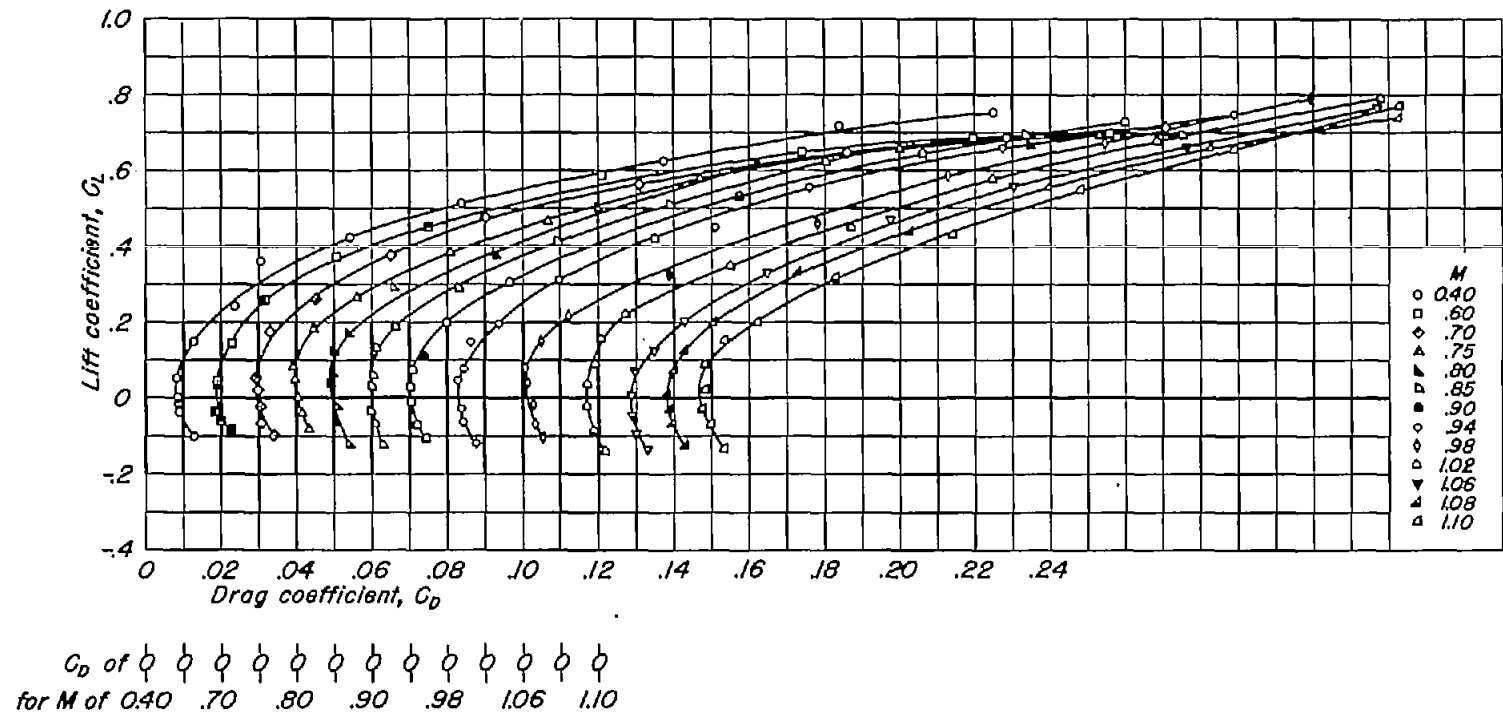
(h) A, 3, t/c , 0.04.
Figure 9.-Continued.



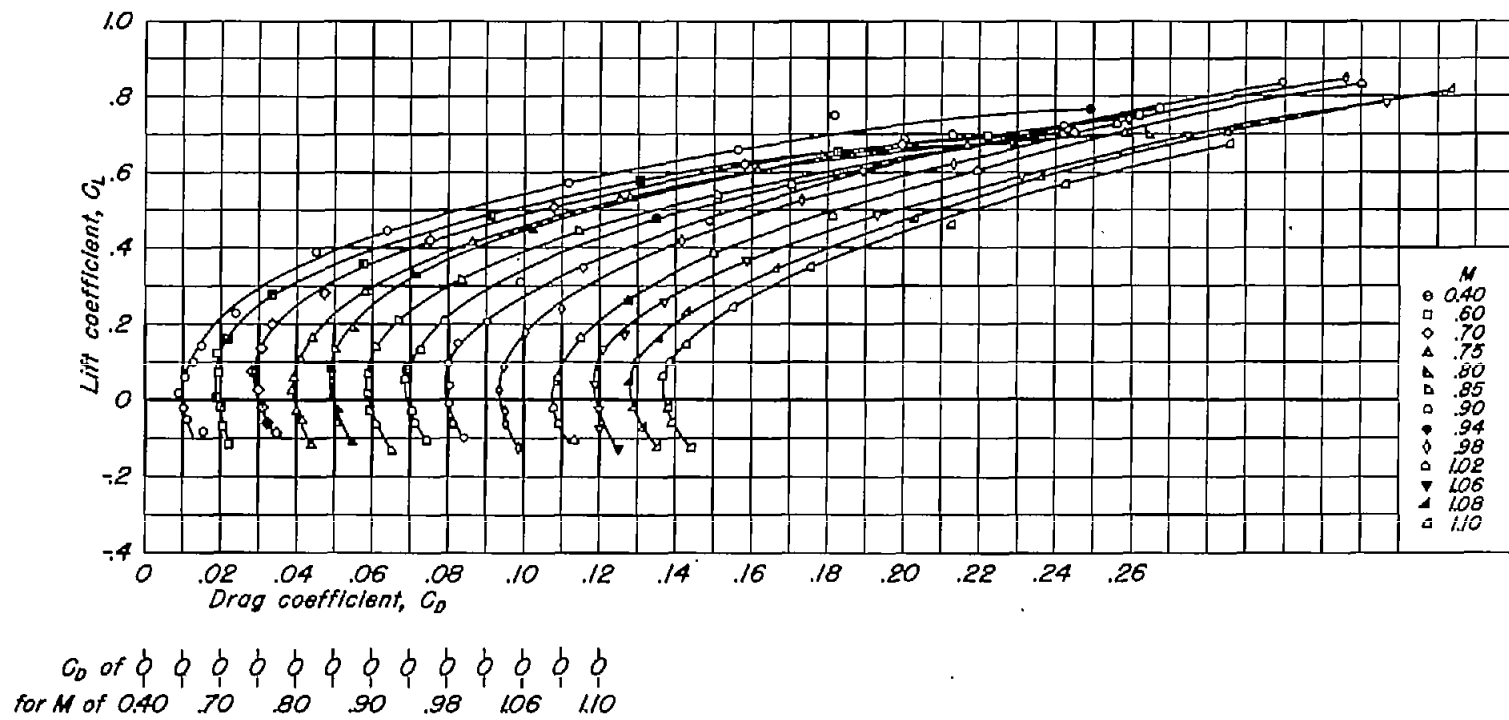
(i) A.2; t/c , 0.10.
Figure 9.-Continued.



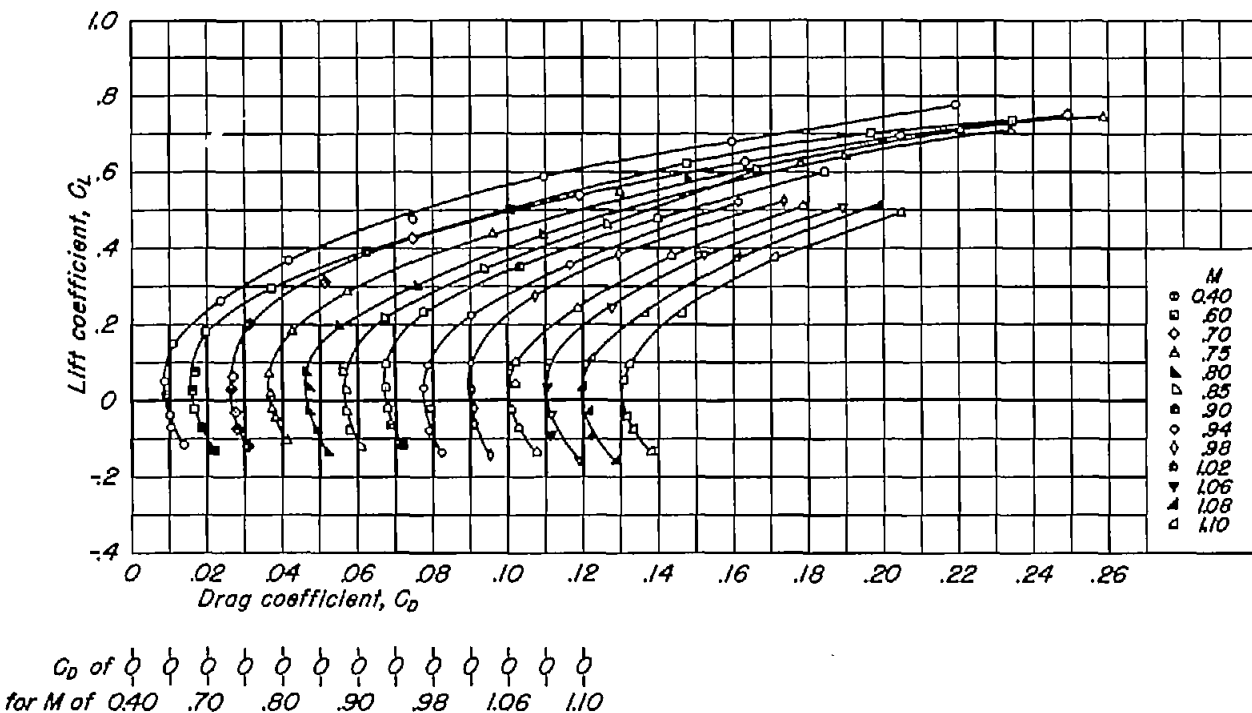
(j) A, 2; t/c, 0.08.
Figure 9.-Continued.



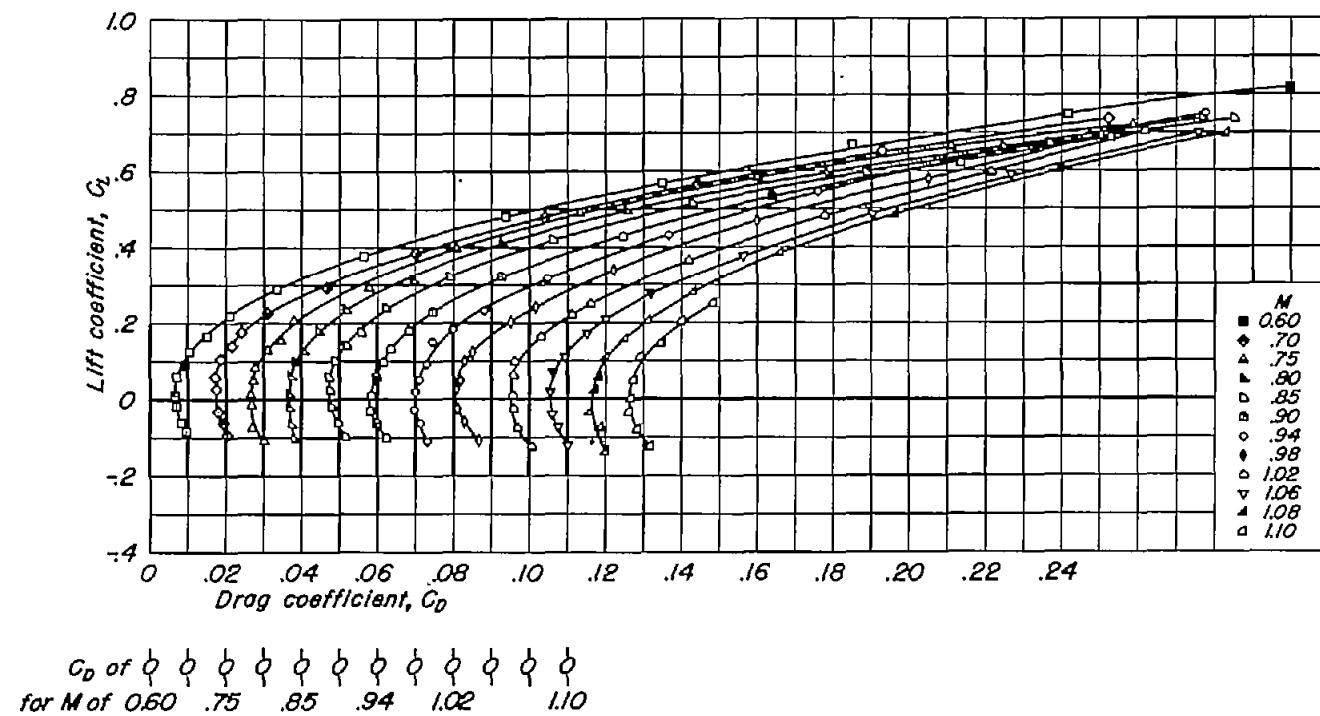
(k) A,2; t/c , 0.06.
Figure 9-Continued.



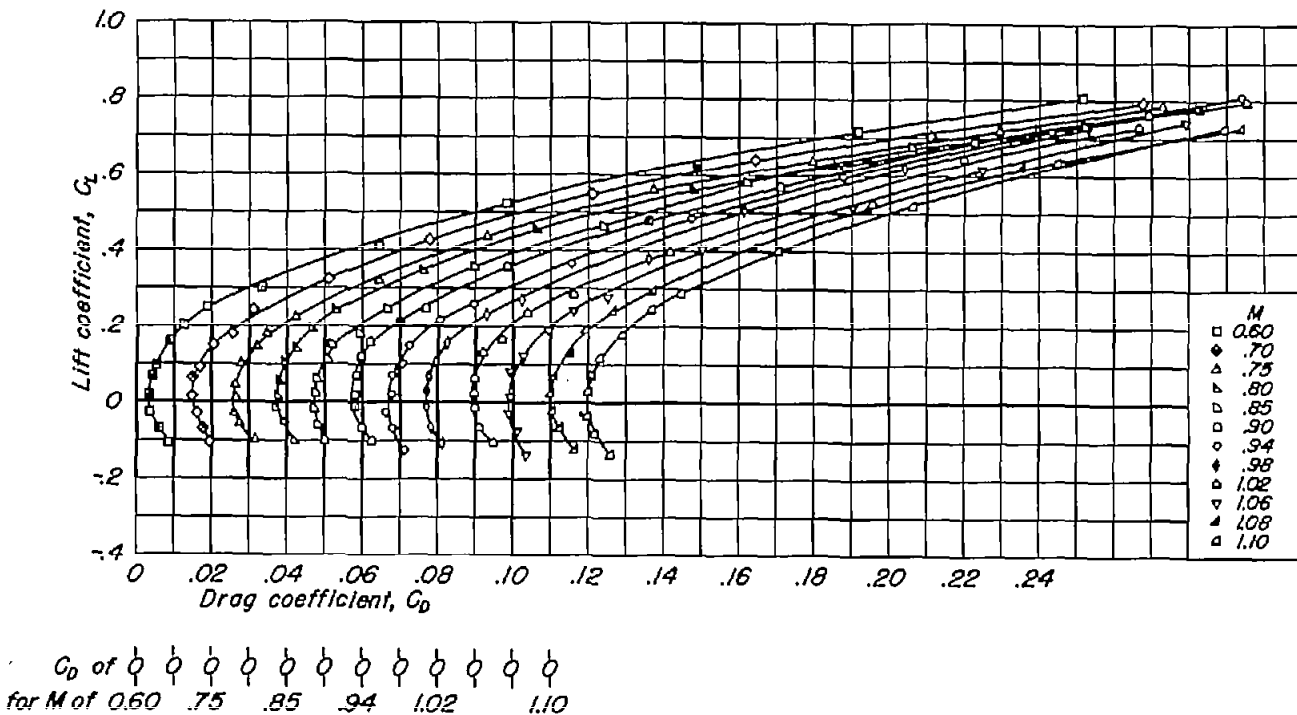
(1) $A, 2; t/c, 0.04$.
Figure 9.-Continued.



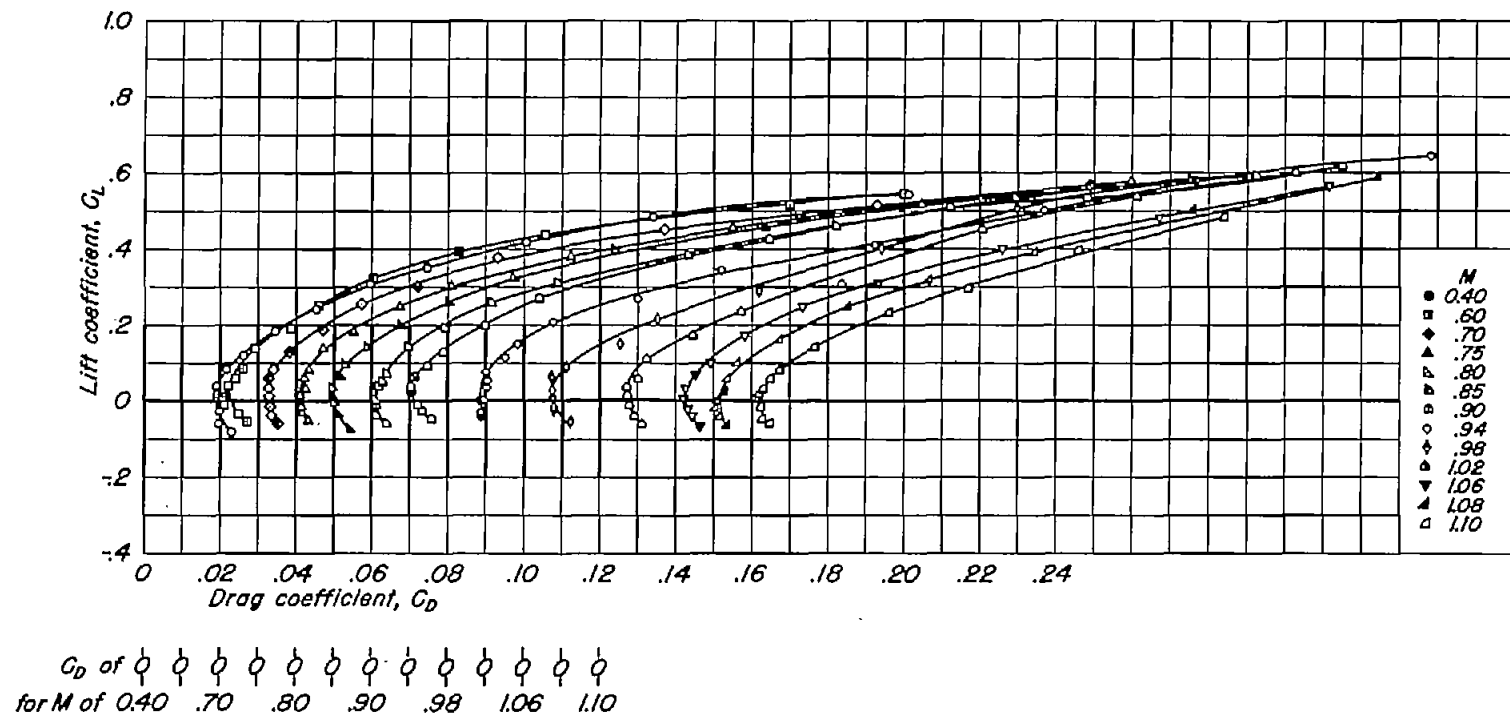
(m) A, 2; $1/c$, 0.02.
Figure 9.-Continued.



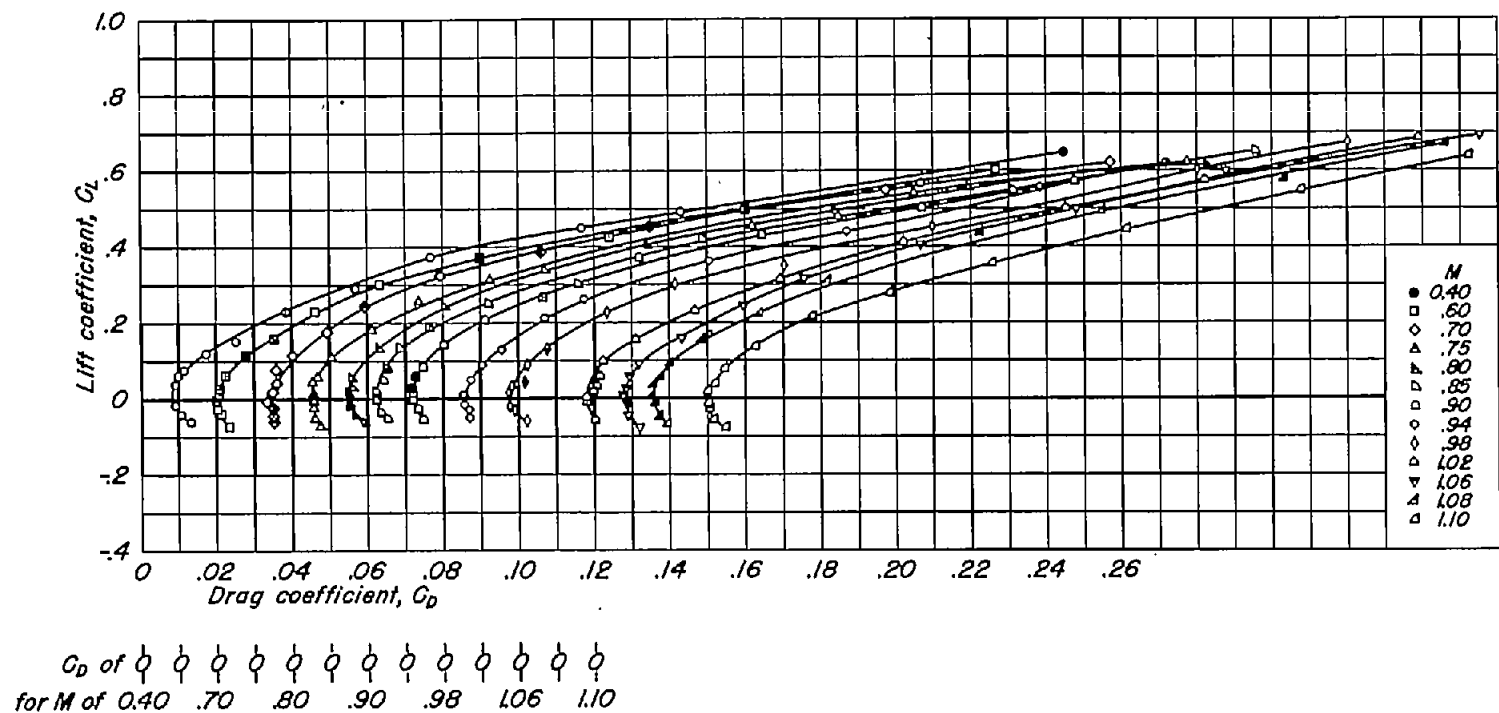
(n) $A, 1.5; t/c, 0.04$.
Figure 9- Continued.



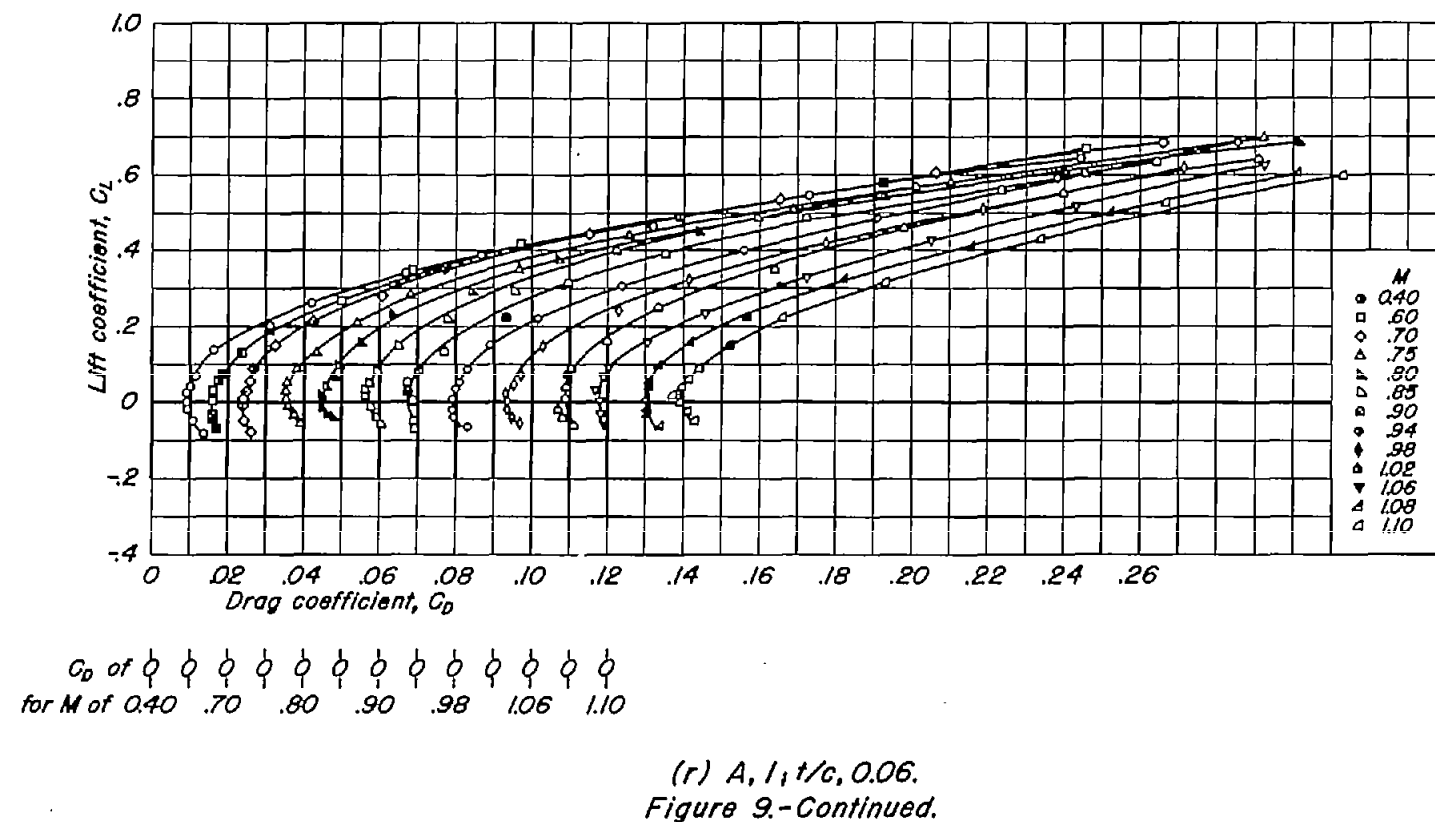
(o) A, 1.5, t/c , 0.02.
Figure 9- Continued.

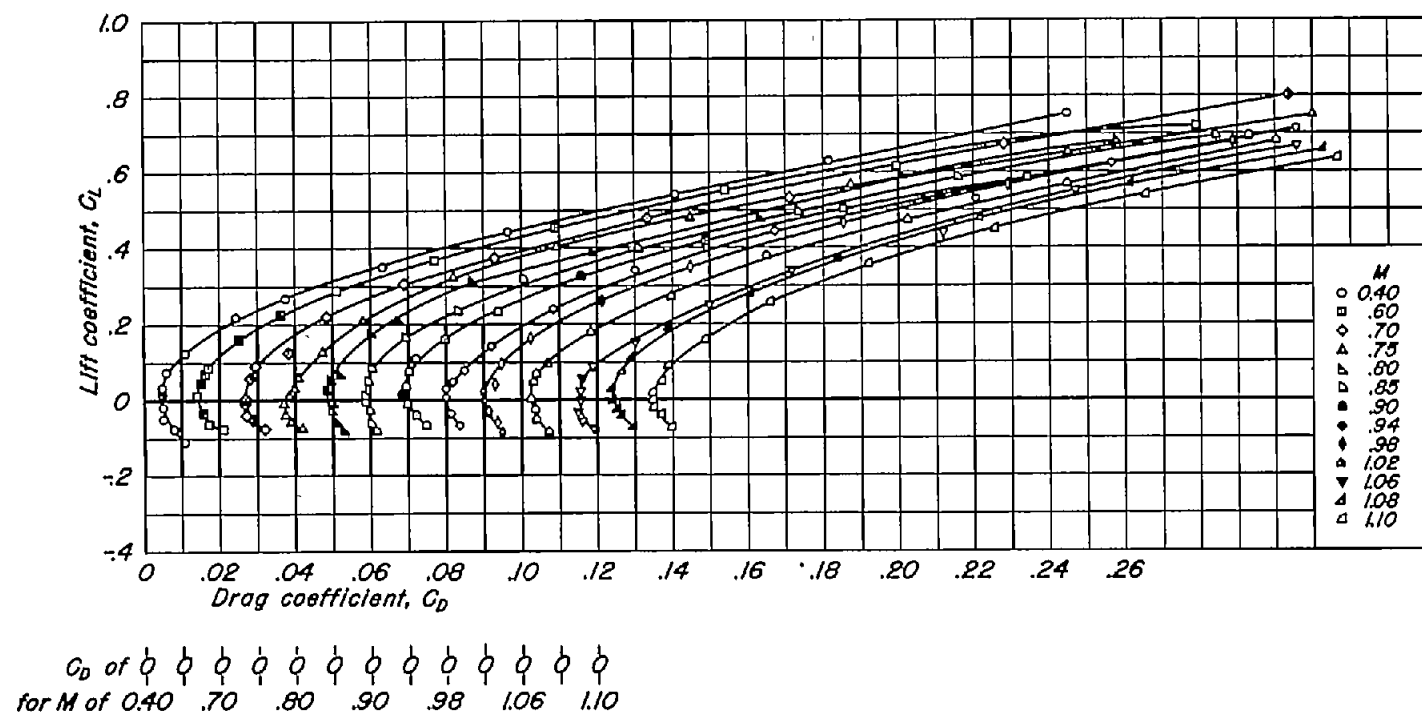


(p) $A, 1; t/c, 0.10.$
Figure 9.—Continued.

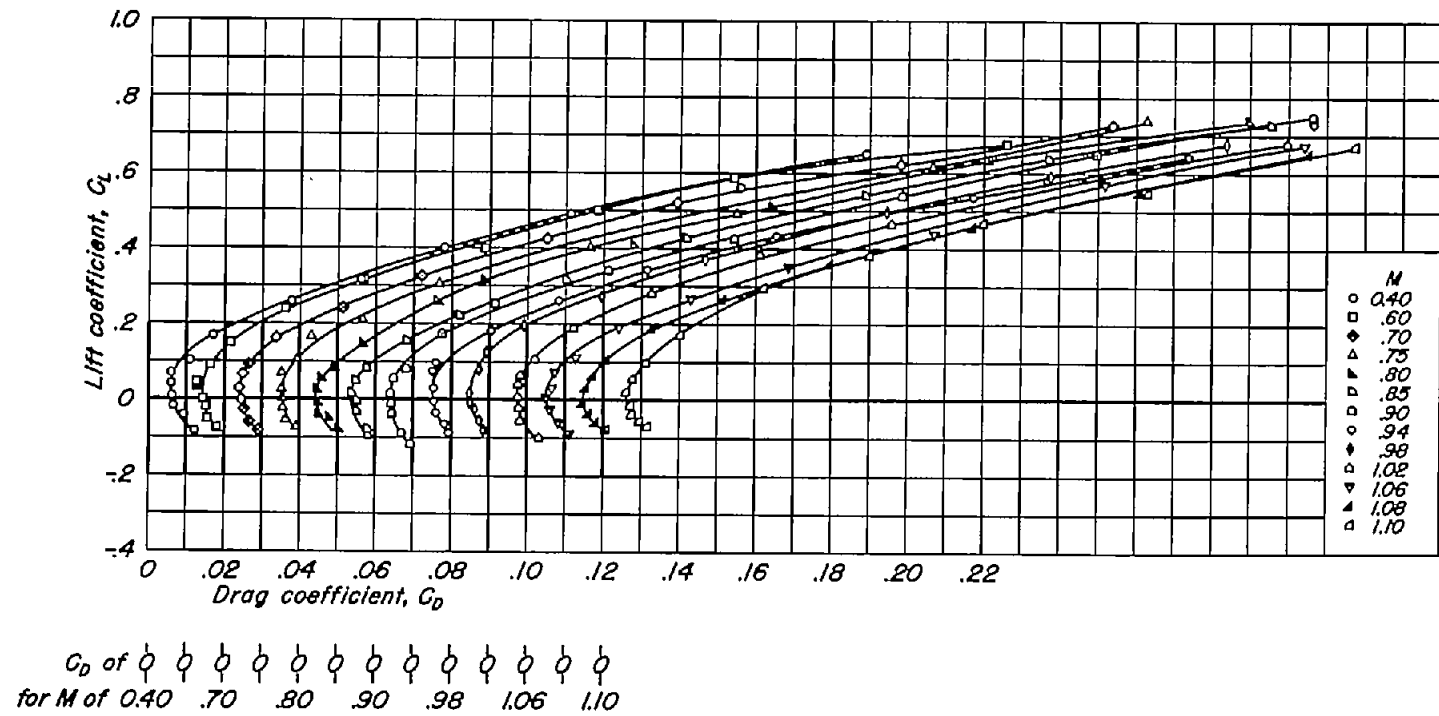


(q) $A, l_1 t/c, 0.08$.
Figure 9.-Continued.

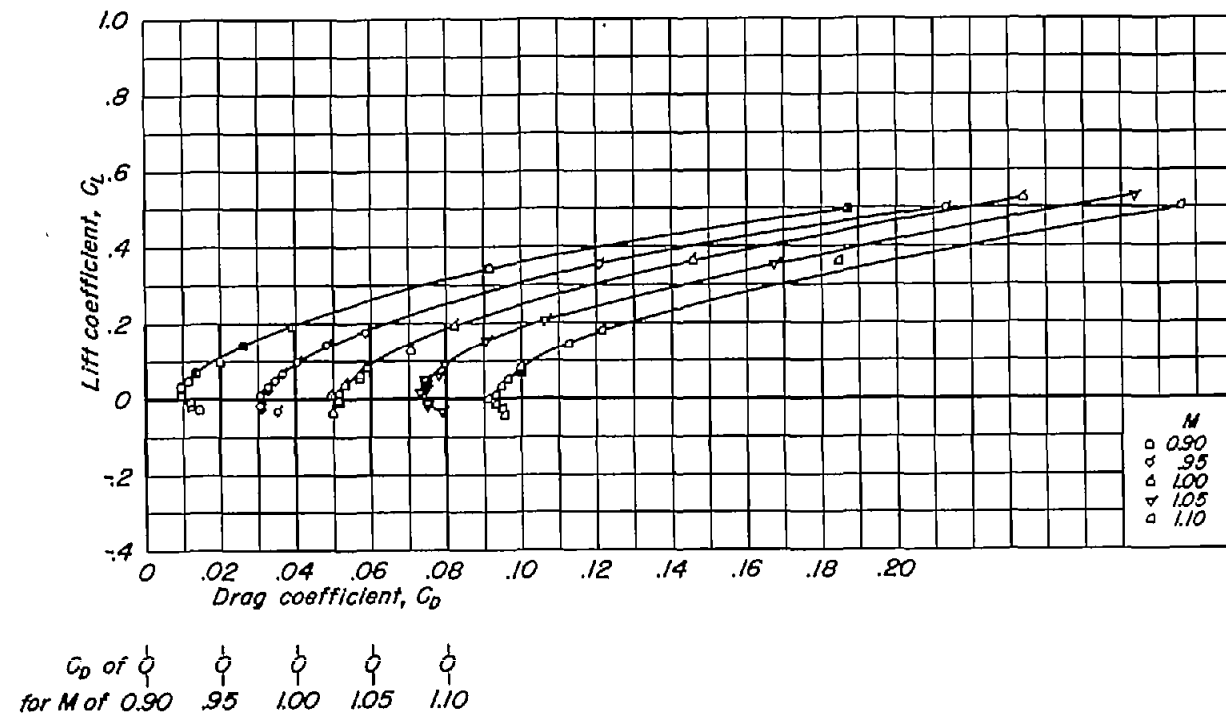




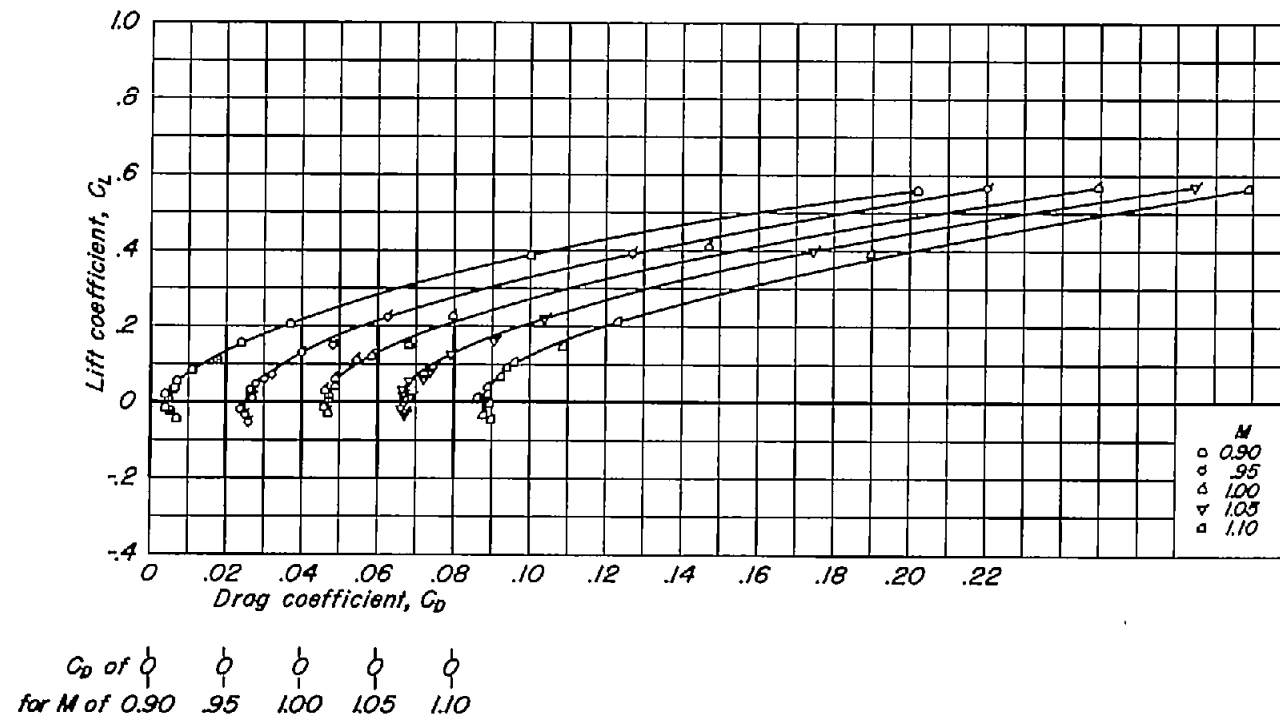
(s) A, 1; t/c , 0.04.
Figure 9.-Continued.



(1) $A, 1; t/c, 0.02$.
Figure 9.-Continued.



(u) $A, 0.5; t/c, 0.04.$
Figure 9- Continued.



(v) A, 0.5, t/c , 0.02.
Figure 9:- Concluded.

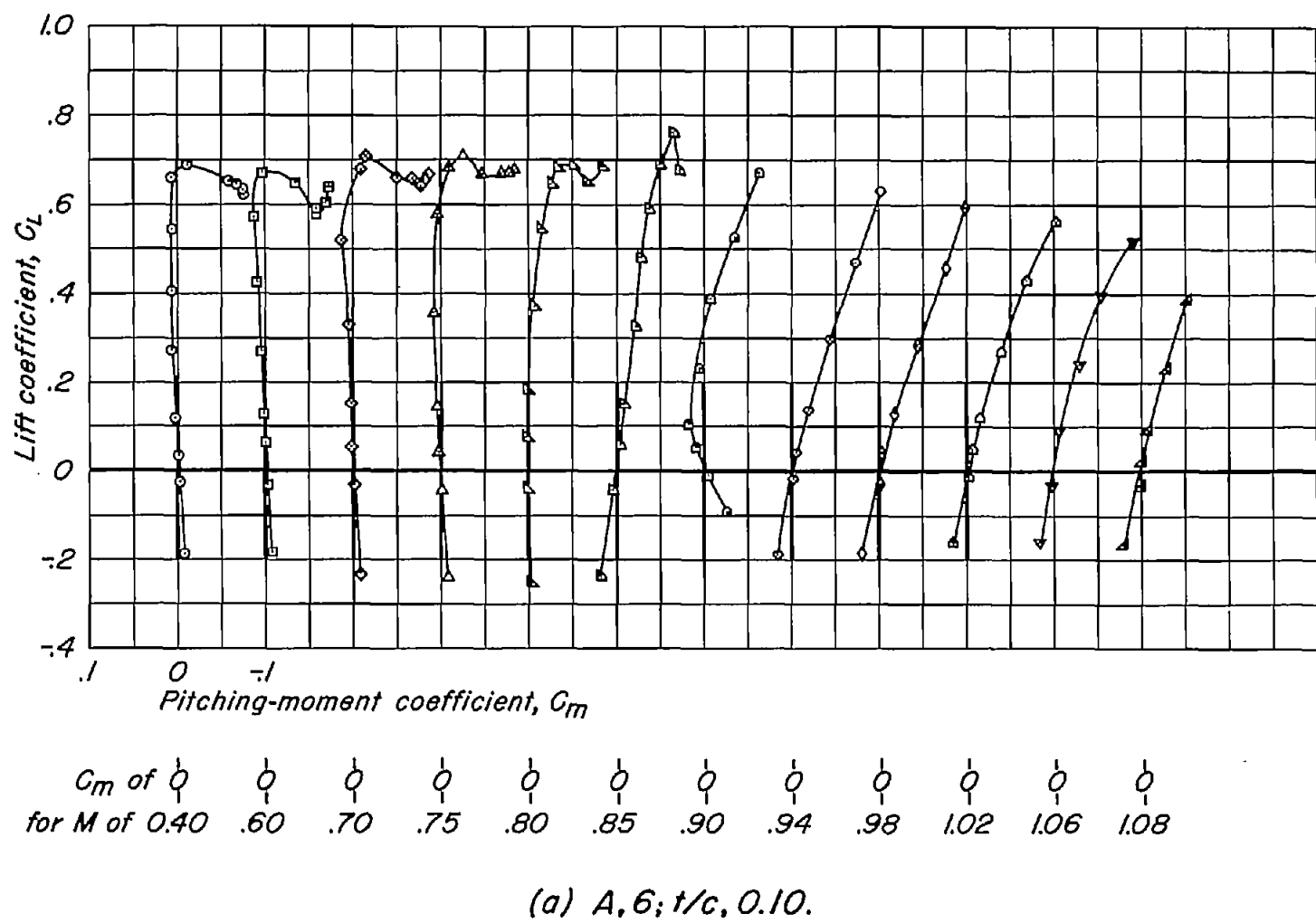
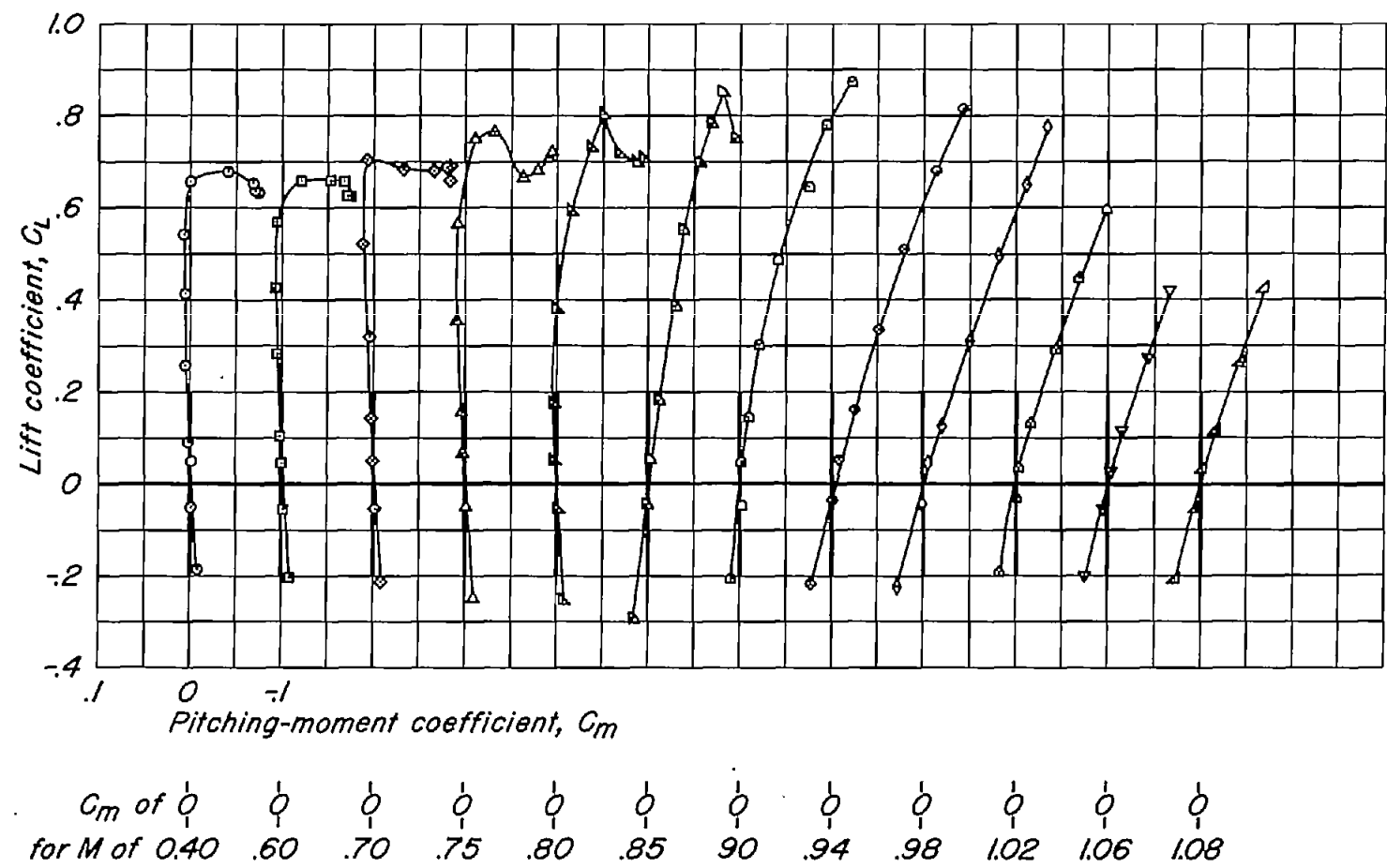
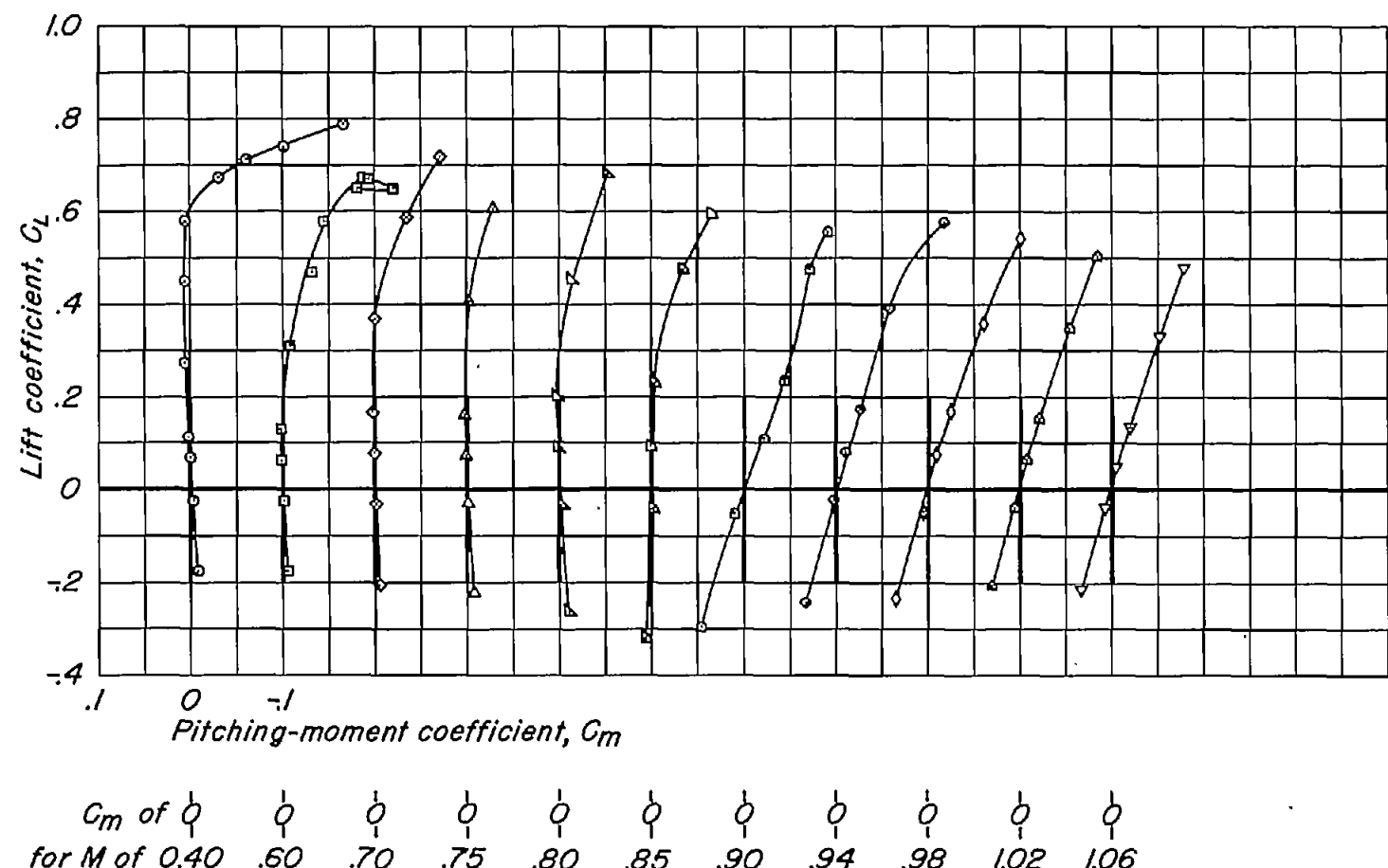


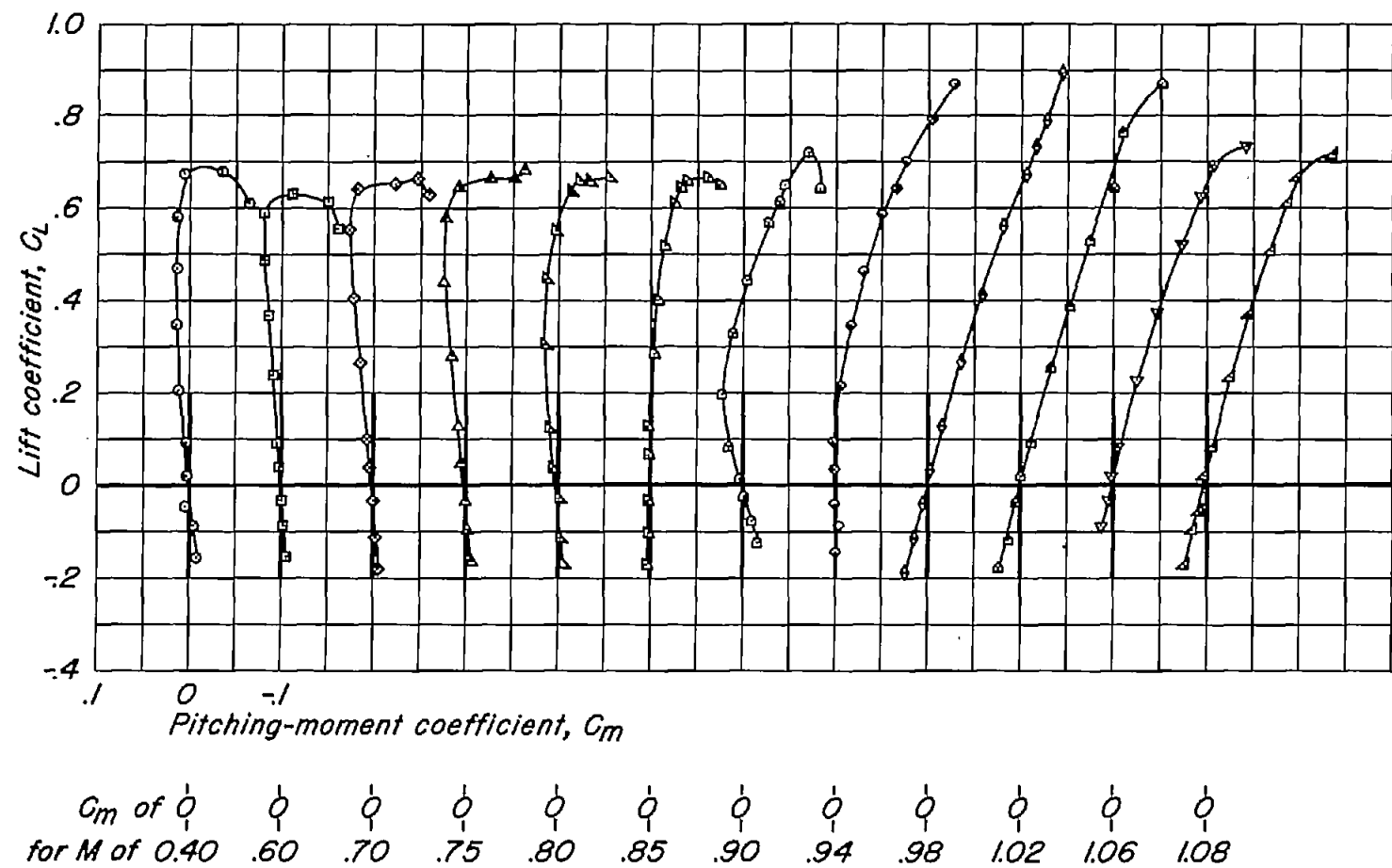
Figure 10.- The variation of pitching-moment coefficient with lift coefficient for the rectangular wings with NACA 63AOXX sections.



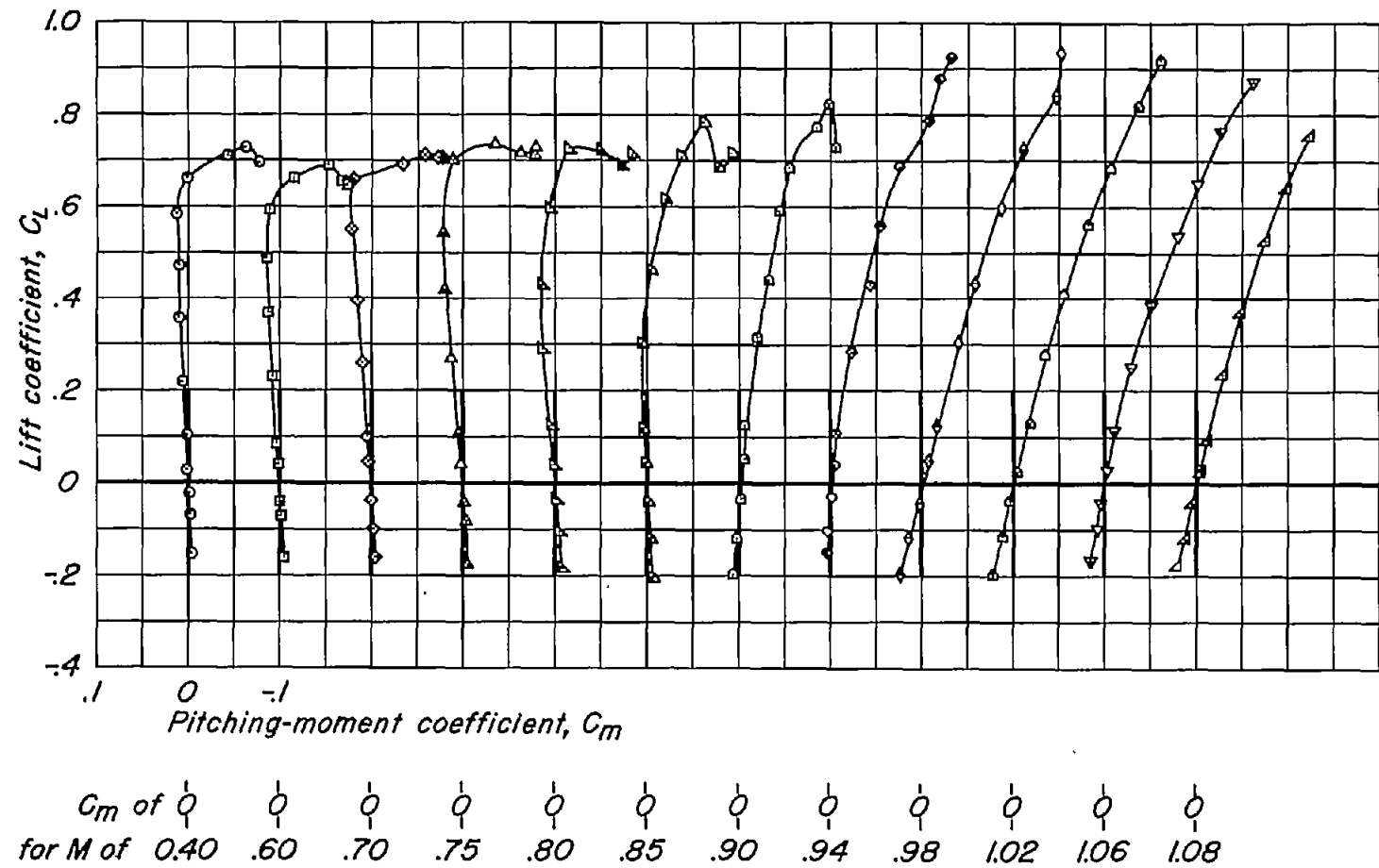
(b) A,6; t/c , 0.08.
Figure 10.—Continued.



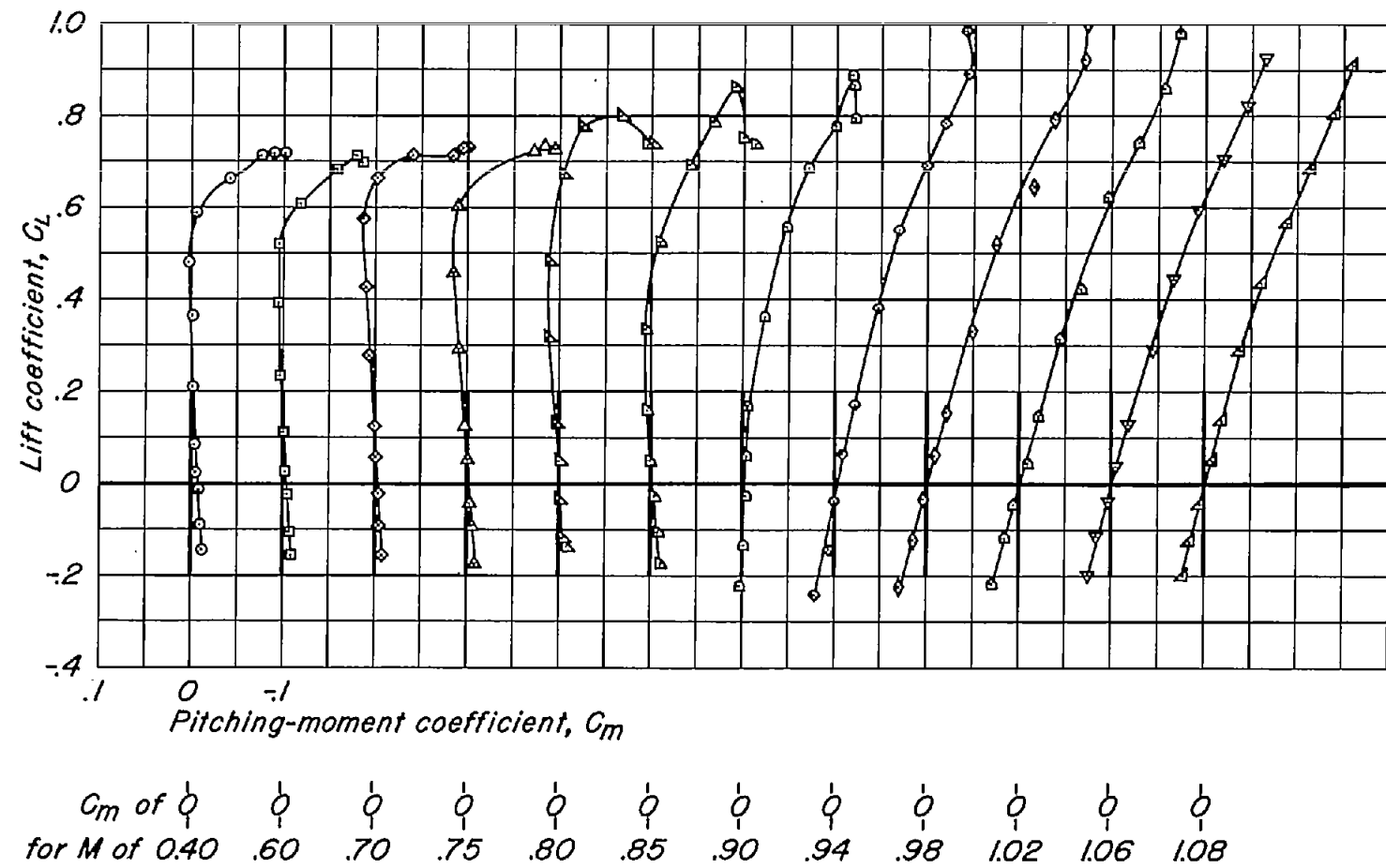
(c) A,6; t/c , 0.06.
Figure 10.-Continued.



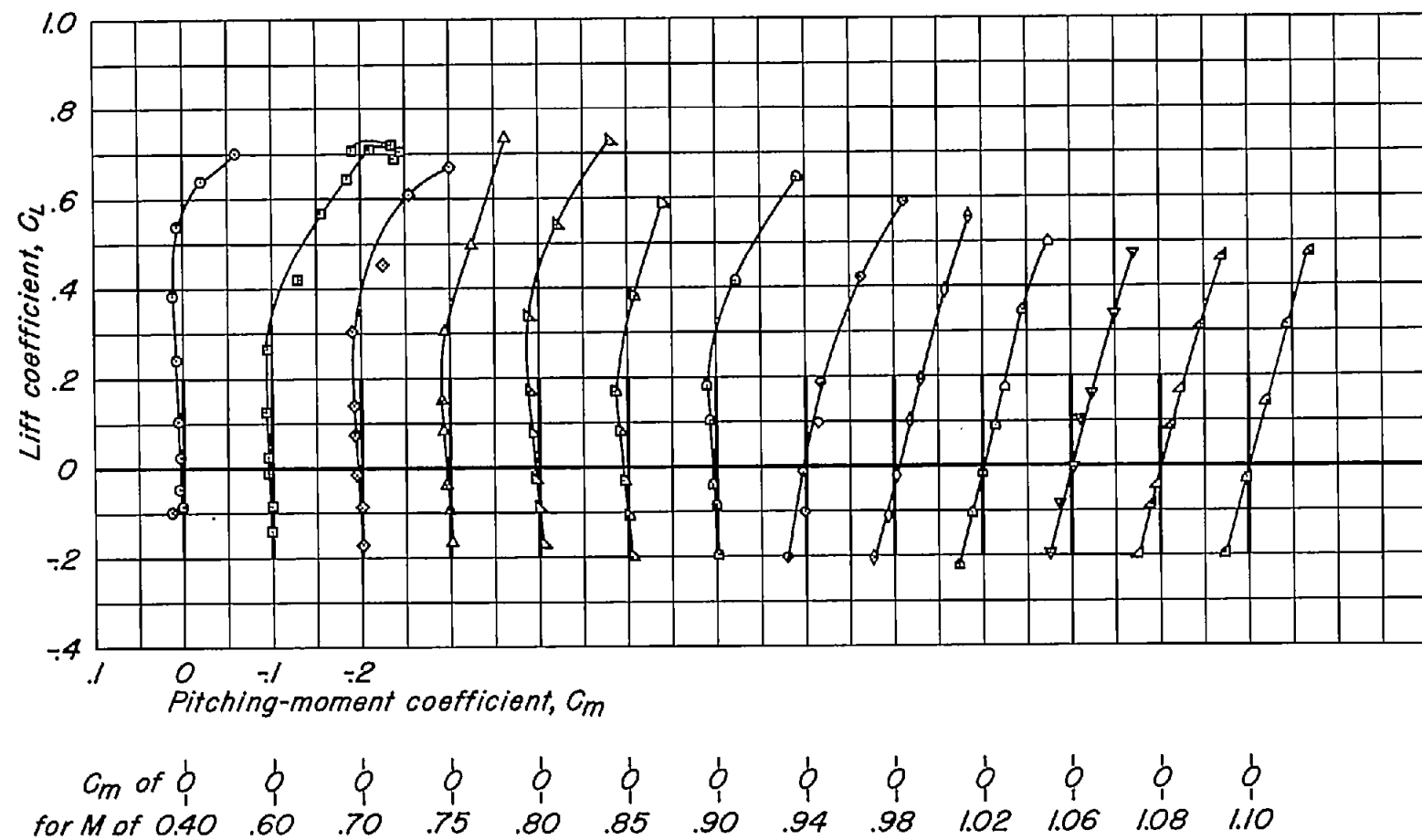
(d) $A, 4; t/c, 0.10.$
Figure 10.-Continued.



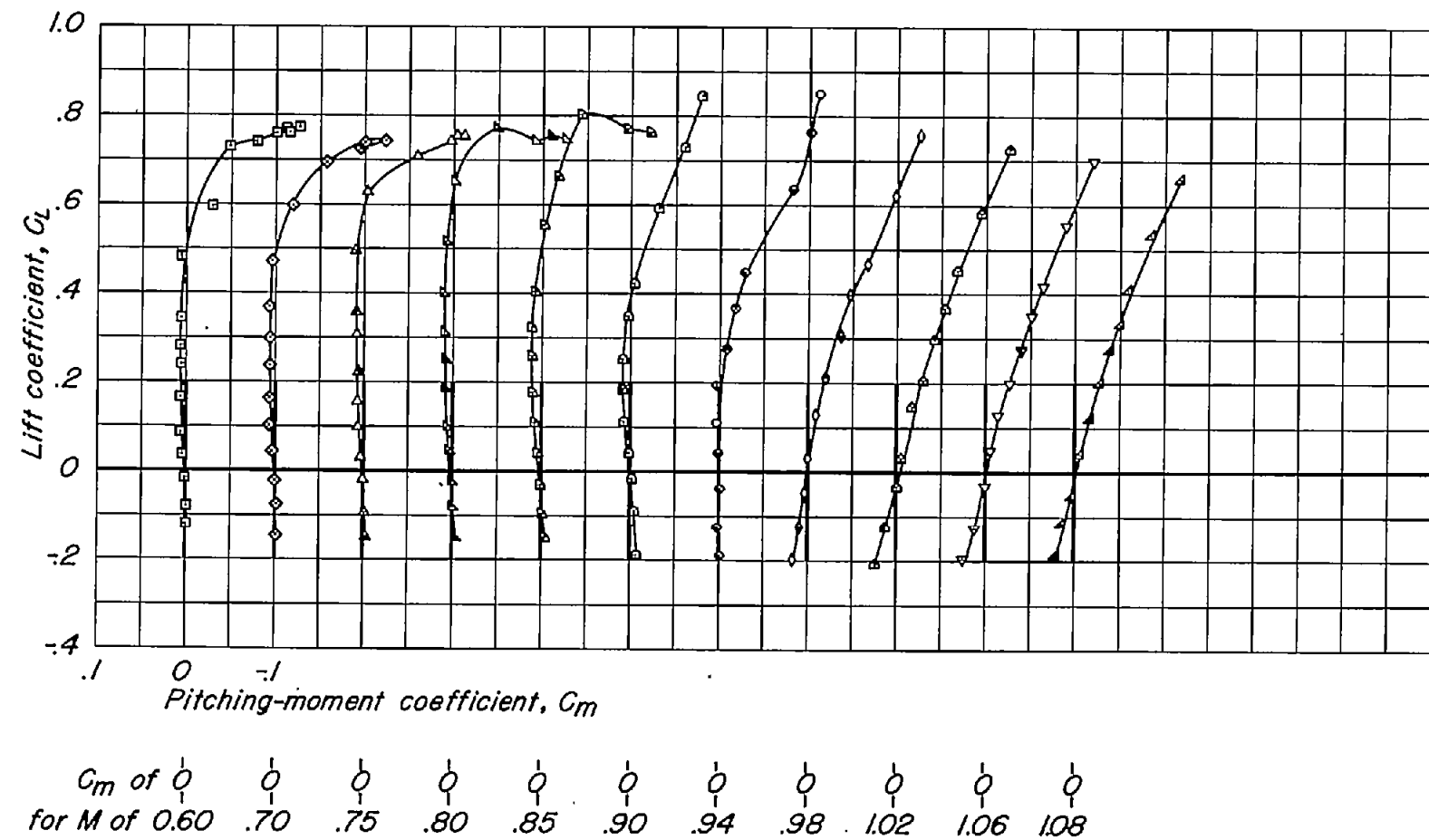
(e) $A, 4; t/c, 0.08.$
Figure 10.-Continued.



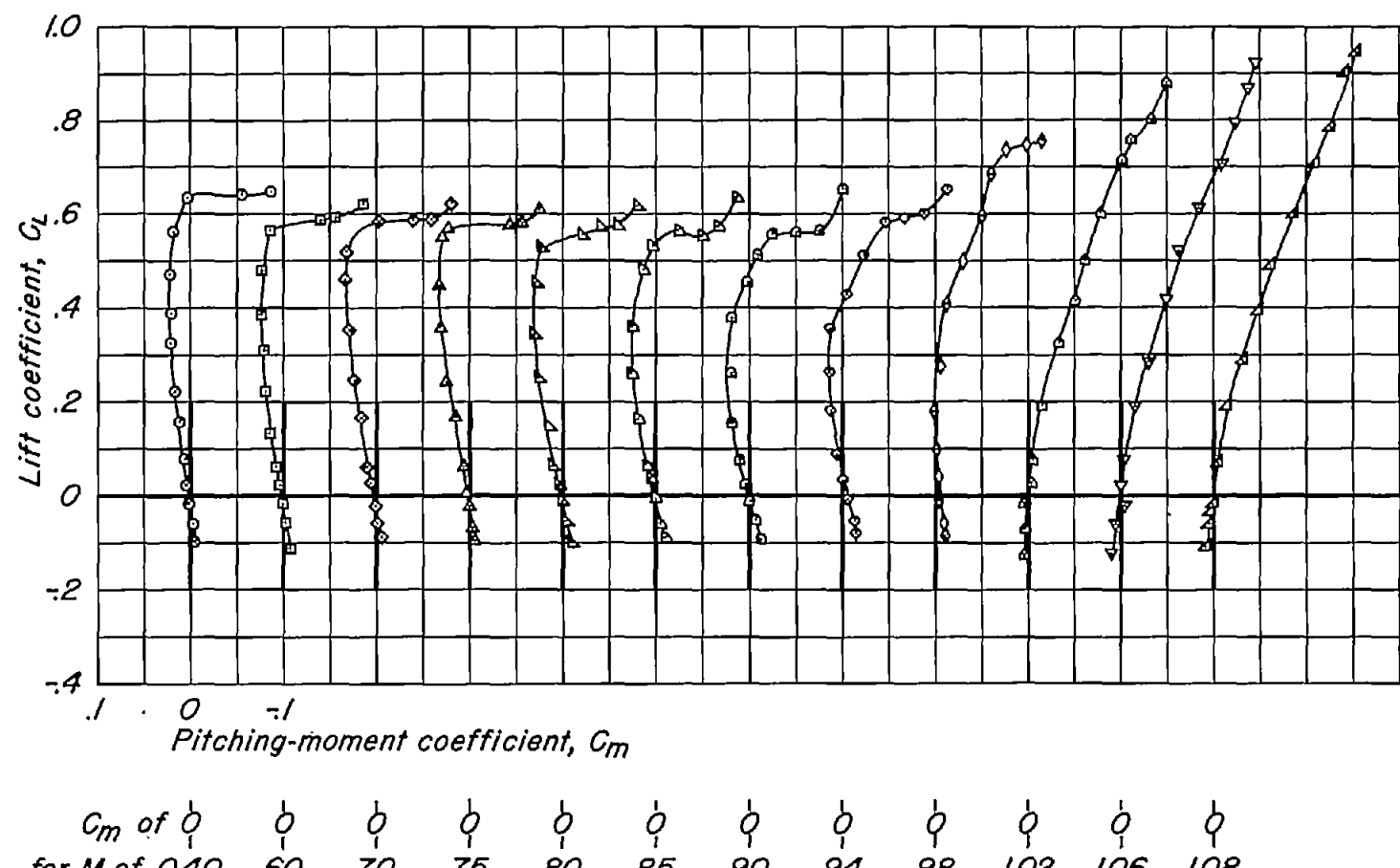
(f) $A, 4; t/c, 0.06.$
Figure 10-Continued.



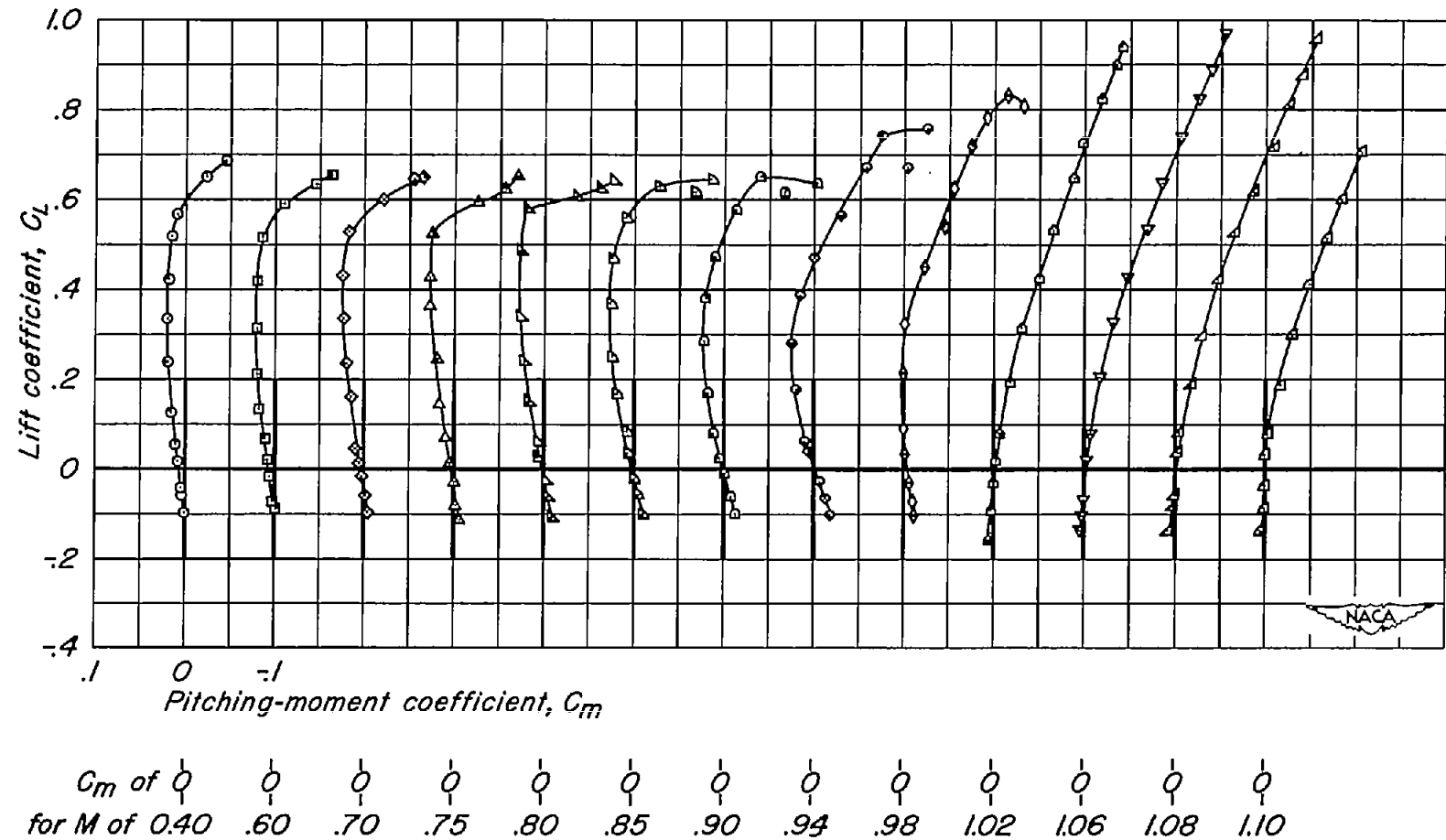
(g) $A, 4; t/c, 0.04.$
Figure 10.-Continued.



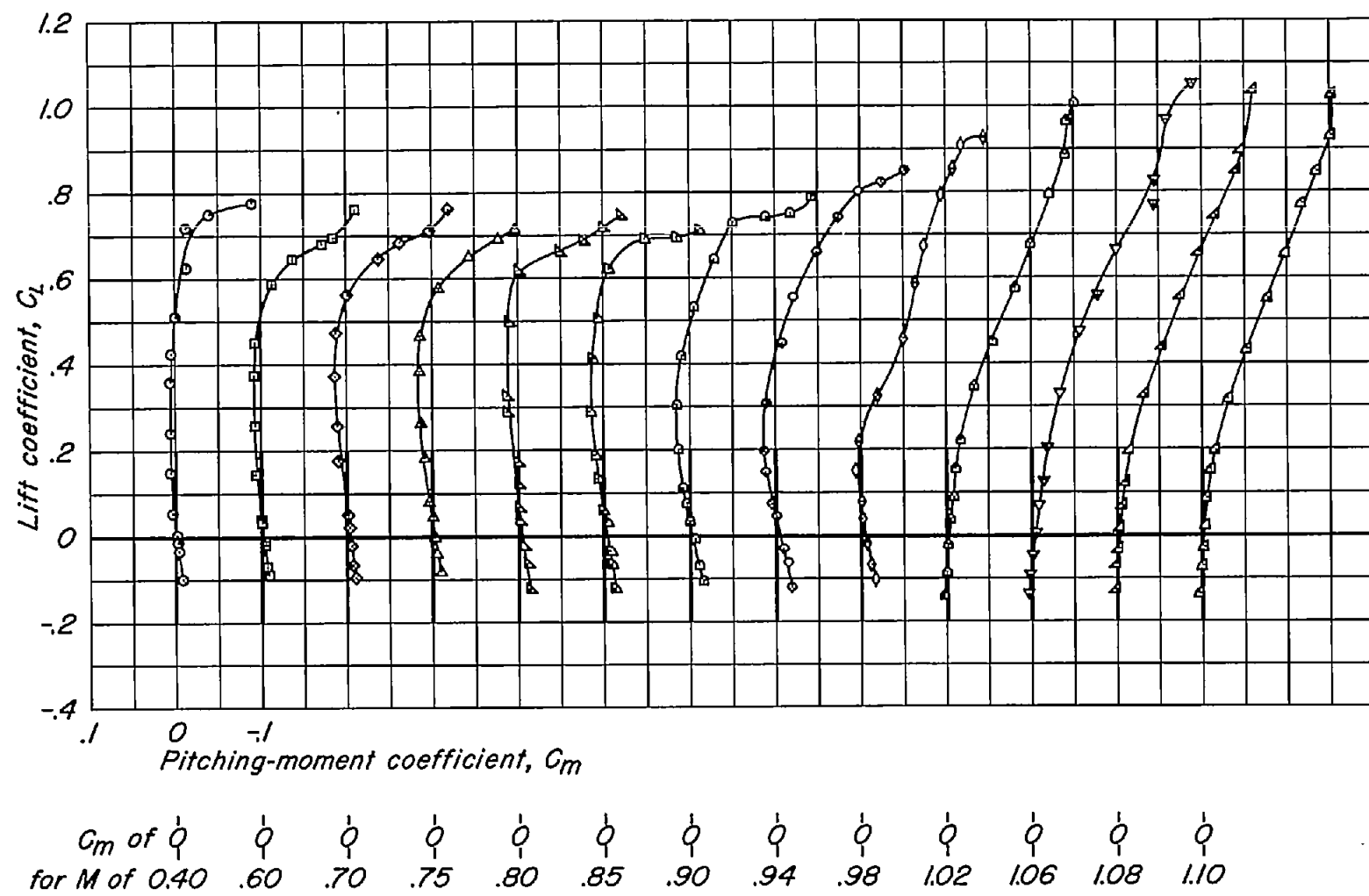
(h) A,3; t/c, 0.04.
Figure 10.-Continued.



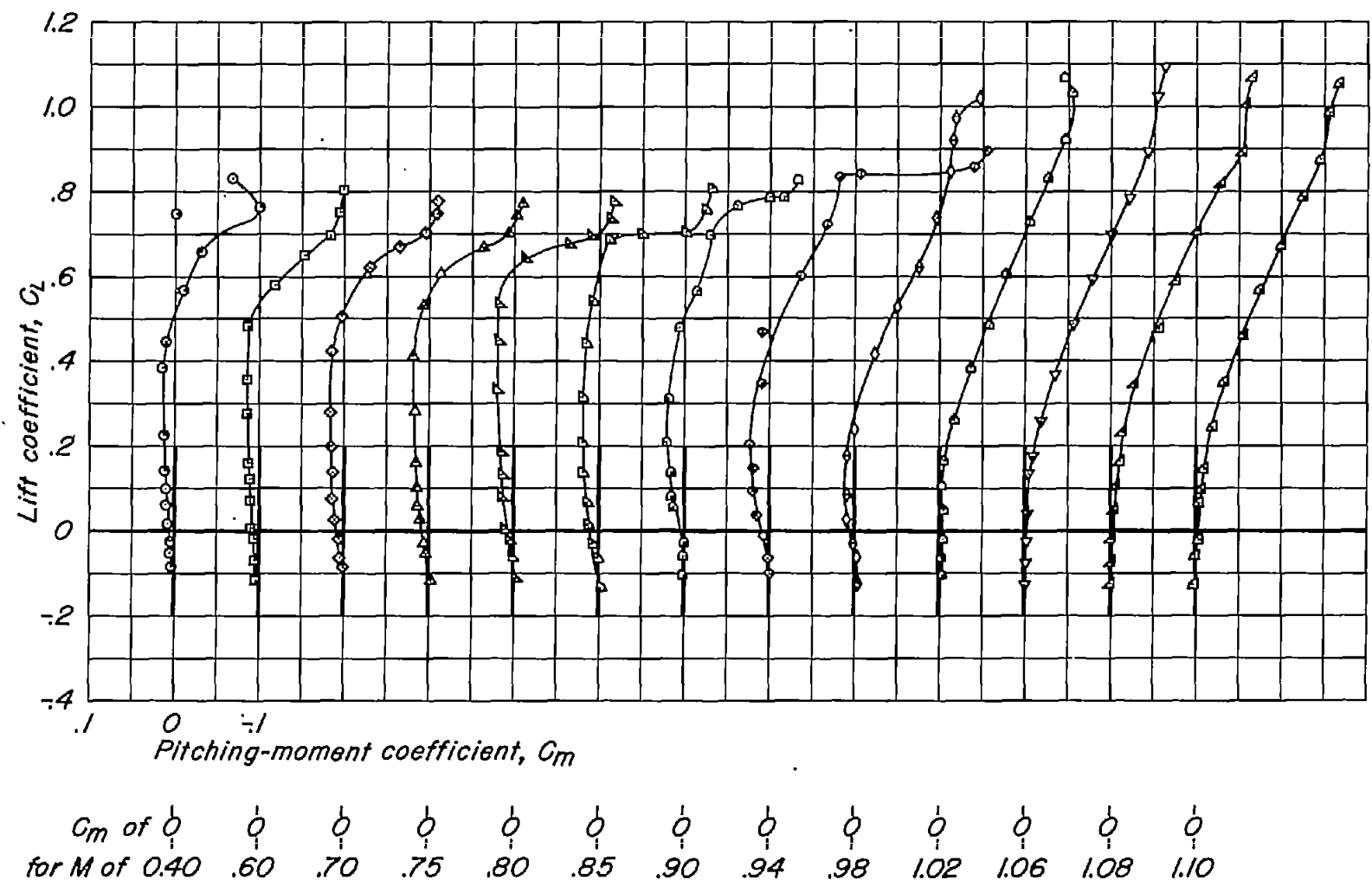
(i) $A, 2; t/c, 0.10.$
Figure 10.-Continued.



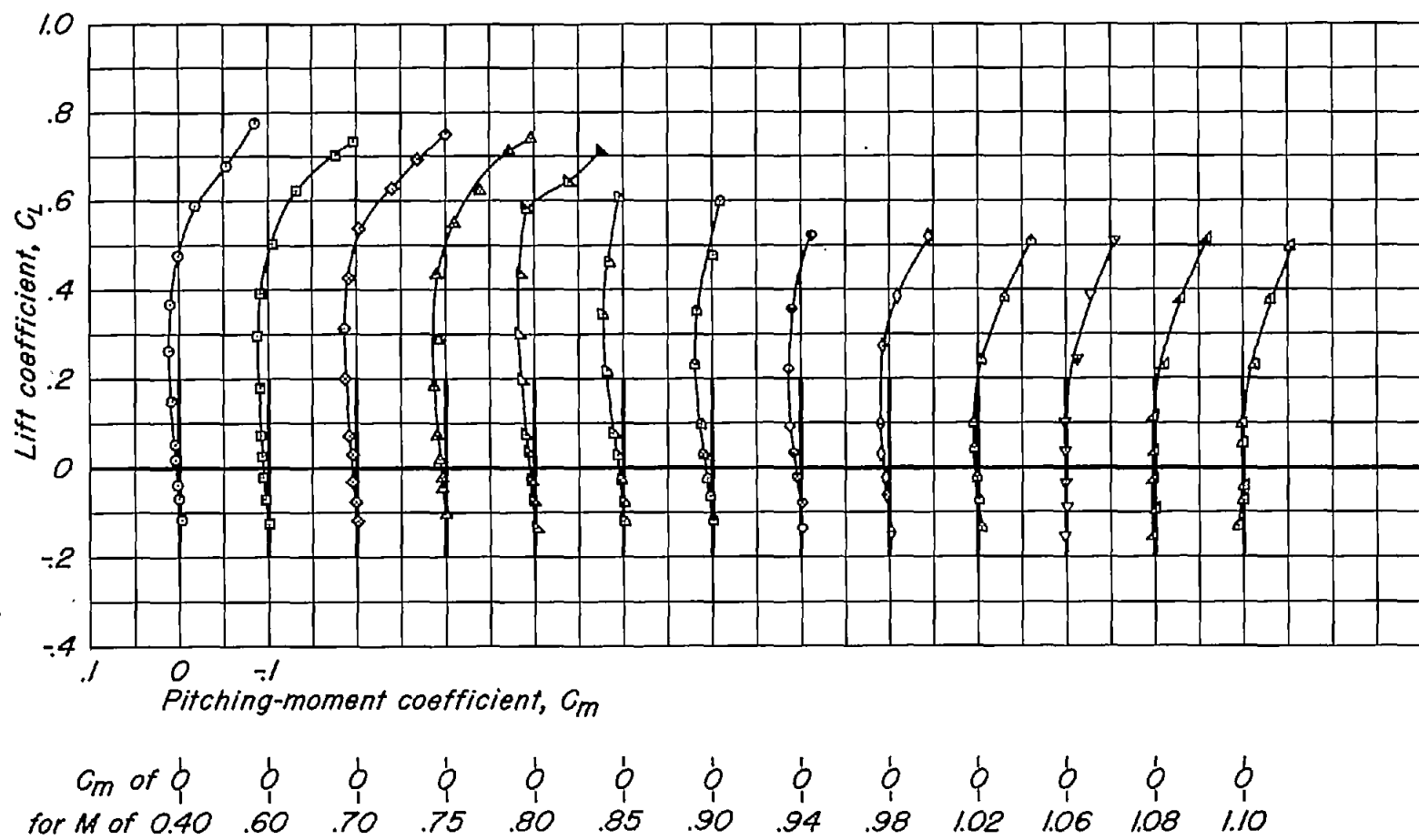
(j) $A, 2; t/c, 0.08.$
Figure 10.-Continued.



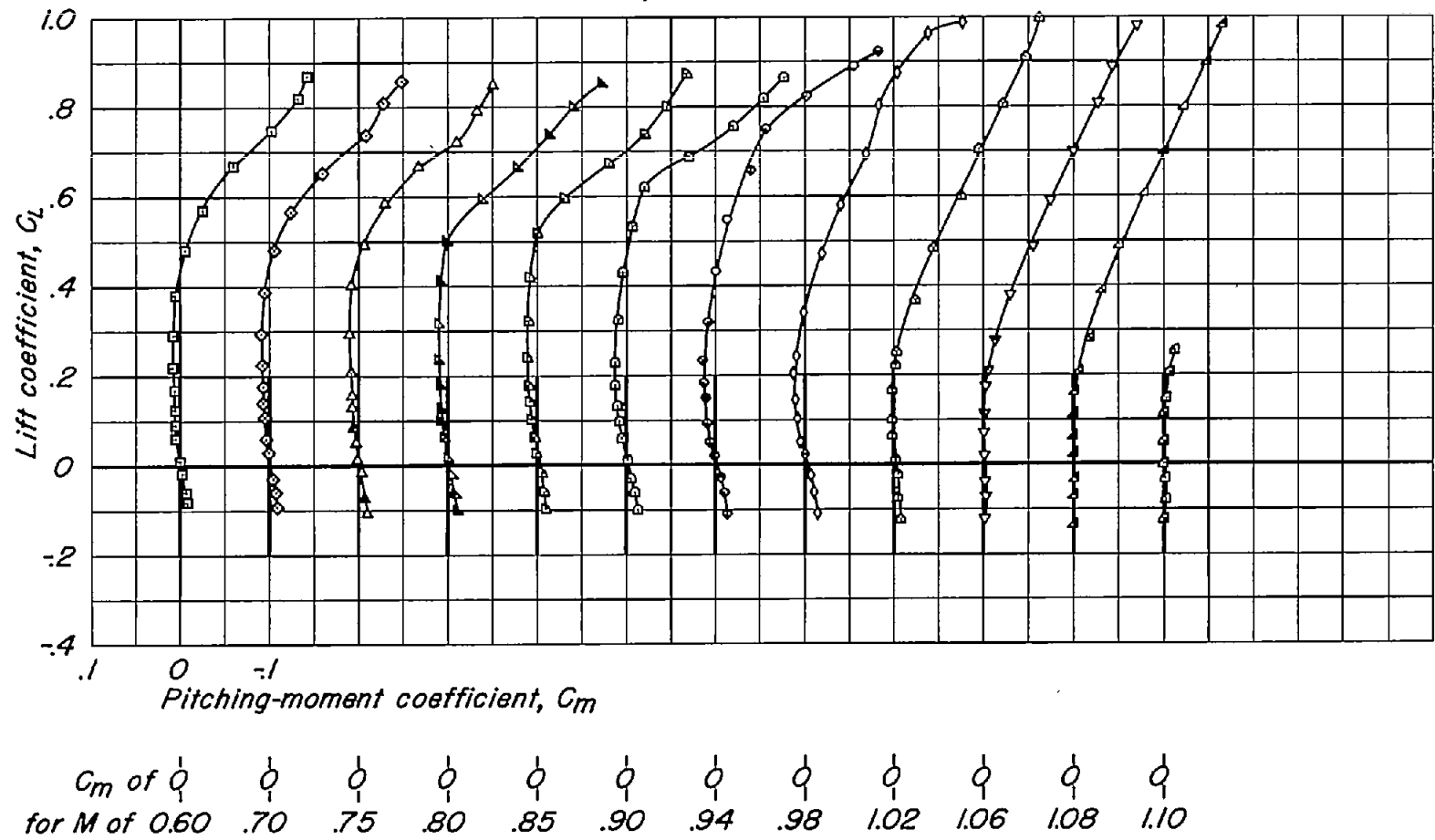
(k) $A, 2; t/c, 0.06.$
Figure 10.-Continued.



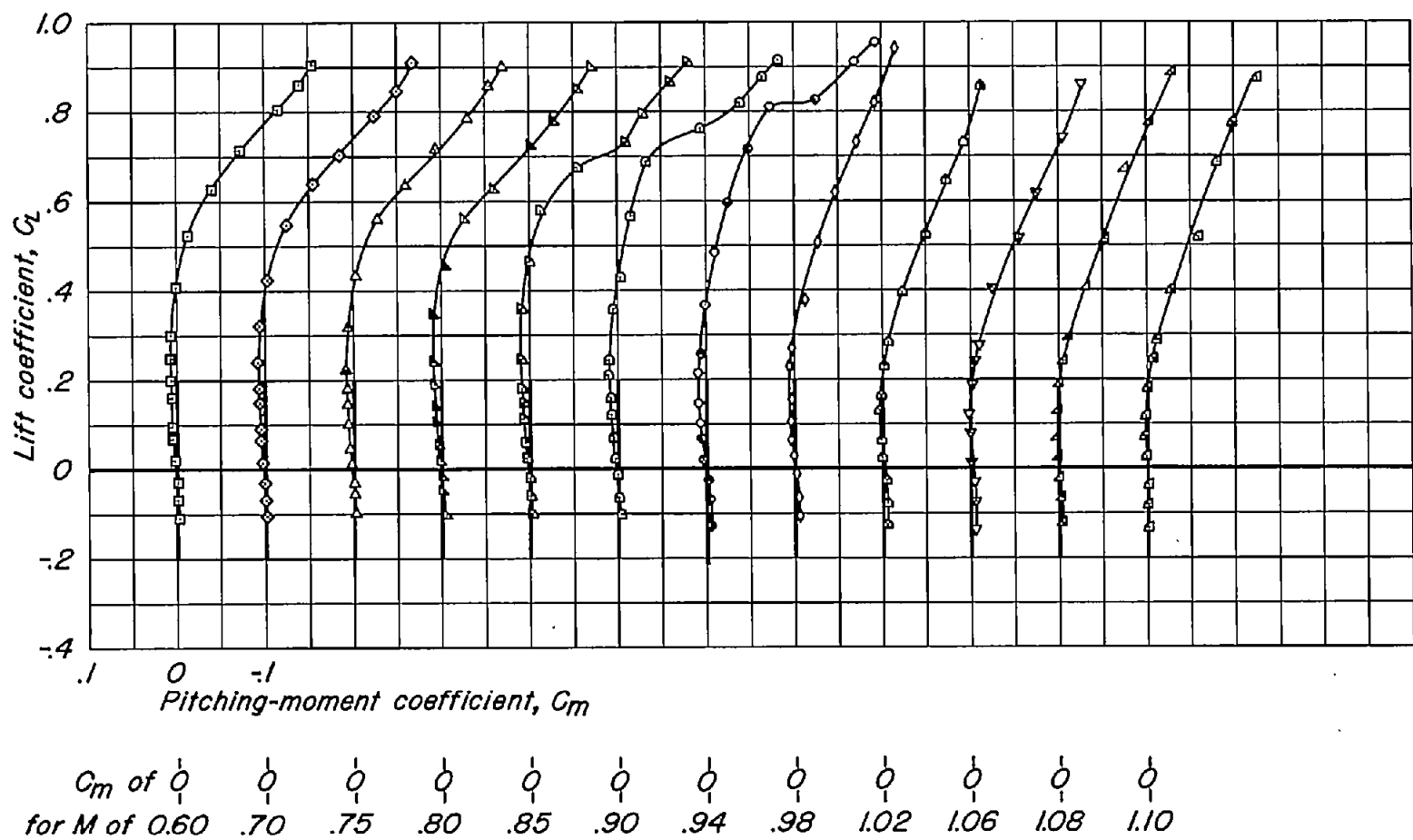
(1) A, 2; t/c, 0.04.
Figure 10.-Continued.



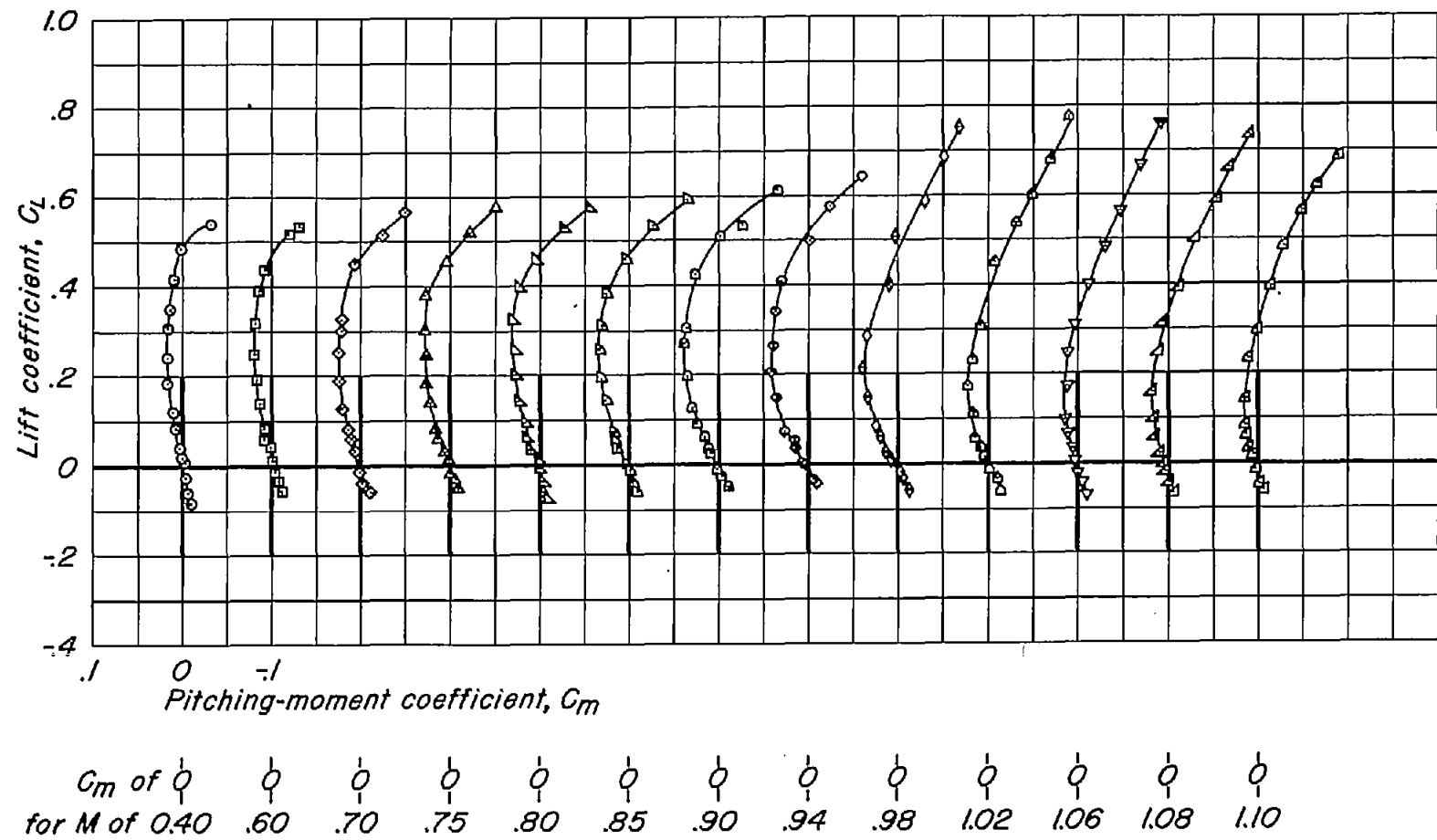
(m) A, 2; t/c , 0.02.
Figure 10.-Continued.



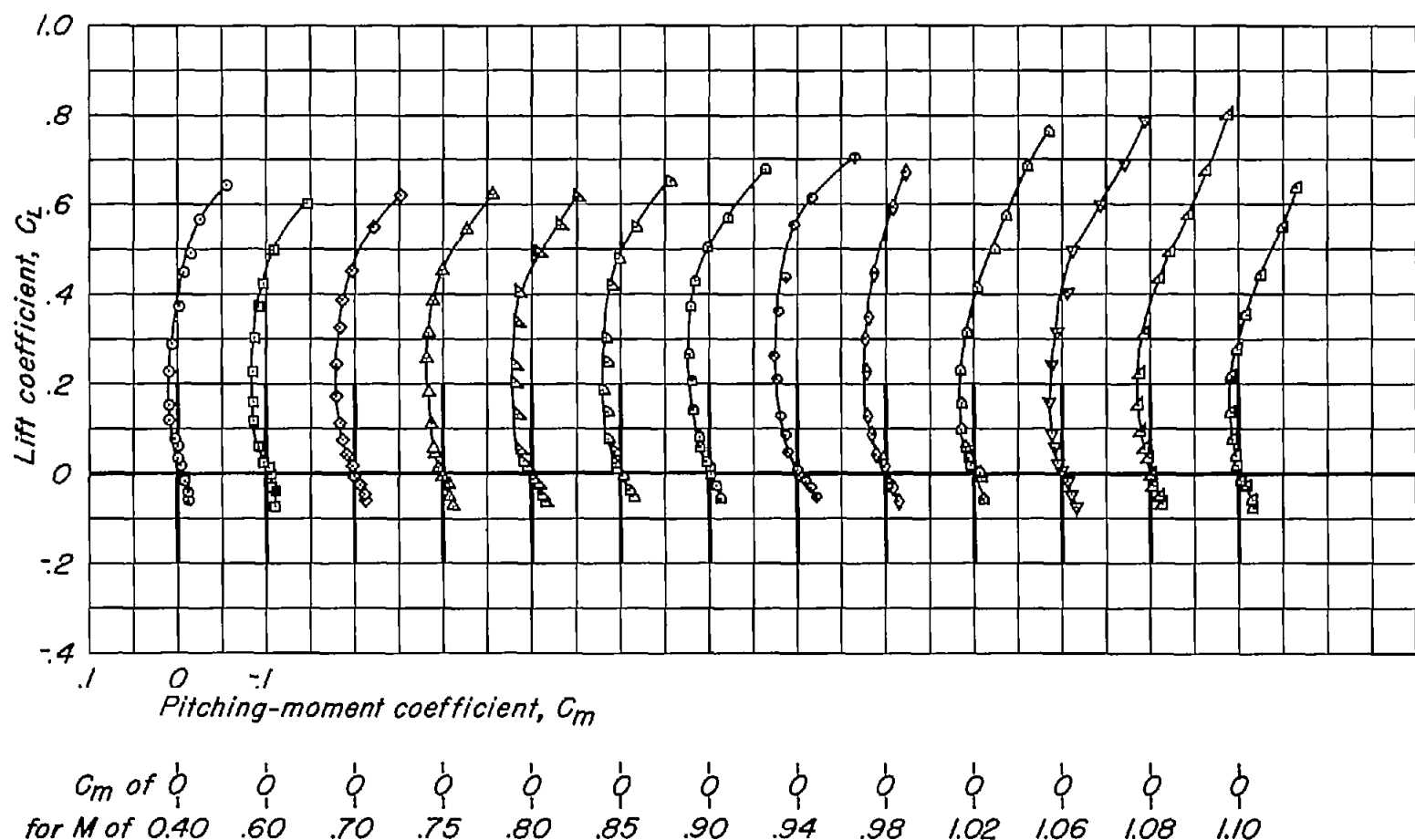
(n) $A, 1.5; t/c, 0.04$.
Figure 10.- Continued.



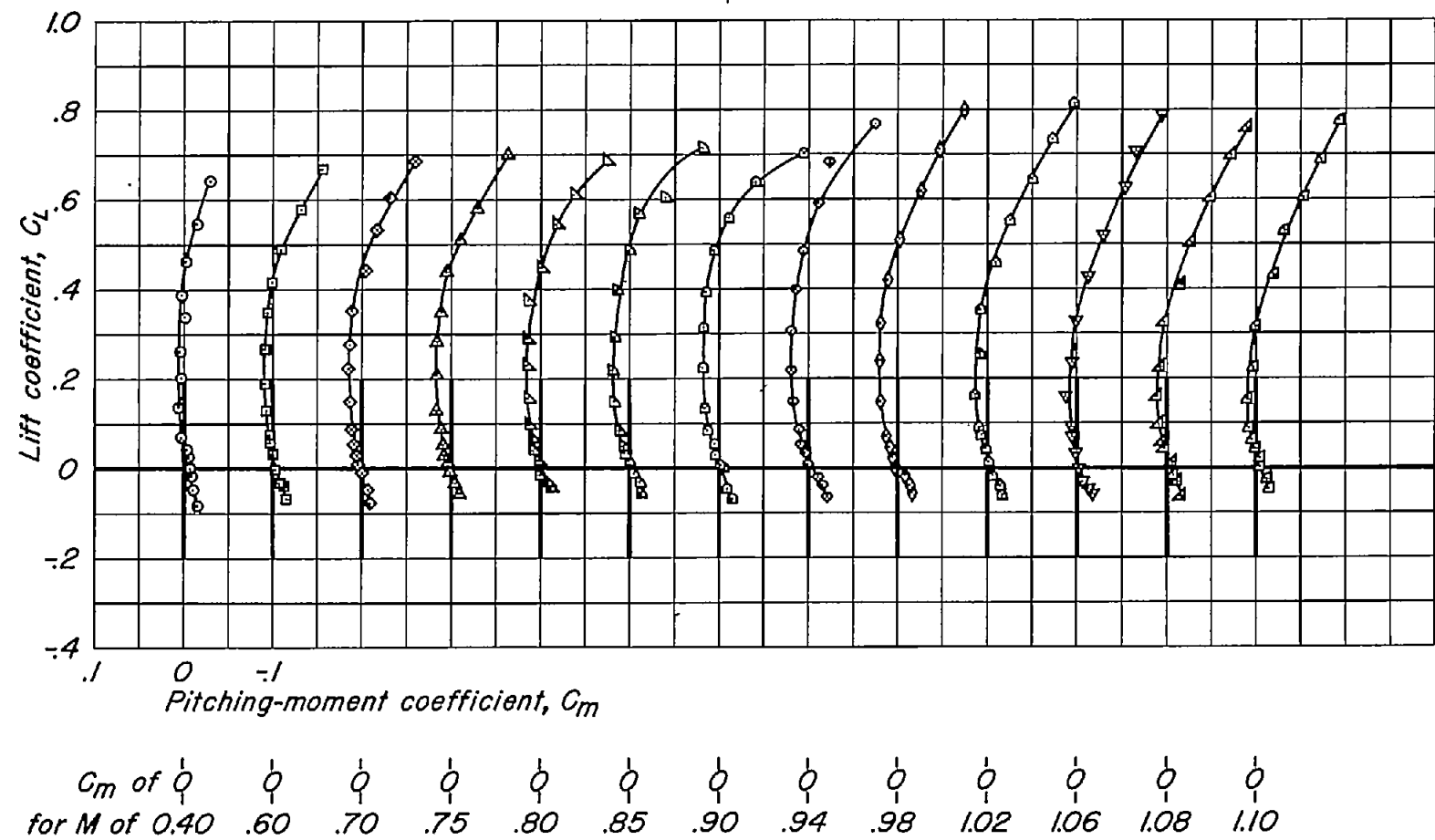
(o) $A, 1.5; t/c, 0.02$.
Figure 10.-Continued.



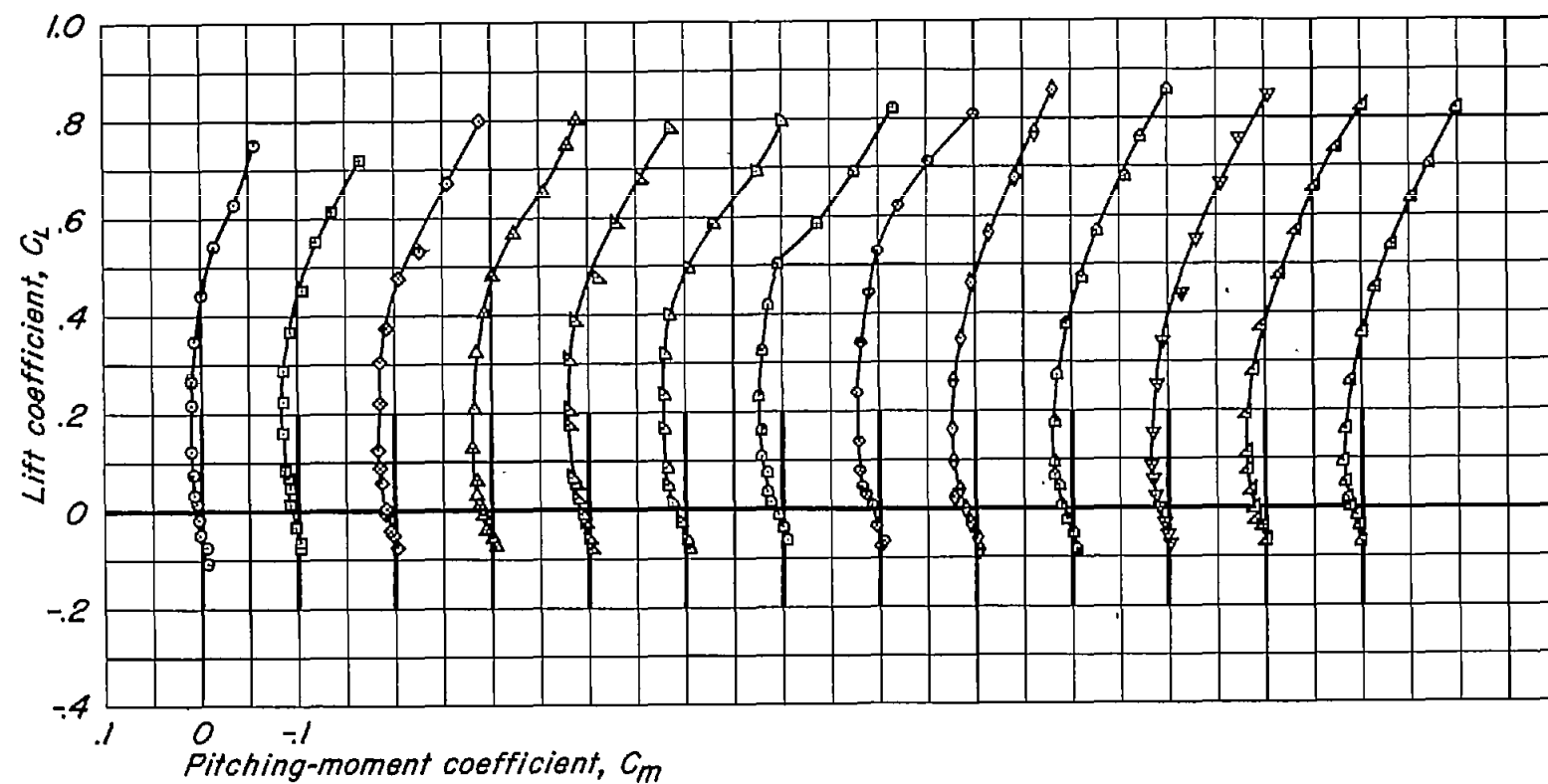
(p) A, 1; t/c , 0.10.
Figure 10.—Continued.



(q) A, 1; t/c , 0.08.
Figure 10.-Continued.

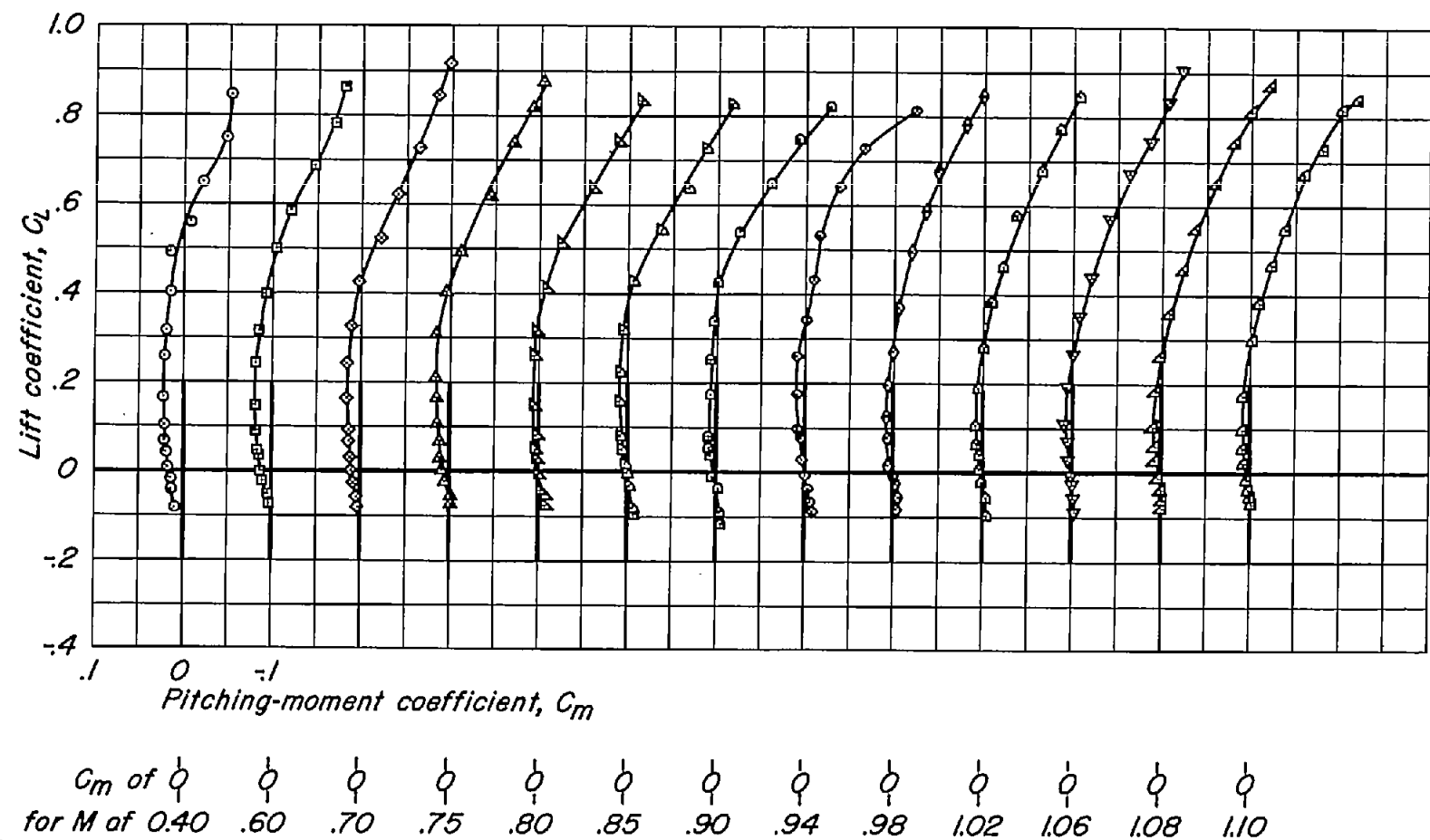


(r) $A, 1; t/c, 0.06.$
Figure 10.-Continued.

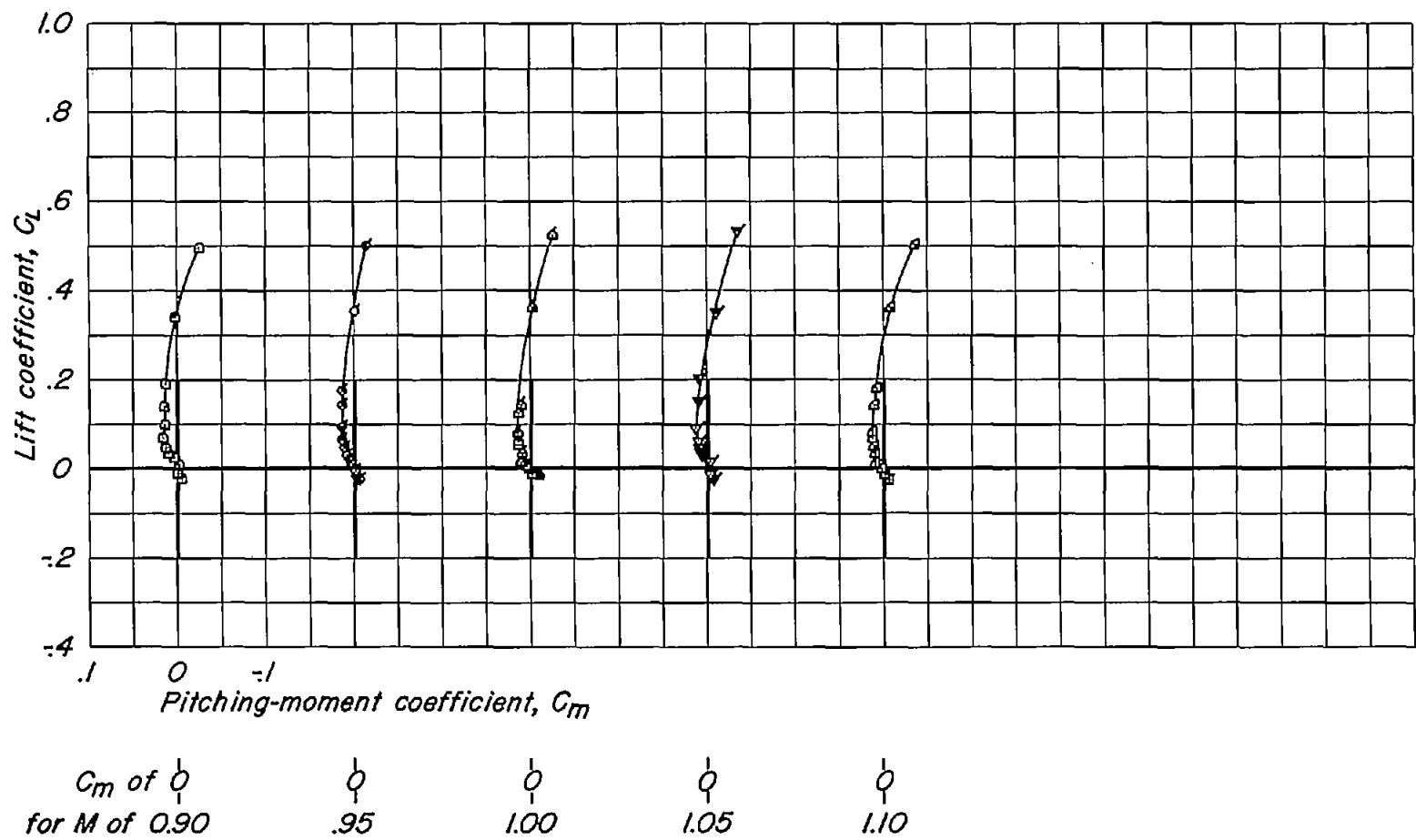


C_m of 0
for M of 0.40 .60 .70 .75 .80 .85 .90 .94 .98 1.02 1.06 1.08 1.10

(s) $A, 1; t/c, 0.04$.
Figure 10.-Continued.



(t) A, 1; t/c , 0.02.
Figure 10.—Continued.



C_m of 0
for M of 0.90

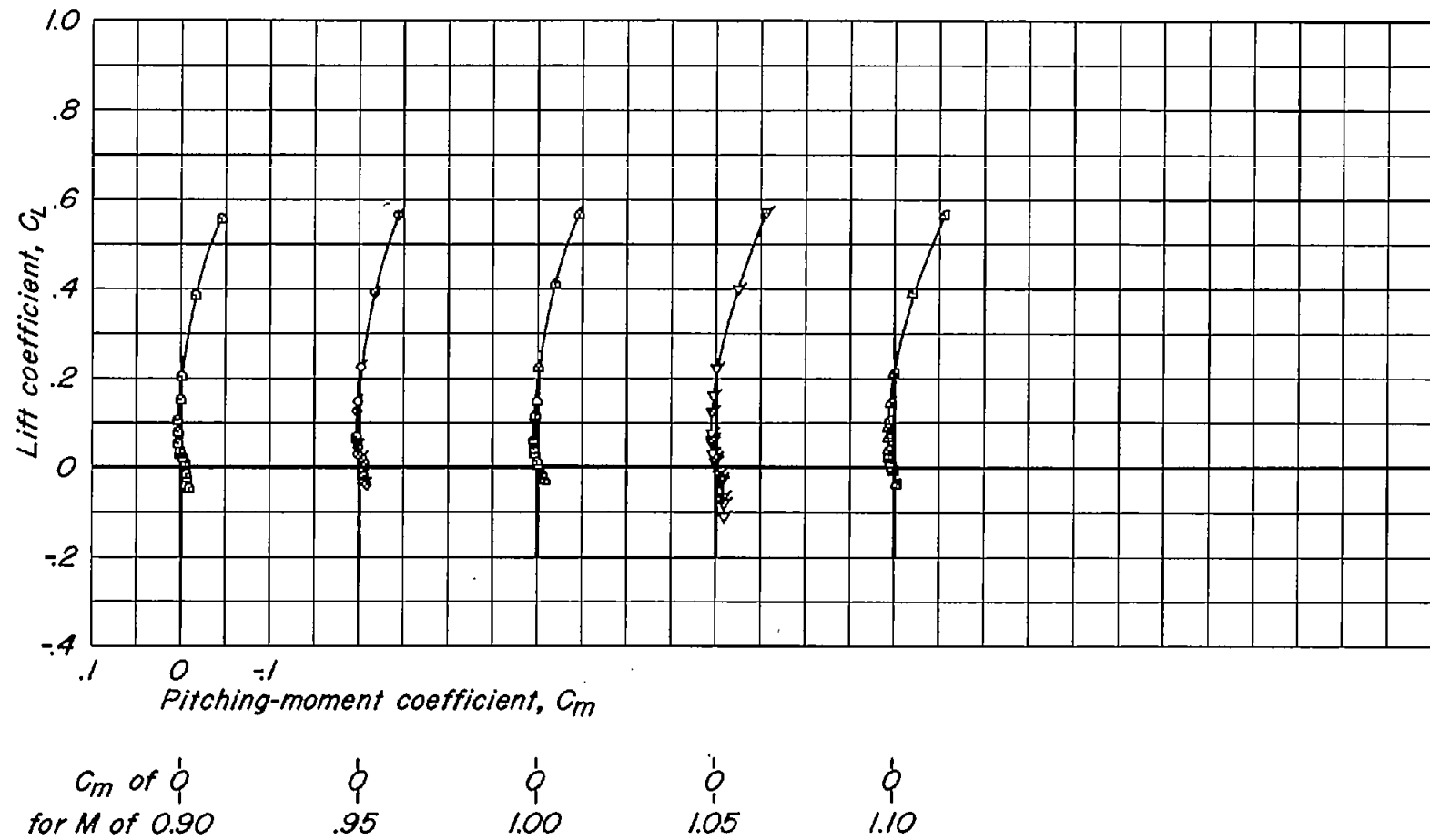
0

0

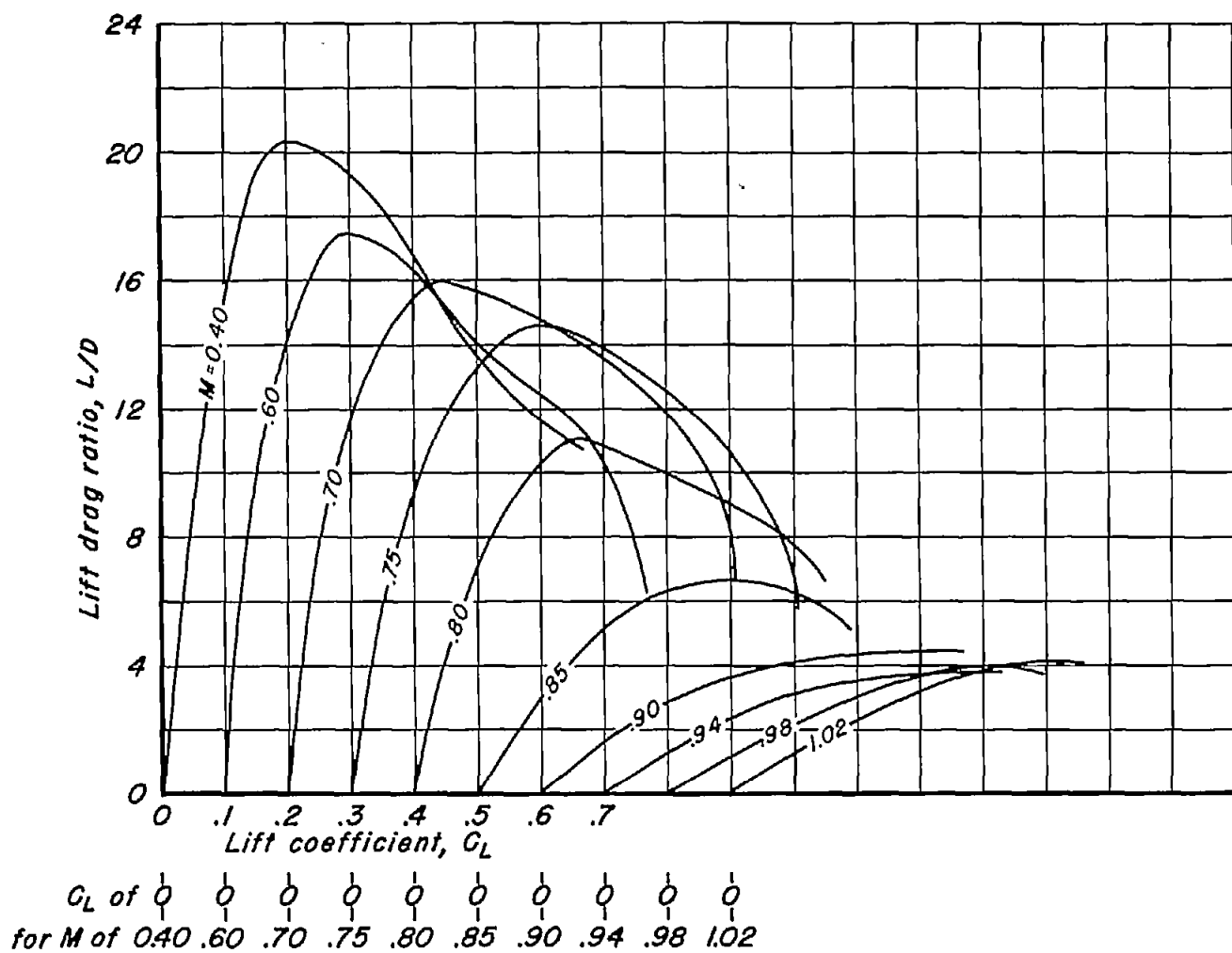
0

0

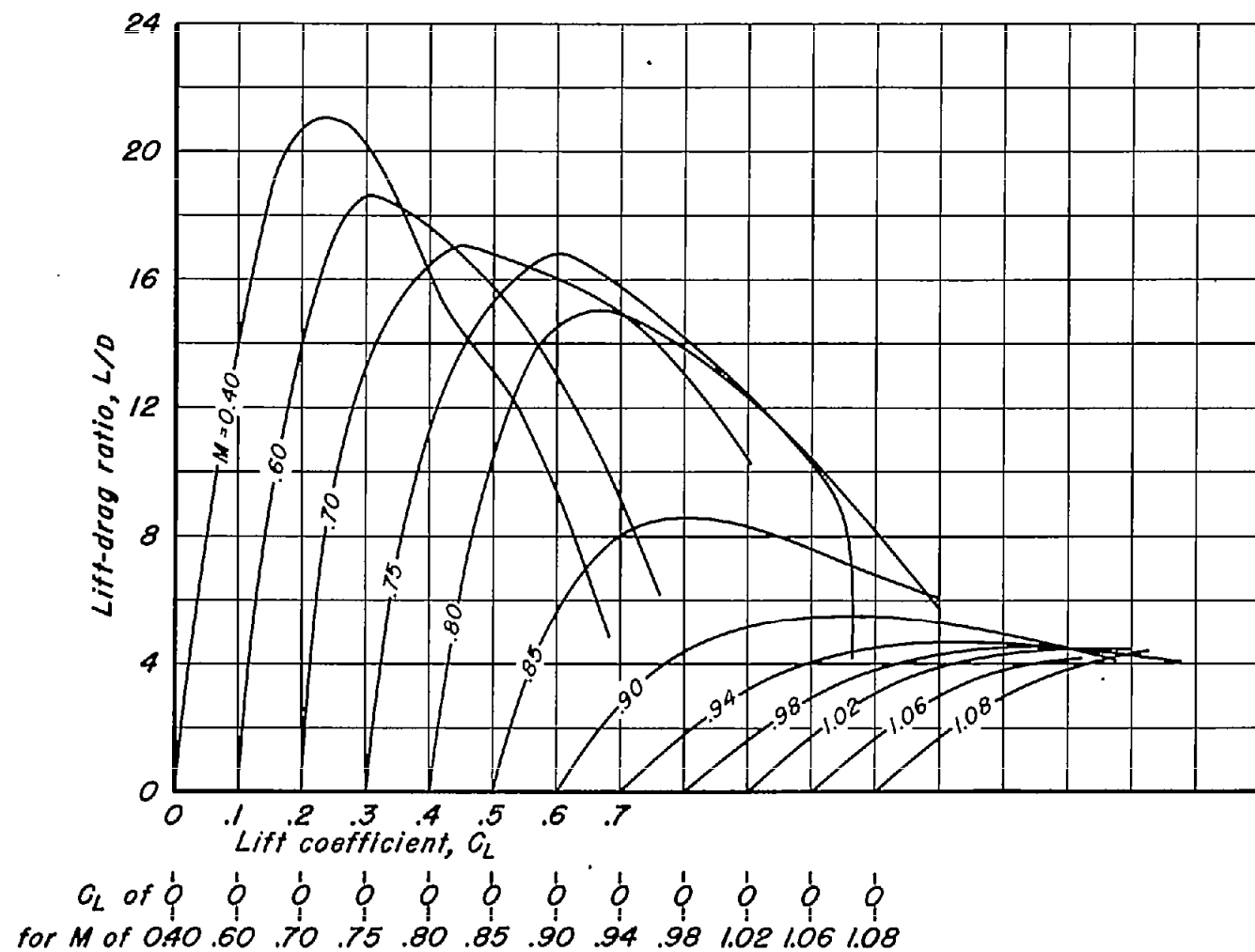
(u) $A, 0.5; t/c, 0.04$.
Figure 10.-Continued.



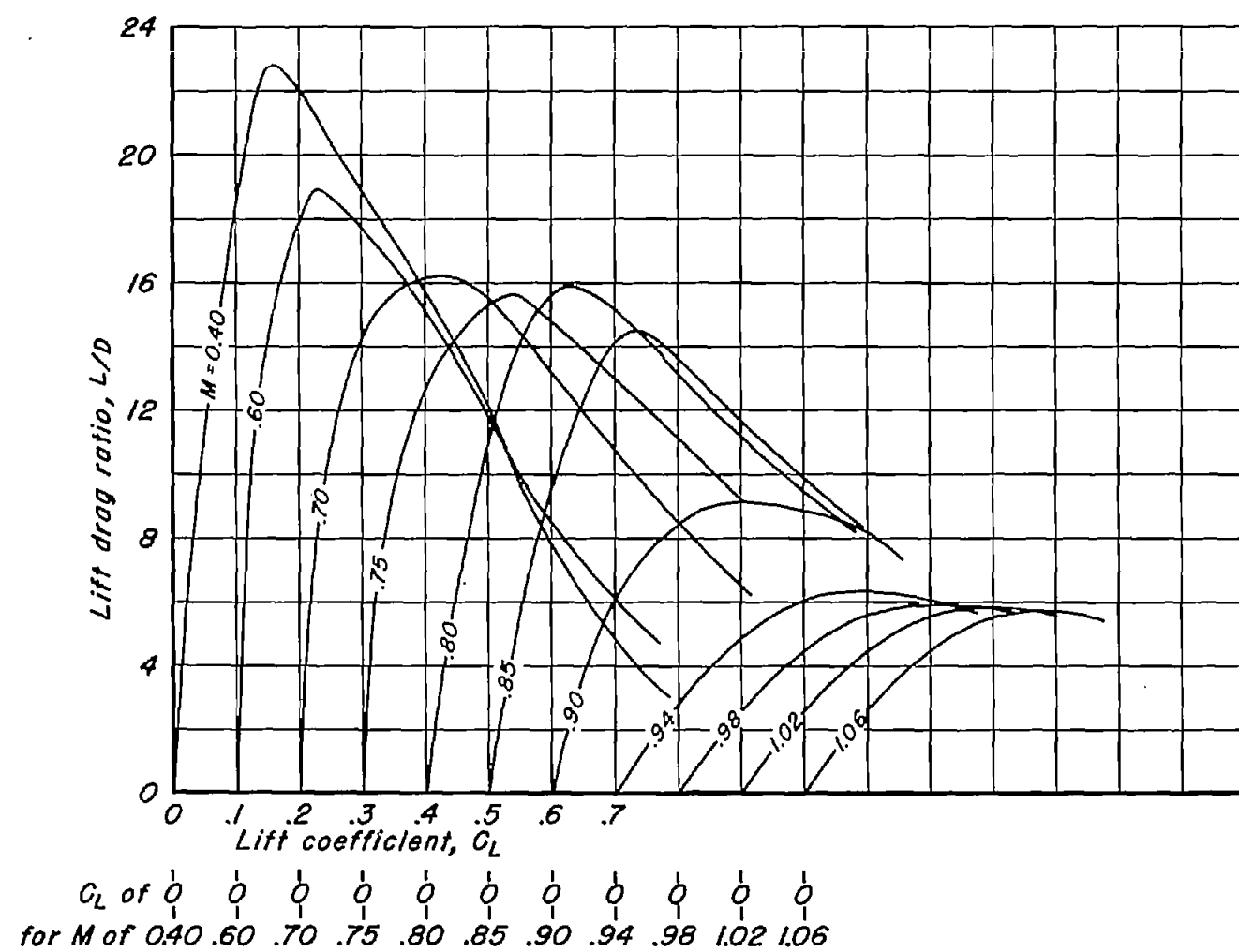
(v) $A, 0.5; t/c, 0.02$.
Figure 10.- Concluded.



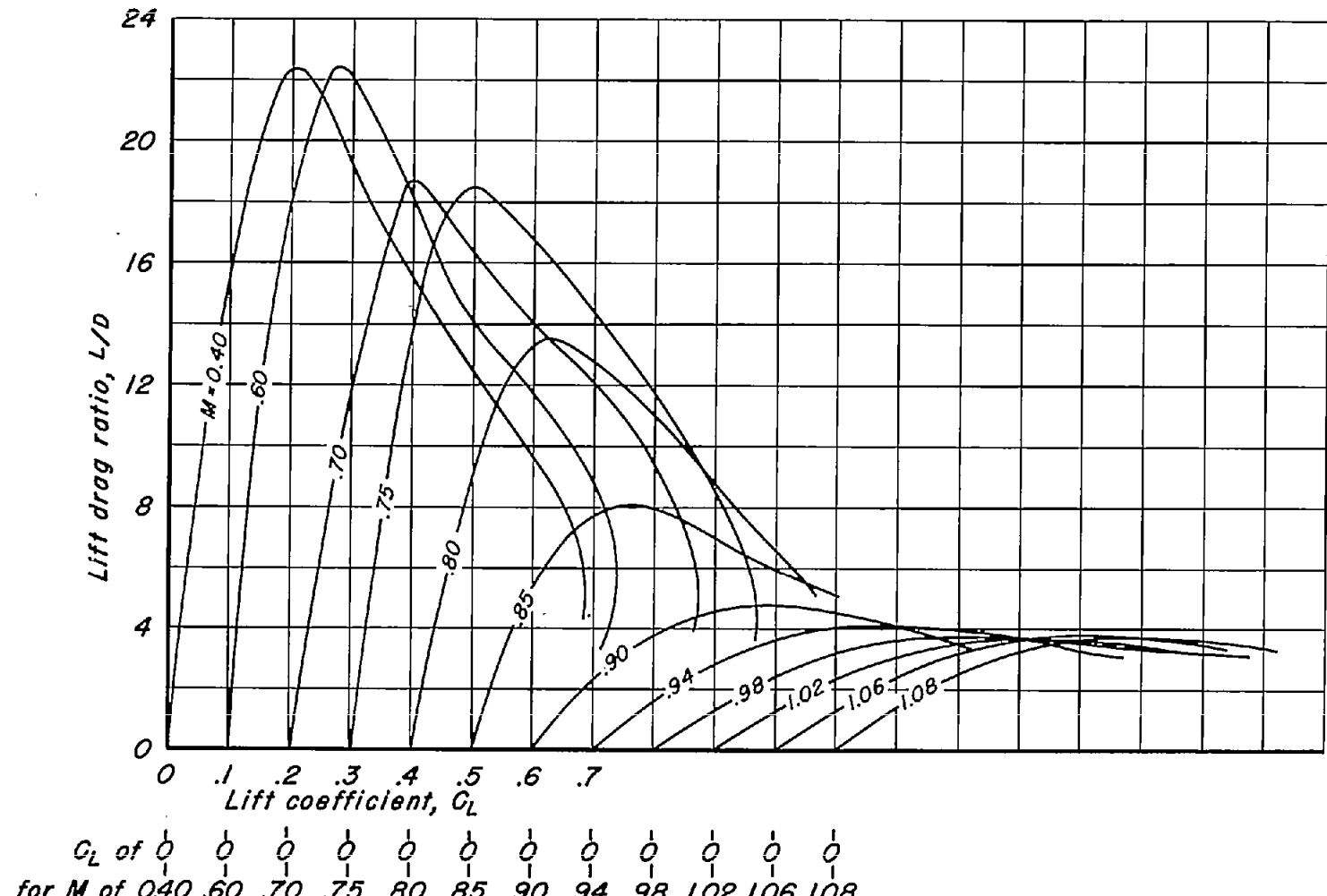
(a) A, 6; t/c , 0.10.
Figure 11.- The variation of lift-drag ratio with lift coefficient for the rectangular wings with NACA 63AOXX sections.



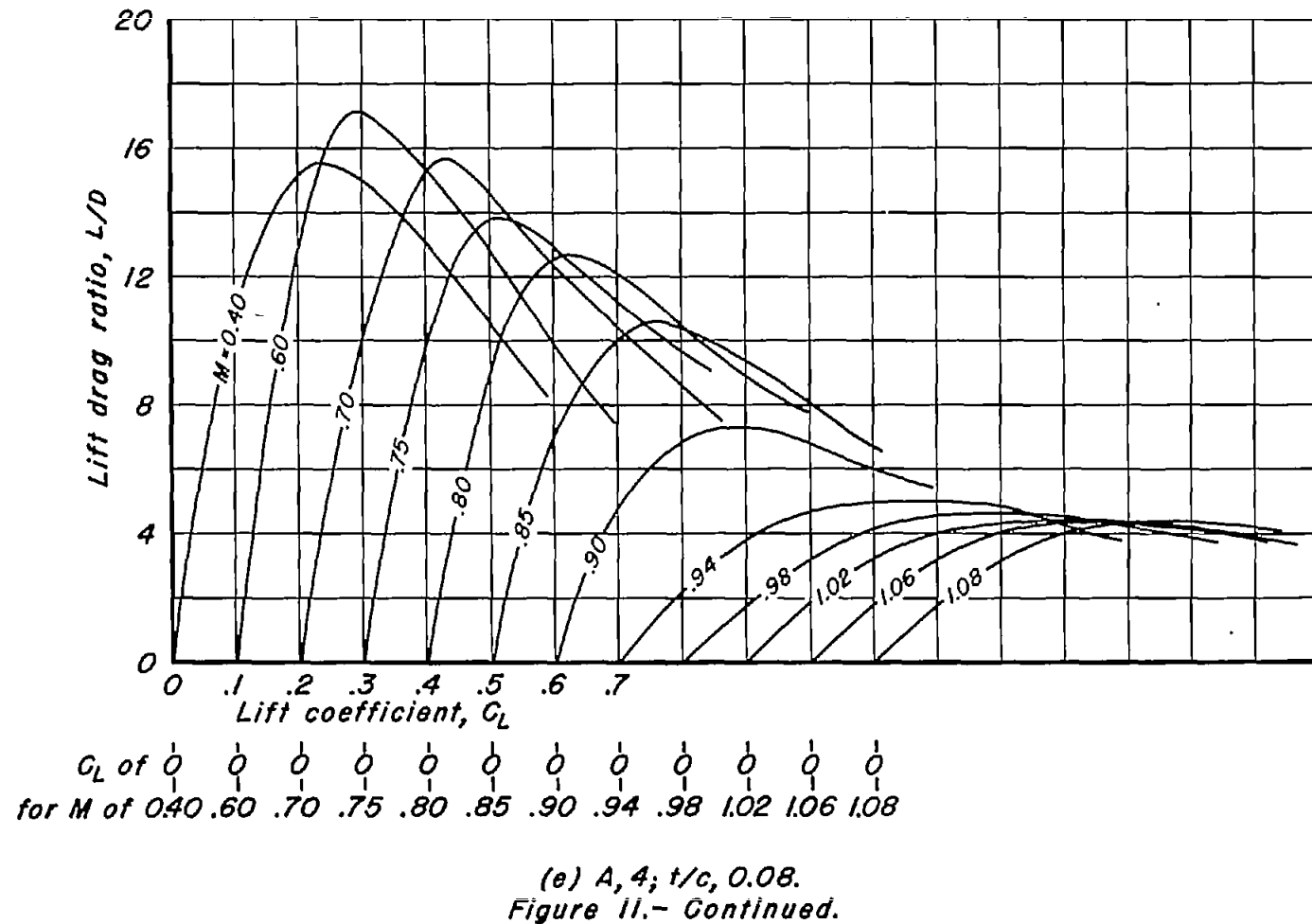
(b) $A, 6; t/c, 0.08.$
Figure 11.- Continued.

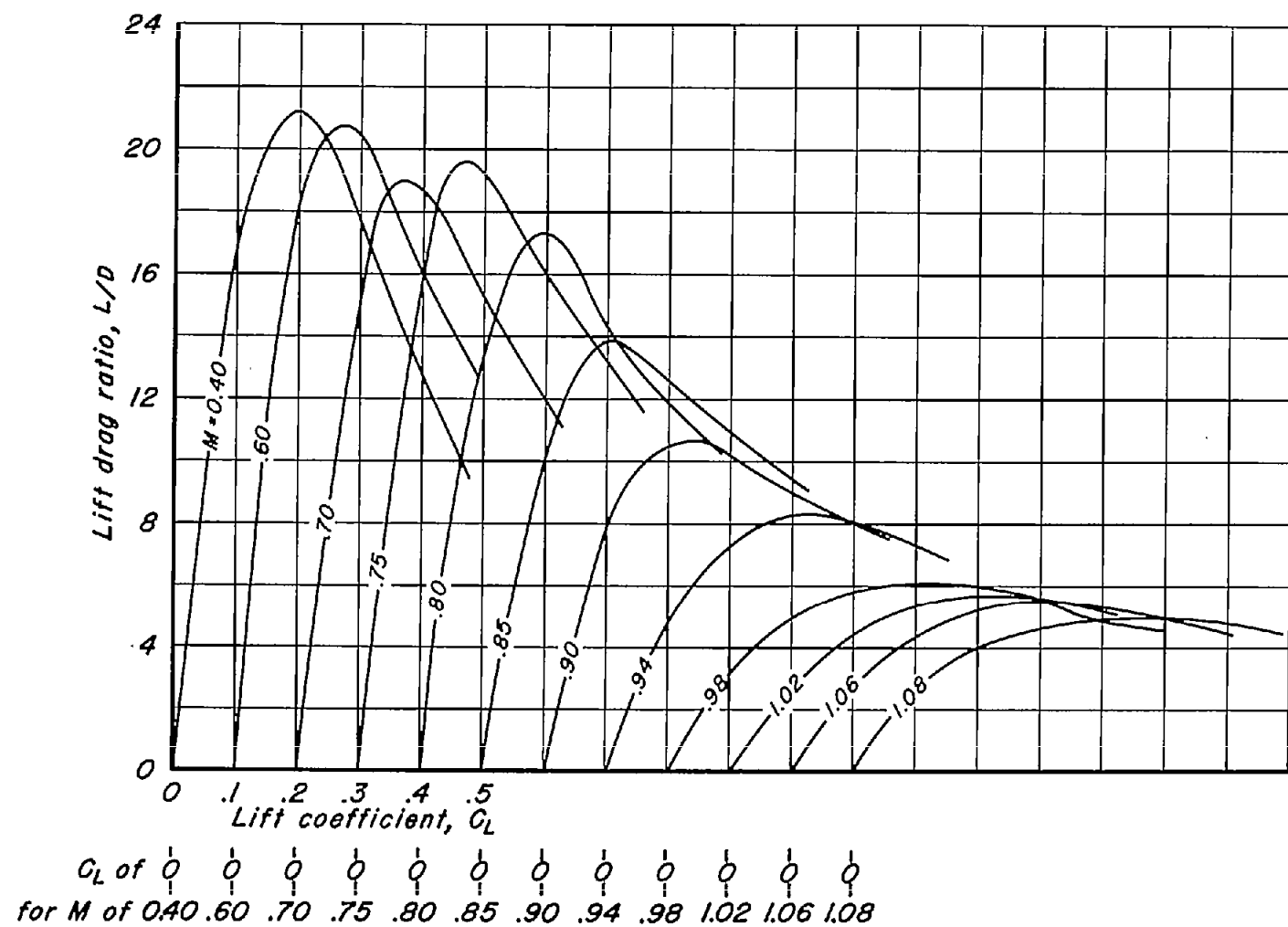


(c) $A, 6; t/c, 0.06.$
Figure 11.—Continued.

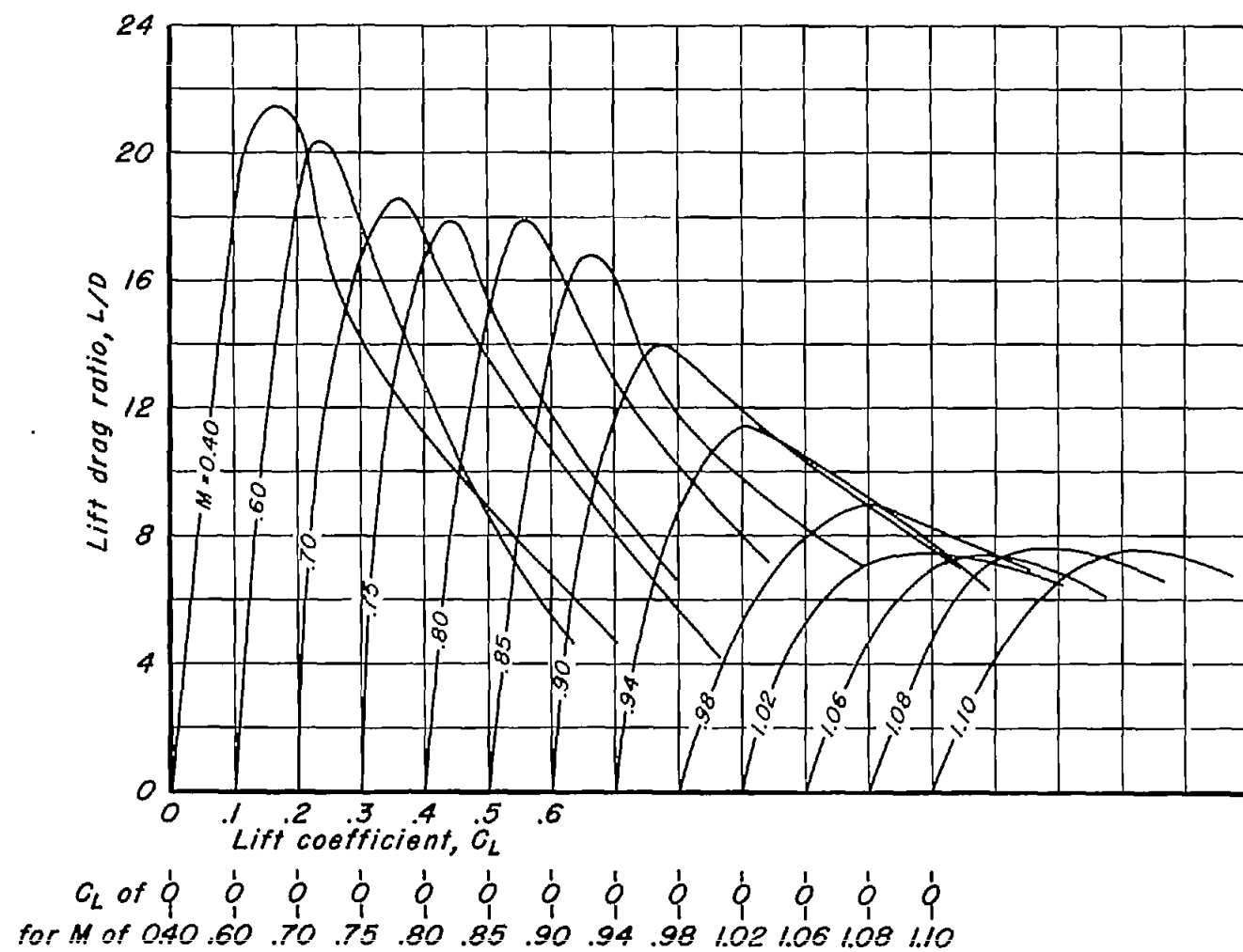


(d) $A, 4; t/c, 0.10$.
Figure 11.- Continued.

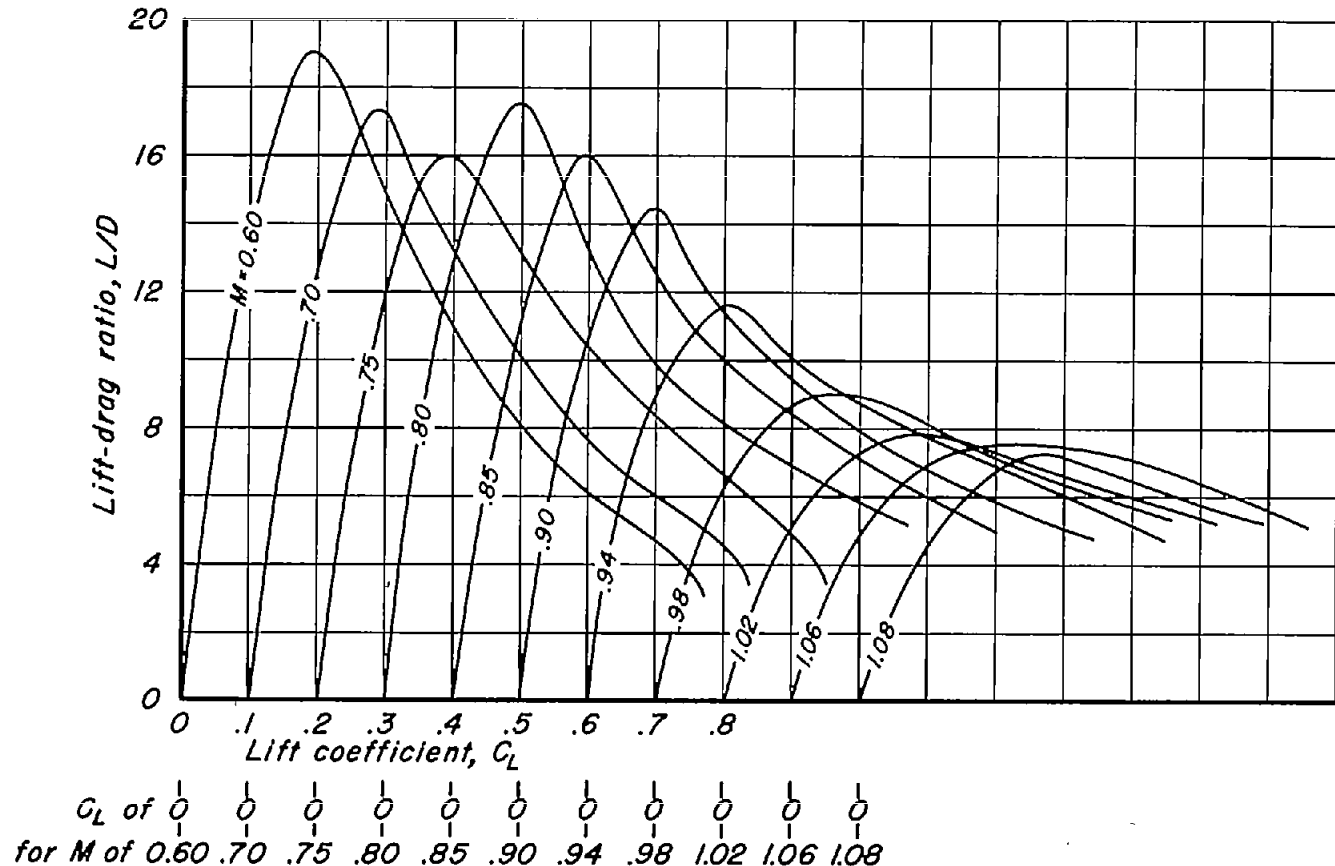




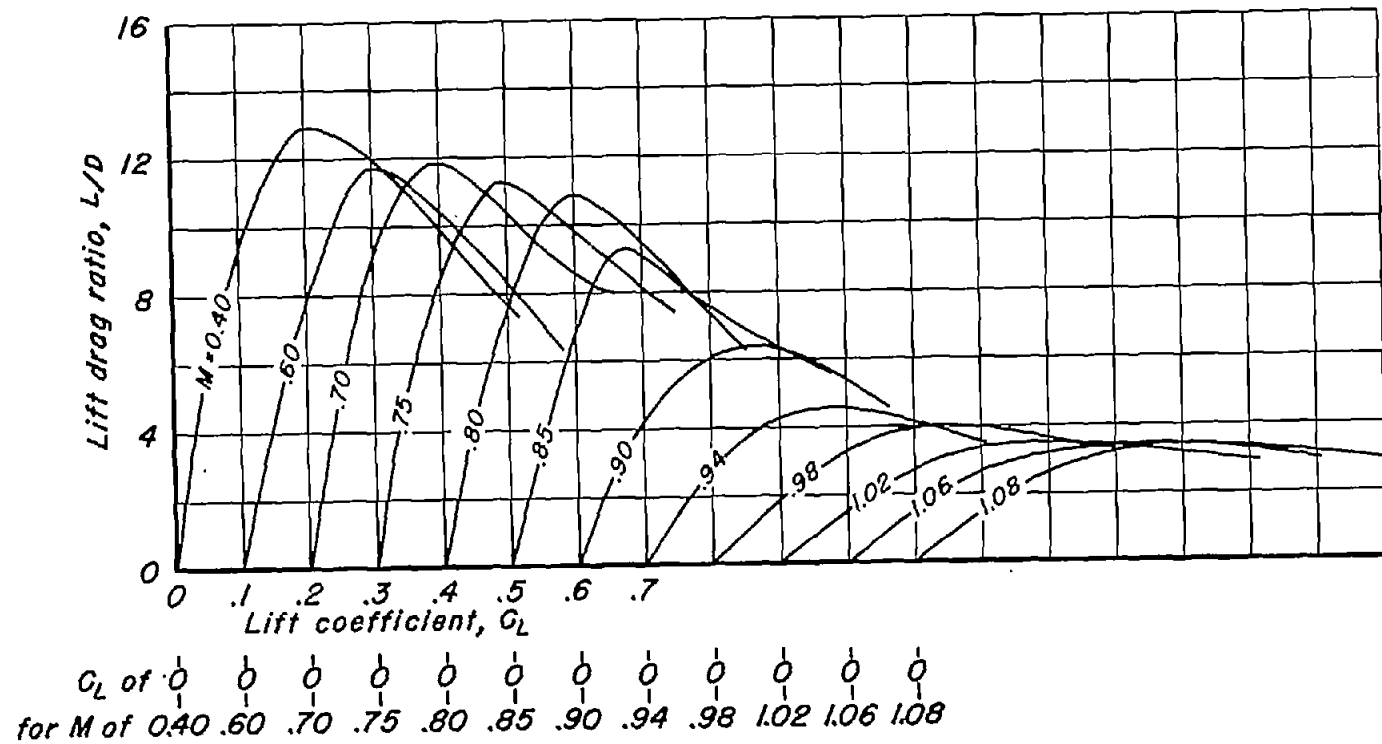
(f) $A, 4; 1/c, 0.06$.
Figure 11.- Continued.



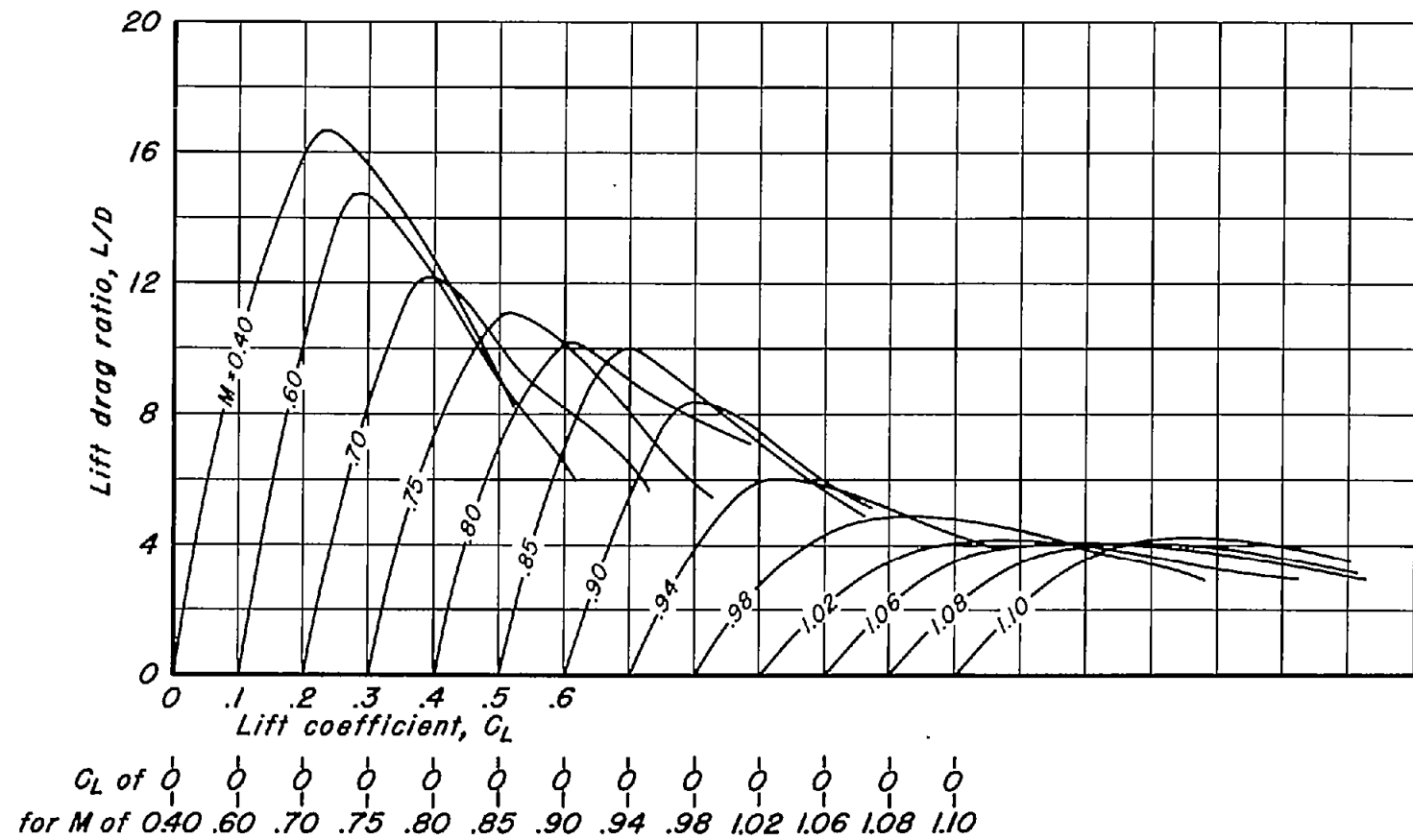
(g) $A, 4; t/c, 0.04$.
Figure 11.—Continued.



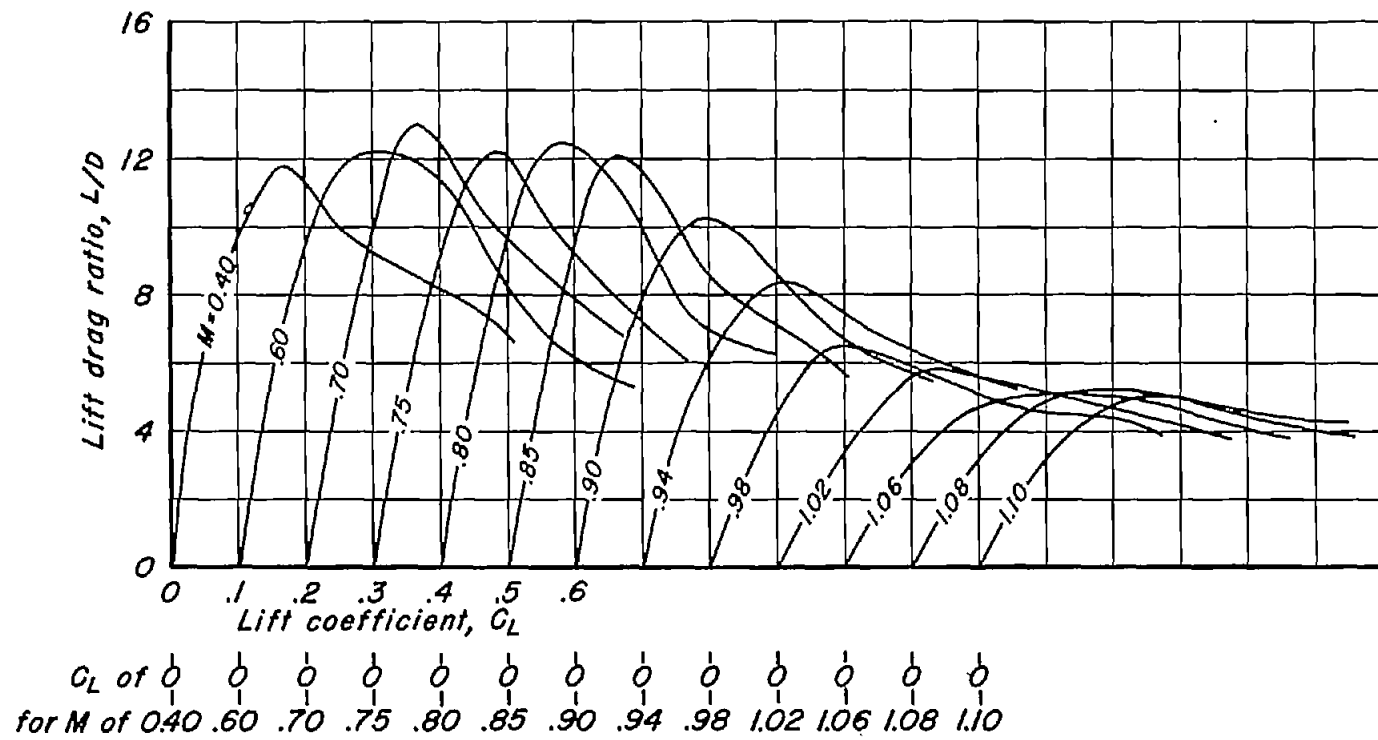
(h) $A, 3; t/c, 0.04$.
Figure 11.- Continued.



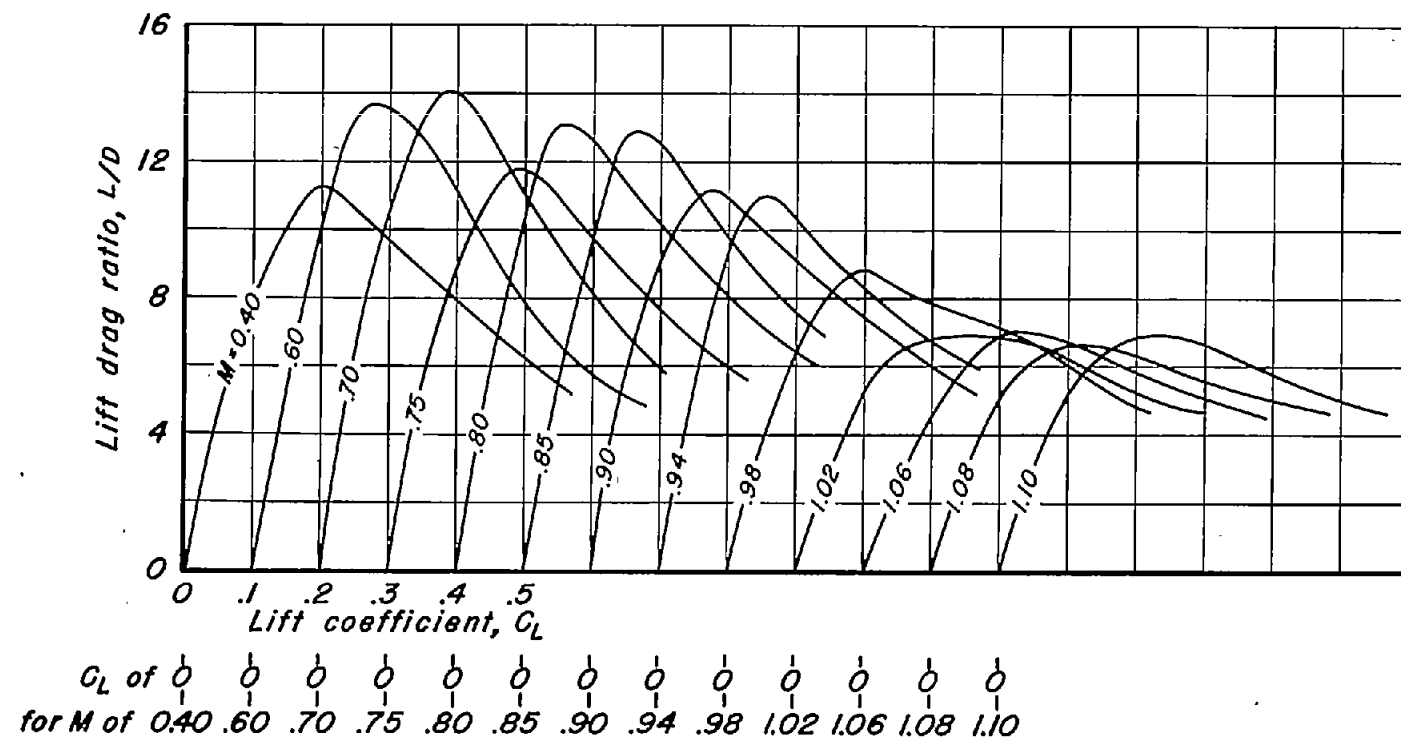
(i) $A, 2; t/c, 0.10$.
Figure 11.—Continued.



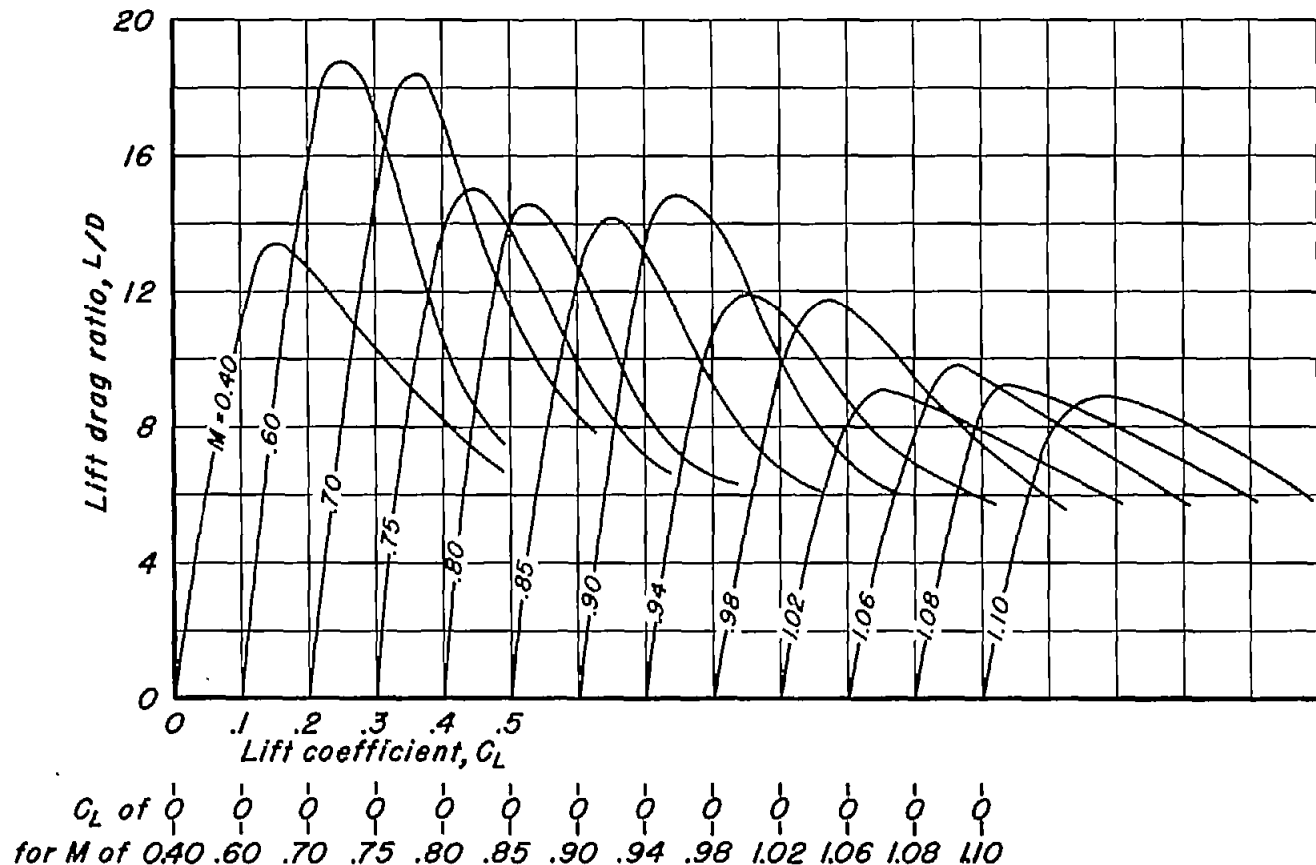
(j) $A, 2; t/c, 0.08$.
Figure 11.- Continued.



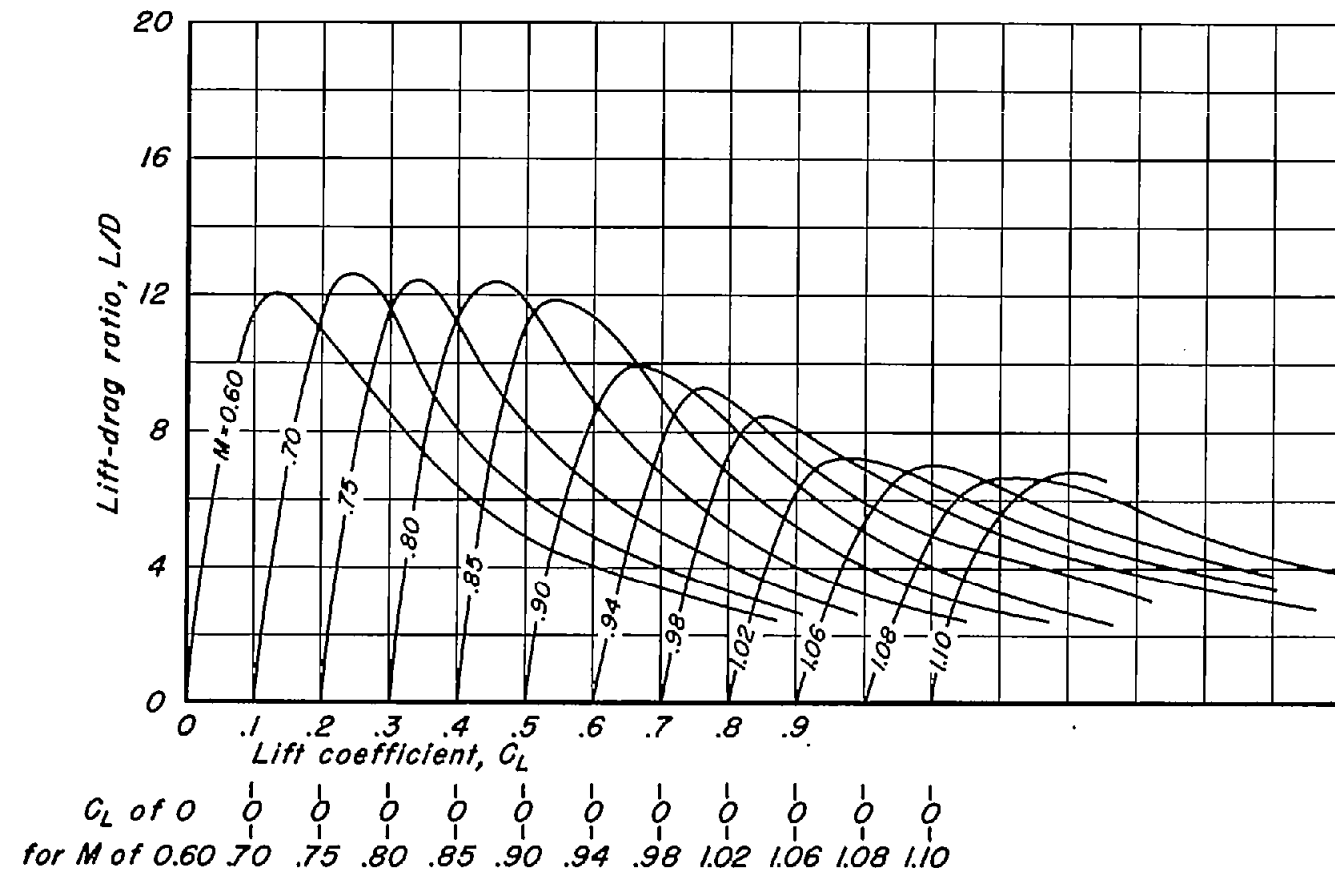
(k) A, 2; t/c , 0.06.
Figure 11.—Continued.



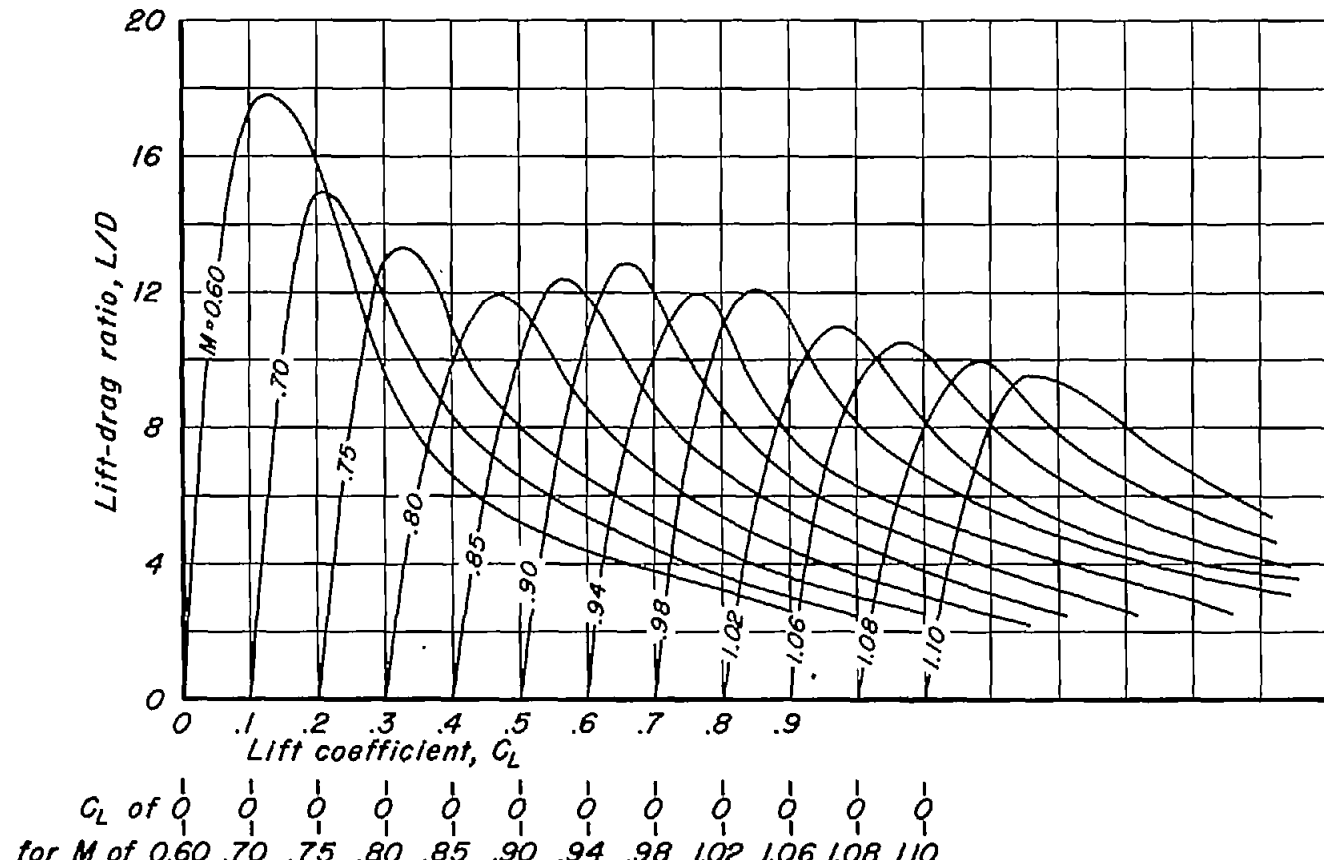
(1) $A, 2; t/c, 0.04$.
Figure 11.- Continued.



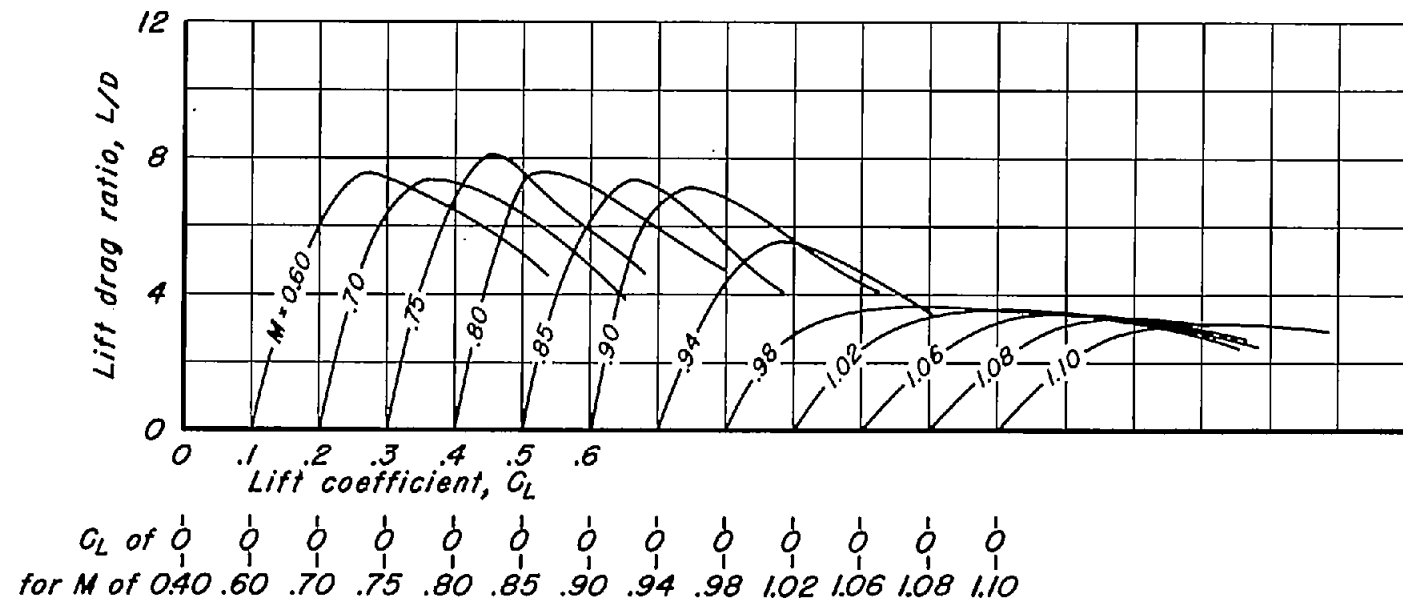
(m) $A, 2; t/c, 0.02$.
Figure 11.- Continued.



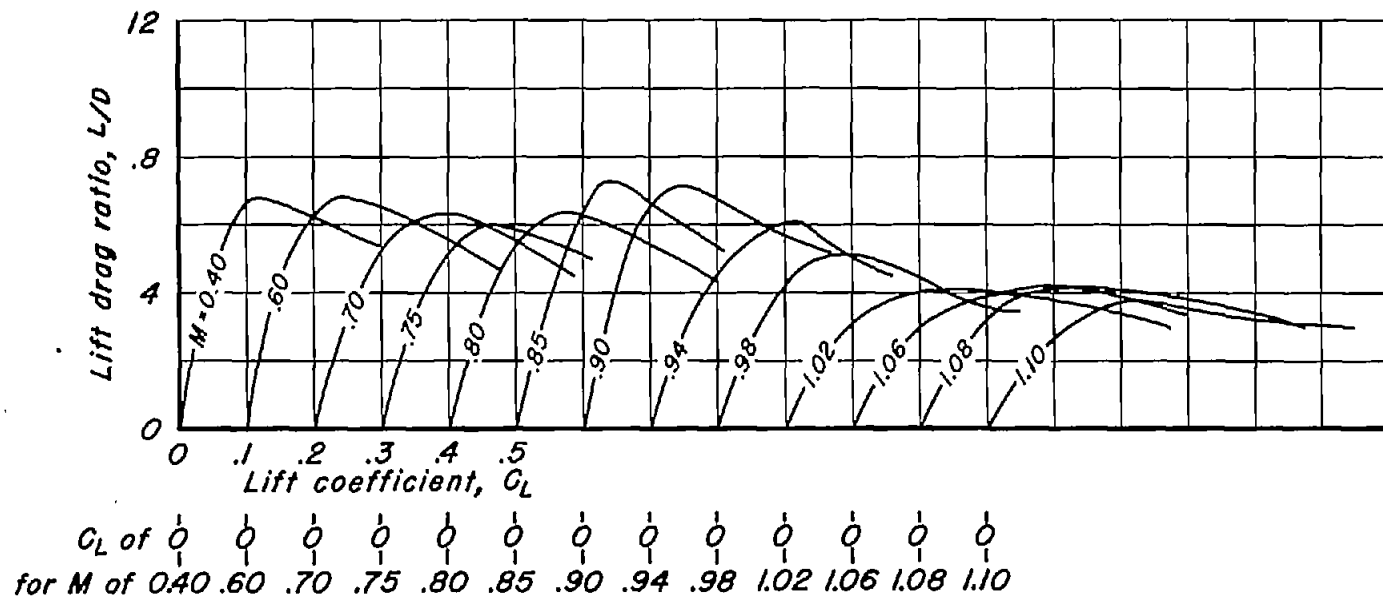
(n) $A, 1.5, t/c, 0.04.$
Figure 11.- Continued.



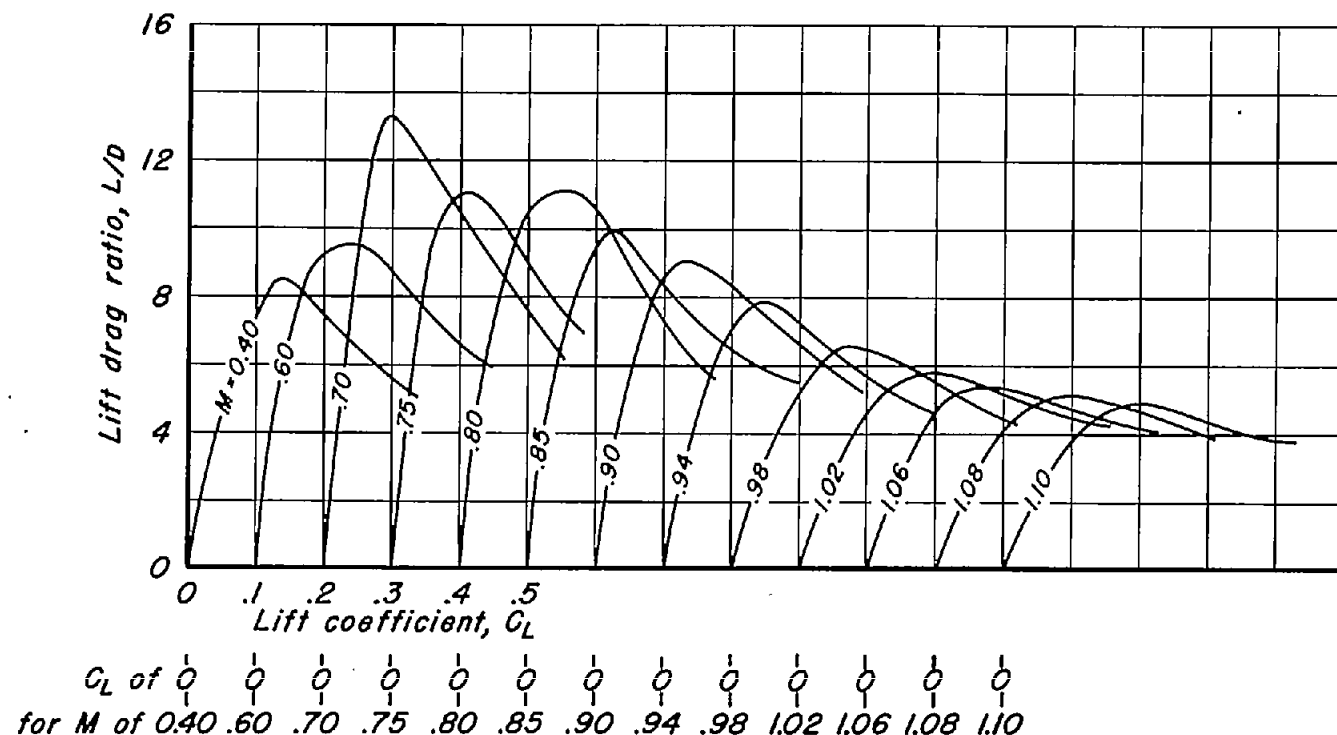
(o) $A, 1.5; t/c, 0.02$.
Figure 11.- Continued.



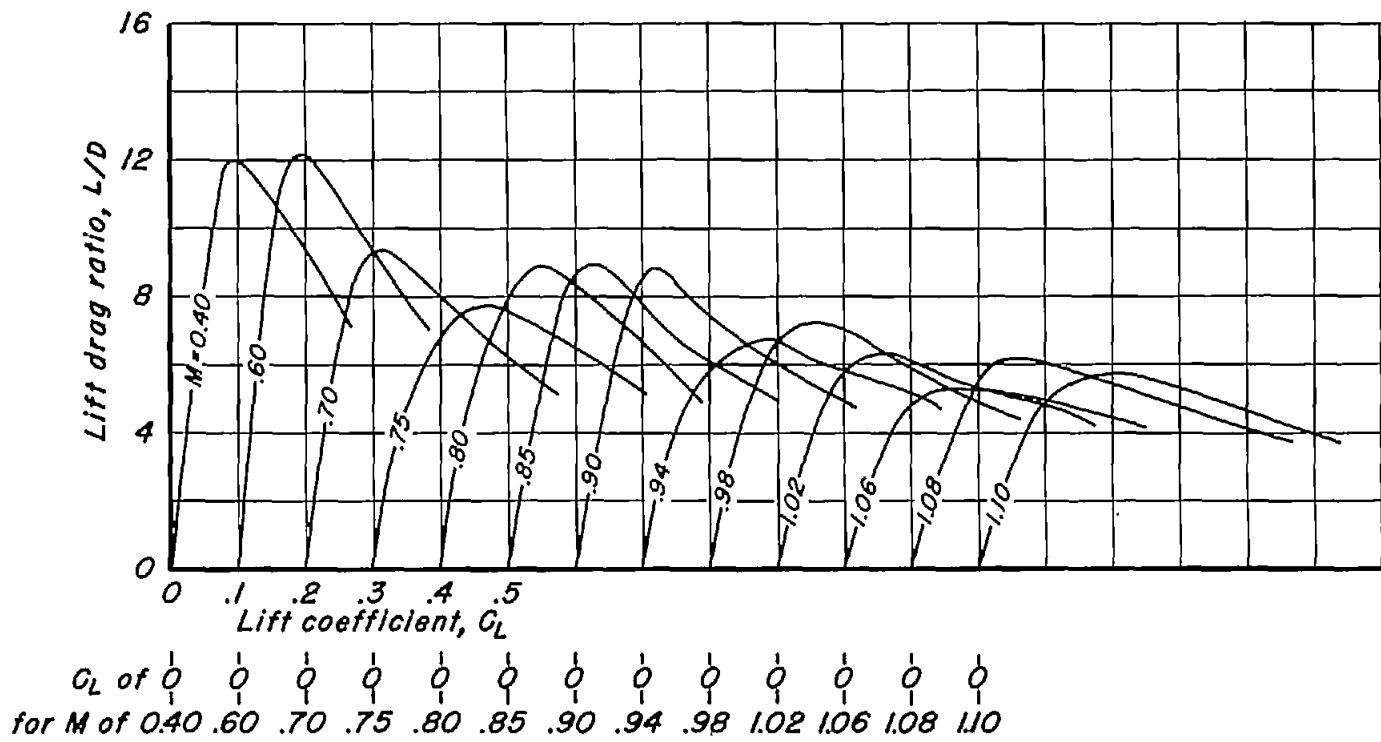
(p) $A, l; t/c, 0.10$.
Figure 11.—Continued.



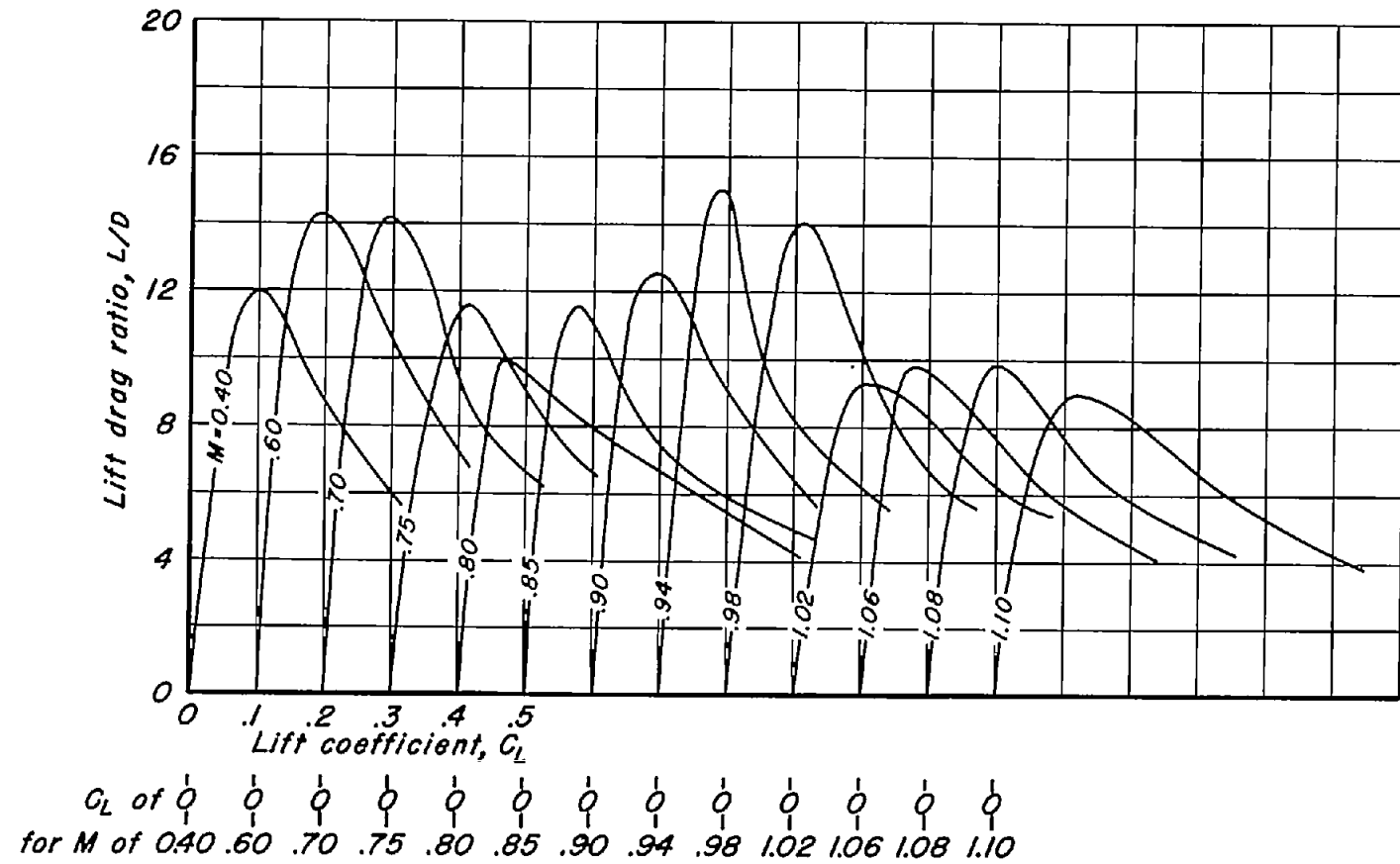
(q) $A, l; t/c, 0.08$.
Figure 11.- Continued.



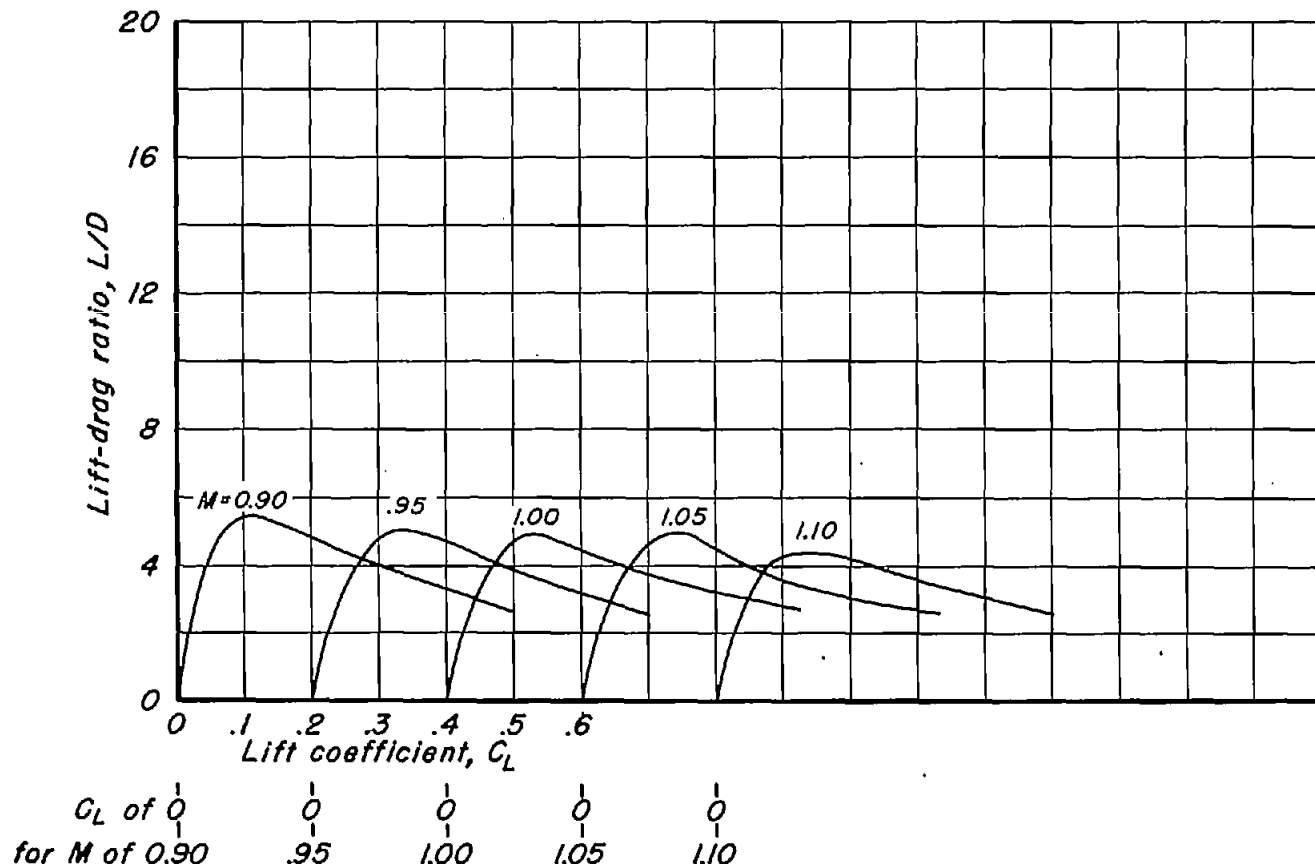
(r) $A, l; t/c, 0.06$.
Figure II.- Continued.



(s) $A, l; t/c, 0.04$.
Figure 11.- Continued.

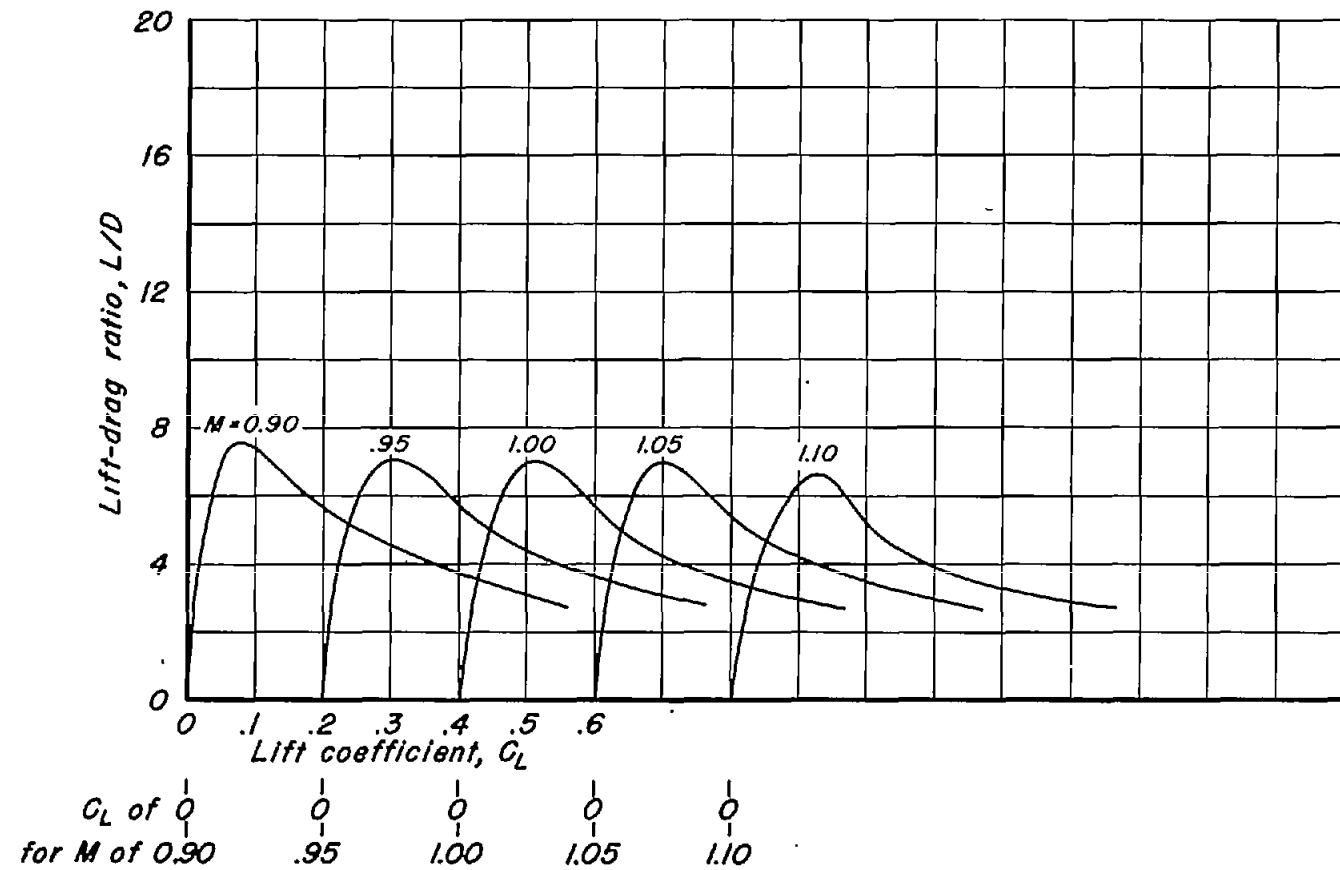


(t) $A, l; t/c, 0.02.$
Figure 11.- Continued.



C_L of 0
for M of 0.90 0.95 1.00 1.05 1.10

(u) $A, 0.5; t/c, 0.04$.
Figure 11.- Continued.



(v) $A, 0.5; t/c, 0.02$.
Figure 11.- Concluded.

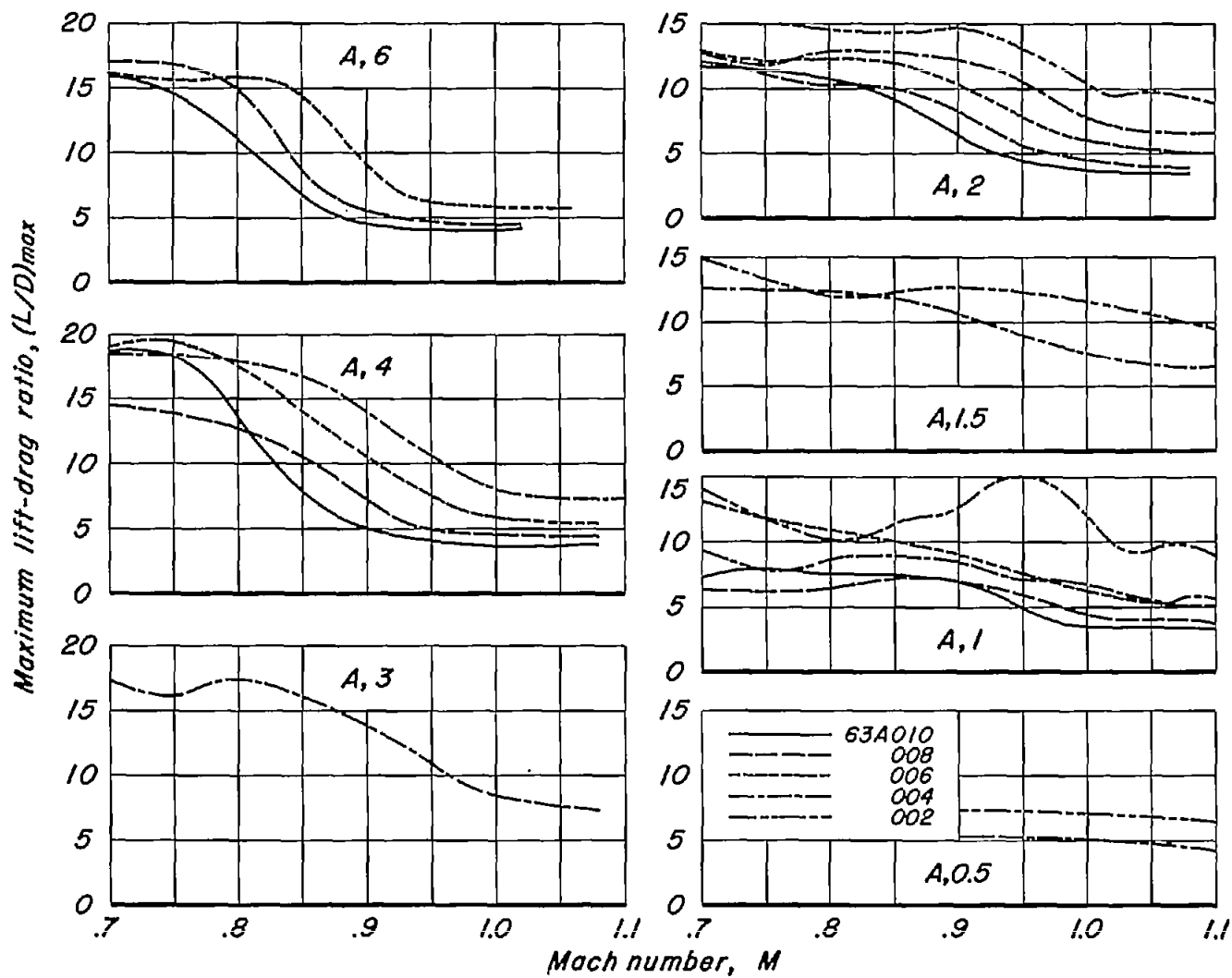


Figure 12.- The variation of maximum lift-drag ratio with Mach number for the rectangular wings with NACA 63AOXX sections.

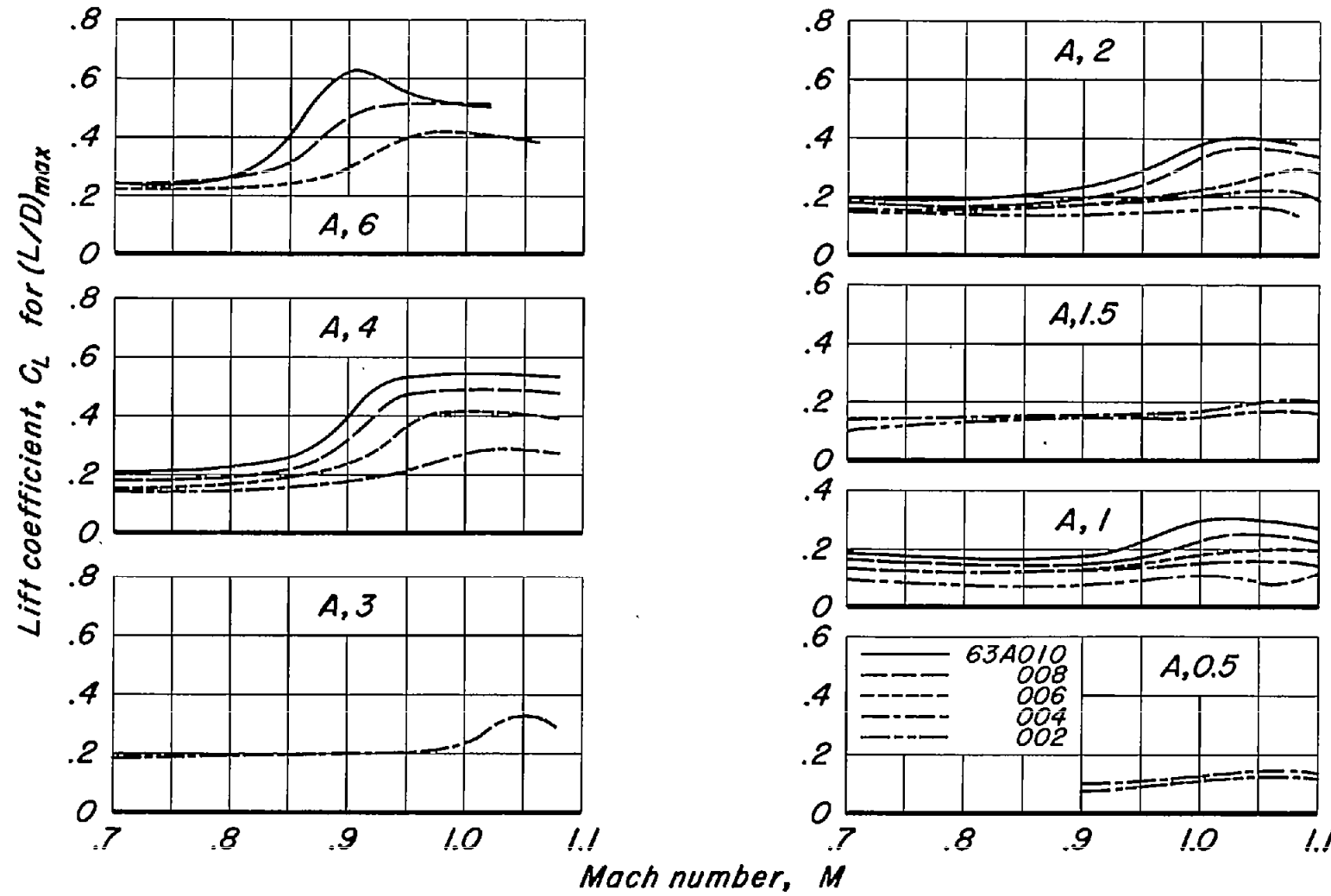


Figure 13.- The variation of lift coefficient for maximum lift-drag ratio with Mach number for the rectangular wings with NACA 63AOXX sections.

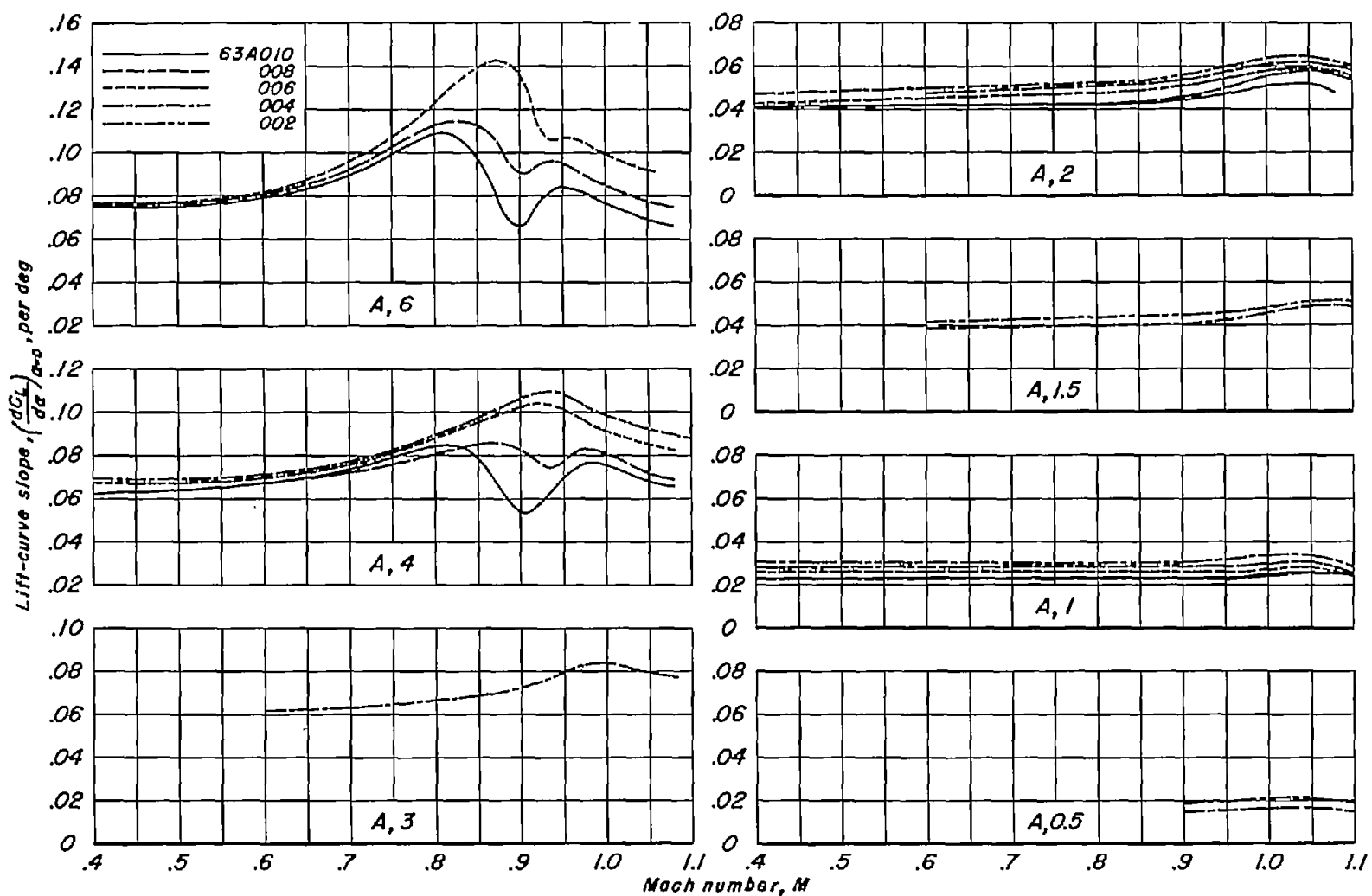


Figure 14.- The variation of lift-curve slope with Mach number for the rectangular wings with NACA 63AOXX sections.

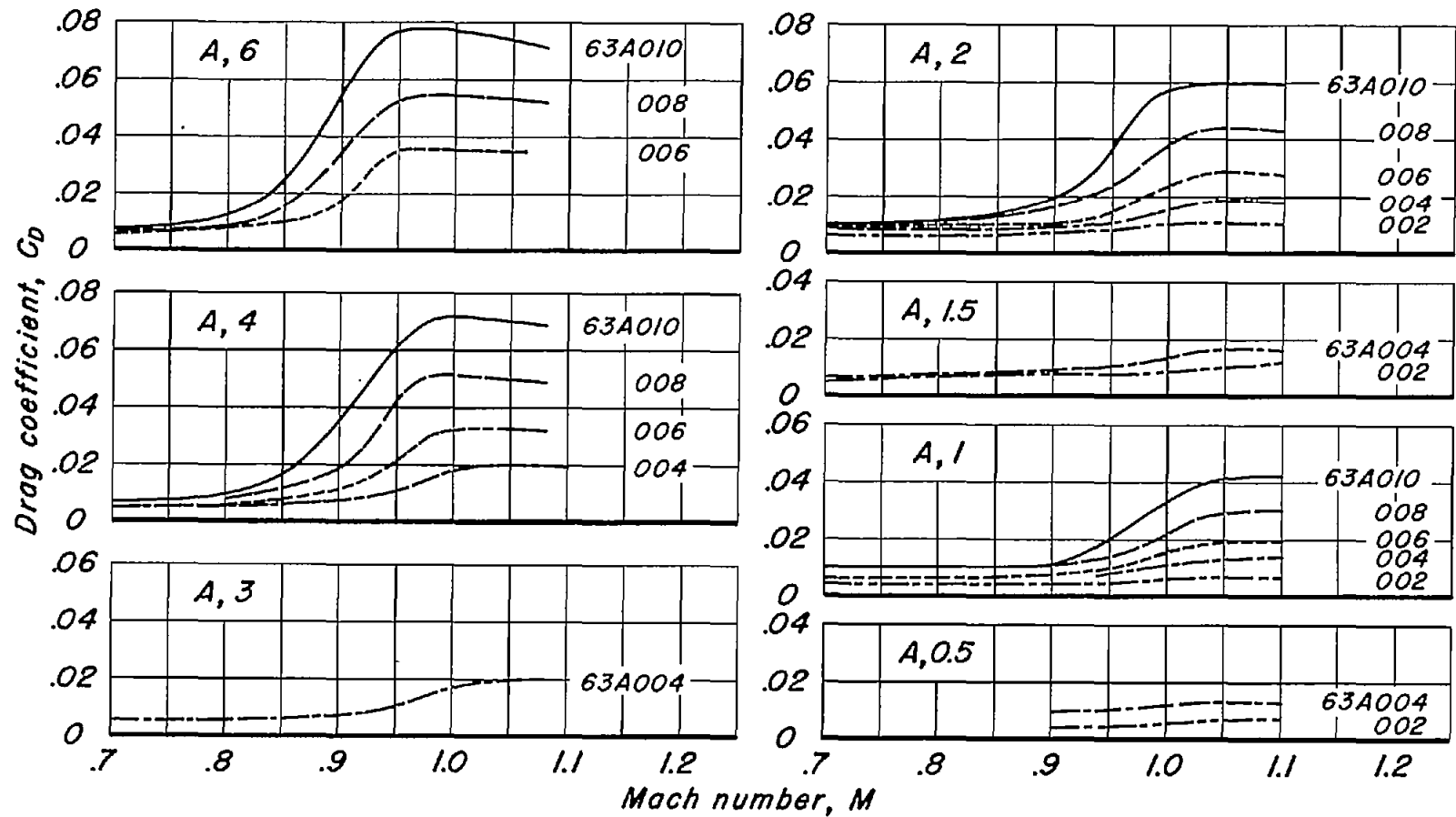
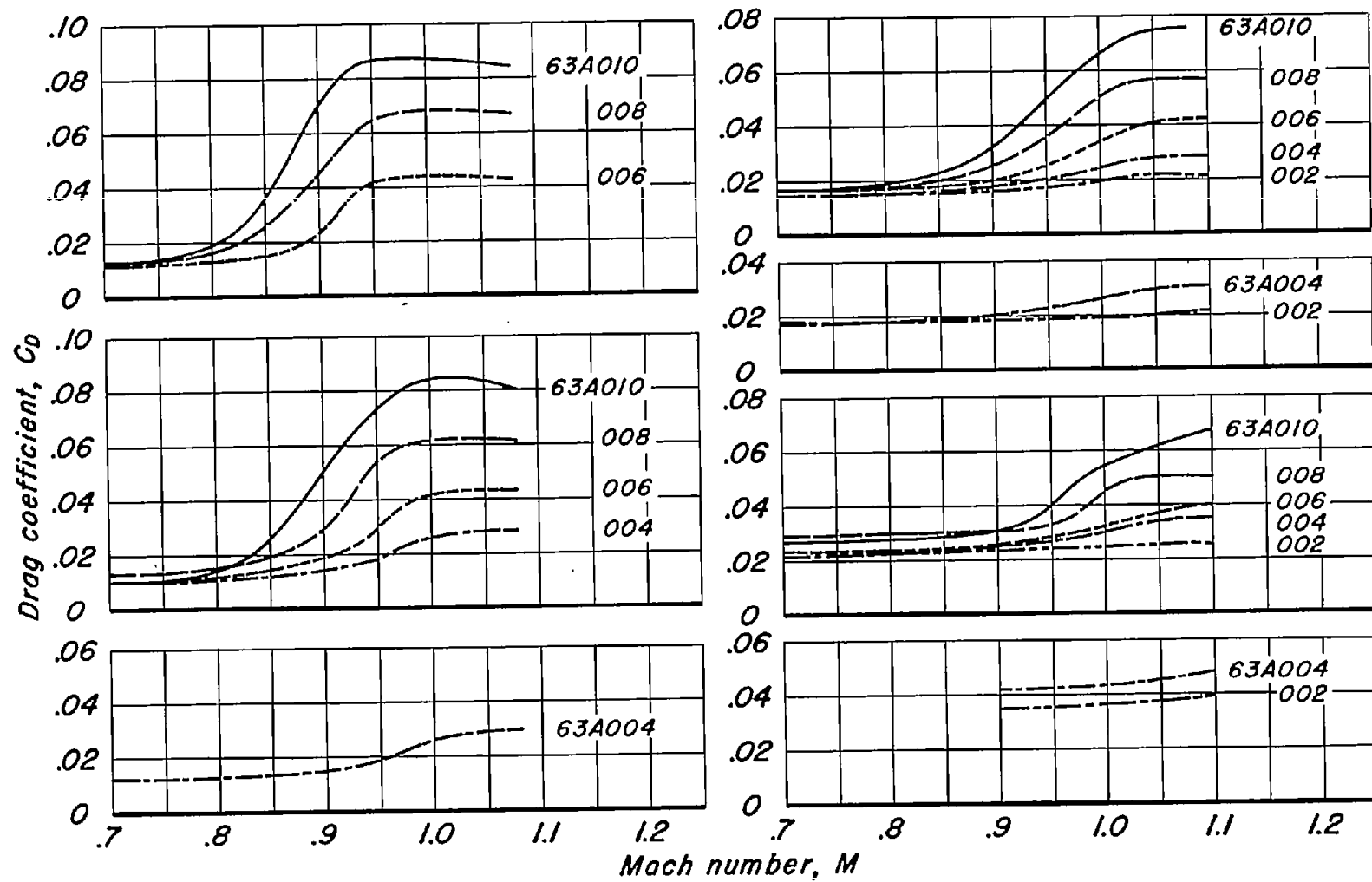


Figure 15.- The variation of drag coefficient with Mach number for the rectangular wings with NACA 63AOXX sections.



(b) $C_L, 0.2.$
Figure 15.- Concluded.

NACA-TN-3501-4A-2-9-1000

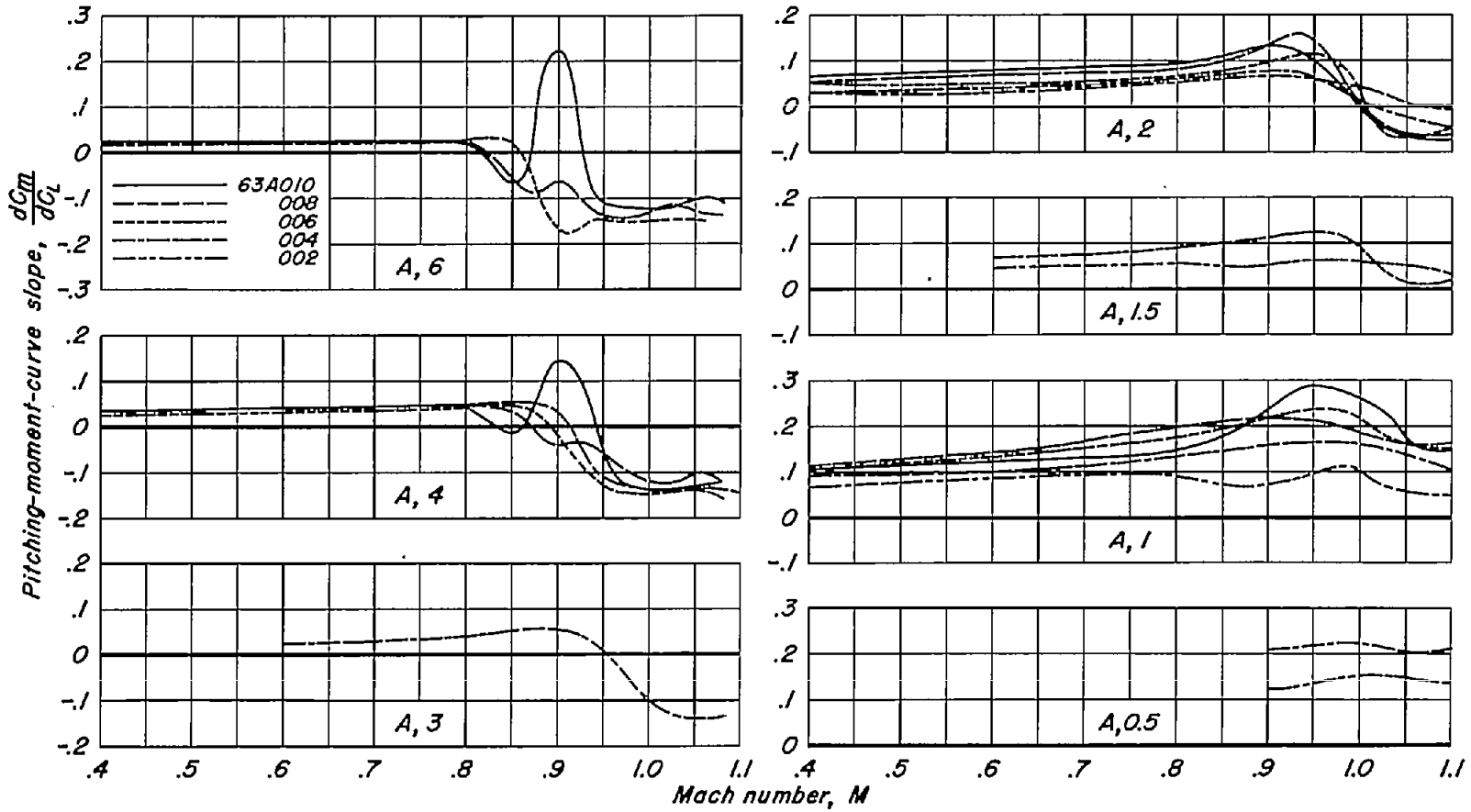


Figure 16.—The variation of pitching-moment-curve slope with Mach number for the rectangular wings with NACA 63AOXX sections.